Use Authorization

In presenting this thesis in partial fulfillment of the requirements for an advanced degree at Idaho State University, I agree that the Library shall make it freely available for inspection. I further state that permission to download and/or print my thesis for scholarly purposes may be granted by the Dean of the Graduate School, Dean of my academic division, or by the University Librarian. It is understood that any copying or publication of this thesis for financial gain shall not be allowed without my written permission.

Signature ______________________________

Date ______________________________

FINITE ELEMENT MODELING OF FIELD-CAST BRIDGE CONNECTIONS

by

Nate Oldham

A thesis

submitted in partial fulfillment

of the requirements for the degree of

Master of Science in the Department of Civil and Environmental Engineering

Idaho State University

Spring 2020

Committee Approval

To the Graduate Faculty:

The members of the committee appointed to examine the thesis of NATE OLDHAM find it satisfactory and recommend that it be accepted.

Major Advisor

Dr. Arya Ebrahimpour

Committee Member

Dr. Mustafa Mashal

Graduate Faculty Representative

Dr. Marco Schoen

Acknowledgments

First and foremost, I would like to thank my precious wife, Kari Oldham for her support, encouragement and endless unwavering love during my academic studies which provided me with the bedrock upon which I could rise. Because of you, I gained so much drive and determination to overcome any challenge in my life.

Personally, I would like to thank my advisor Dr. Arya Ebrahimpour for his patience, motivation, immense knowledge and continuous support throughout my study and research. I could not have imagined having a better advisor than him.

To my children, Keegan and Hailie, thank you for your understanding and encouragement in my many, many moments of crisis. I hope that my experience and education show through hard work and dedication, you can accomplish anything.

Table of Contents

List of Figures

List of Tables

FINITE ELEMENT MODELING OF FIELD-CAST BRIDGE CONNECTIONS

Thesis Abstract – Idaho State University (2020)

Ultra-High Performance Concrete (UHPC) is typically used as connection between precast bridge girders in Accelerated Bridge Construction (ABC). An alternative low-cost mix design using polypropylene fiber-reinforced High-Early Strength (HES) concrete was proposed by the Idaho Transportation Department (ITD). In this thesis, finite element models using Abaqus bending tests of beams representing a 1-foot strip of the bridge deck were developed for a performance comparison between UHPC and HES. The "concrete damaged plasticity" material model was used for concrete and cohesive surface interaction represented the interface bond showed good results in representing the interface between the closure pour and precast concrete. The finite element models were able to produce results similar to the experimental results and also show that HES provides a comparable replacement for UHPC.

Keywords: Abaqus, UHPC, HES, closure pour, finite element modeling

Nomenclature

Abaqus/CAE – Software application also known as Abaqus used for both the modeling and analysis of mechanical components using finite element analysis. Complete Abaqus Environment (CAE)

Accelerated Bridge Construction (ABC) – Bridge construction method using precast deck elements to reduce costs and construction time.

ASTM International (ASTM) – An international standards organization that develops and publishes voluntary consensus technical standards for a wide range of materials. Formerly, American Society for Testing and Materials.

Axisymmetric Model – A two-dimensional model in which the geometry, loadings, and boundary conditions are symmetric with respect to an axis. The model represents a three-dimensional shape with the simplification benefits of a two-dimensional analysis.

Bond-Slip – Interaction relationship of the bond between the reinforcing bar and concrete can slip longitudinally in a reinforced concrete member under flexural loading.

Clear Cover – The distance from outer surface of concrete member to the outer surface of reinforcment steel.

Concrete – Mixture of Portland cement or any other hydraulic cement, fine aggregate, coarse aggregate, and water, with or without admixtures.

Concrete, Normal Weight – Normal weight concrete typically has a density (unit weight) between 135 and 160 lb/ft^3, and is normally taken as 145 to 150 lb/ft^3.

Concrete Compressive Strength – The ultimate strength of hardened concrete material measured in a uniaxial compressive stress test. This is typically called the 28-day strength.

Development Length – Region of straight rebar that bonds with the concrete.

Edge Distance – Distance from the edge of the concrete to the center line of the reinforcement bar.

Embedment Depth – Distance, parallel with the bar, measured from the head, to a critical section (a point of maximum stress in the bar).

Finite Element Analysis (FEA) – Studying or analyzing a phenomenon with FEM.

Finite Element Method (FEM) – A numerical method for solving problems of engineering and mathematical physics.

Headed Reinforcement Bar (Headed Rebar) – Rebar with a head attached to the end as an alternate method of terminating rebar in concrete structures. It will typically replace laps, hooks, and bends to reduce congestion around structure joint areas.

High-Early Strength (HES) – Concrete that has a higher early strength and allows for forms to be removed after a shorter time than the normal concrete. ITD typically specifies removing the forms after one day.

Idaho Transportation Department (ITD) – The State of Idaho governmental organization responsible for state transportation infrastructure.

Modulus of Elasticity – Ratio of normal stress to corresponding strain for tensile or compressive stresses below proportional limit of material.

Normal Weight Concrete (NWC) – Concrete that has a weight of approximately 150 lb/ft^3

Plain Concrete – Structural concrete with no reinforcement or with less reinforcement than the minimum amount specified for reinforced concrete.

Rebar – Steel used in combination with concrete to aid in compressive and tensile strength of the material.

Ultra-High Performance Concrete (UHPC) – Concrete that is a high-strength by providing compressive strengths of 17-22 ksi (120-150 MPa).

CHAPTER 1 INTRODUCTION

1.1 – Background and Motivation

The infrastructure in the United States needs upgrades and bridges are no exception. The United States has over 600,000 bridges which support the millions of vehicles that travel over them each day. According to the Federal Highway Administration (2018), every one in nine bridges is structurally deficient or outdated. These numbers do not even include new bridge construction required for the growing population. The cost for bridge construction is extremely high. And the indirect cost of traffic delays and congestion during construction is even higher.

Bridge designers are constantly looking for methods to reduce bridge construction costs and accelerate the bridge construction. Accelerated Bridge Construction (ABC) is one such method that reduces traditional construction time of bridges and thus a reduction in traffic impact and overall cost. Additionally, ABC can produce a safe and reliable bridge (Culmo, 2011).

ABC accelerates bridge construction by fabricating a number of bridge components off site. These pre-fabricated components are produced months in advance of the actual bridge construction and delivered to the construction site. The bridge construction then commences by assembling all of the pre-fabricated components rather than building them in place. The time savings in ABC is due to the fact that the load bearing concrete components are set in place and can immediately carry a load versus the traditional construction where forms stay in place until the concrete is sufficiently cured.

One method of ABC construction typically uses deck bulb-T girders which are precast beams that span the bridge. The deck bulb-T girders are set in place and joined together with a final substructure concrete pour known as the closure pour. Figure 1.1 illustrates the typical components of a deck bulb-T and a closure pour with three closure pours shown. Closure pours are typically cast with Ultra-High Performance Concrete (UHPC) and high-strength grout.

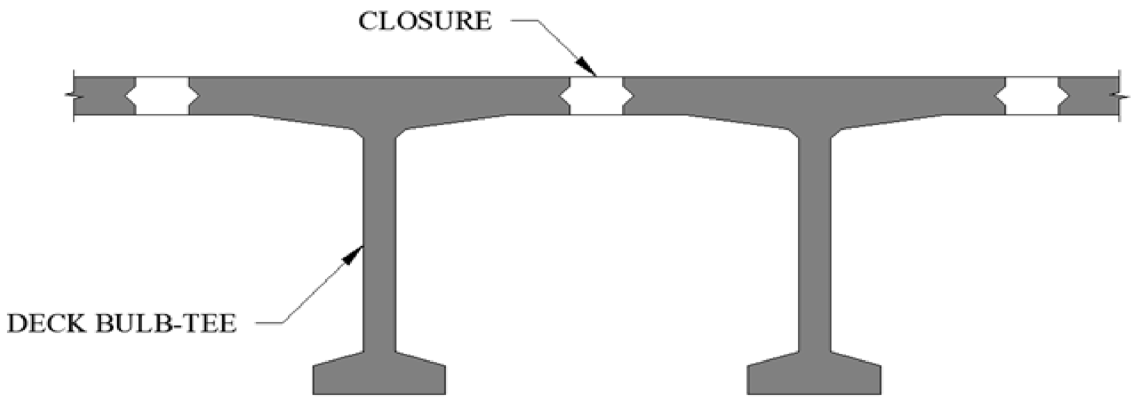

Figure 1.1 ABC Cross Section of Components (Casanova 2018)

1.2 – Problem Statement and Scope

The behavior of ABC joints can be tested in laboratories. The complexity of these large joints can create unknown stress phenomena that is difficult and expensive to test. This is due to the specialized laboratories needed, large testing equipment, and large amounts of technician labor time to perform experiments. Thus, laboratory testing is limited in the number of variables that can be evaluated.

Finite element analysis of composite materials is a useful tool to evaluate the structural performance of large structures and provides a method to evaluate without full-scale testing. Developments in finite element software makes it possible to analyze structures that have different nonlinear materials and different geometries. ABC closure pour joints are a good perfect example of a complex composite because of the different concrete materials and complex reinforcement bars in the connection.

To analyze the response of numerous variables of a closure pour joint, a 3-dimensional finite element analysis must be performed. A successful finite element analysis is validated by comparison to experimental data from several different sources of testing. Finite element modeling has a unique advantage in explaining reasons behind failure in composite concrete joints. The analysis can look inside the material and describe areas of high stress and high strain where it is difficult to instrument in experimentation. The Idaho Transportation Department (ITD) and Idaho State University study on ABC joints is one area where finite element modeling is applicable.

ITD bridges are currently using UHPC or high strength grout as a closure pour material along with headed rebar in ABC projects because of its high-strength properties. UHPC also has some disadvantages that increase time and cost. The material itself is at least 10 times more expensive than the normal concrete. It is a labor-intensive process because the proprietary material must be mixed on site with small portable mixers and then hand poured requiring a large crew. ITD could realize a significant cost savings by using HES concrete with polypropylene fibers because it can be mixed off-site at a local plant and poured using a smaller sized crew. ITD bridge engineers estimate cost savings of HES concrete compared to UHPC can be over $100,000 per project (Casanova, 2018).

The proposed HES concrete possesses lower strength properties than UHPC. Therefore, to evaluate using it as a replacement material, data will need to be obtained to show acceptability. This data can come from physical testing and/or finite element analysis.

1.3 – Objectives

There are many structural analysis software options available to use. These programs are excellent in analyzing large structures from a macro-level modeling perspective. However, they are limited in analyzing complex composite joints such as an ABC closure pour. These programs use simplified finite beam elements to represent objects. This project will develop a three-dimensional nonlinear finite element model using the software Abaqus. The finite element model will evaluate the use of Normal Weight Concrete (NWC) closure pour joint versus a UHPC closure pour joint. The bridge engineer could then use this modeling approach to refine the connection detail and change the geometry and even use a different material.

CHAPTER 2 LITERATURE REVIEW OF PHYSICAL TESTING

This chapter presents a summary of a literature review in the subject of headed rebar in concrete and recent experimental work done at Idaho State University on the behavior of HES concrete with Polypropylene fibers. This chapter is divided into five main sections; development length, hooks/bended ends, headed reinforcement, headed reinforcement physical testing, a summary of experimental work on HES concrete with Polypropylene fibers conducted at Idaho State University, and finite element analysis of reinforced concrete.

Reinforcement bar is used in concrete to enhance the materials behavior in tension. One purpose of rebar is to provide tensile strength in a concrete beam that is subjected to bending stress. The maximum bending stress is typically greatest in the middle of the beam. The rebar must remain fixed in the ends of the beam to ensure that it stays in tension and transfers the tension forces to the concrete. The provided area of reinforcement is not fully effective unless it is fully developed. The fundamental requirement for development of reinforcing bars is that a reinforcing bar must be embedded in concrete enough distance on each side of the critical section to anchor the bar at the section. The reinforcement may also be developed by embedment length, hooks, mechanical anchorage devices, headed deformed reinforcement, or a combination of these methods.

Finite element analysis is a numerical method for solving engineering problems. It is used to find solutions to problems which have complex geometry and non-linear material properties. Analytical solving methods for this type of problem is difficult or impossible to solve because of their complex nature. The numerical method calculates approximate values at a number of points (nodes) that are connected to form a complete solution of the whole body (Logan, 2012).

2.1 – Development Length

Development length is the region of straight rebar that bonds with the concrete. The length must be long enough to anchor the steel with enough strength to match the yield stress of the rebar plus some additional stress due to strain hardening effects. This will ensure that the rebar can yield and achieves its ultimate strength before pullout. The mechanical bond is created through multiple mechanisms. First, is the cohesion of the concrete with the steel surface. Second, is the griping force due to concrete shrinkage. And third is the mechanical interlock of the rib features on the rebar as shown in Figure 2.1. Where the forces on the reinforcing bar are shown in Figure 2.1(a), and the forces on the concrete are shown in Figure 2.1(b).

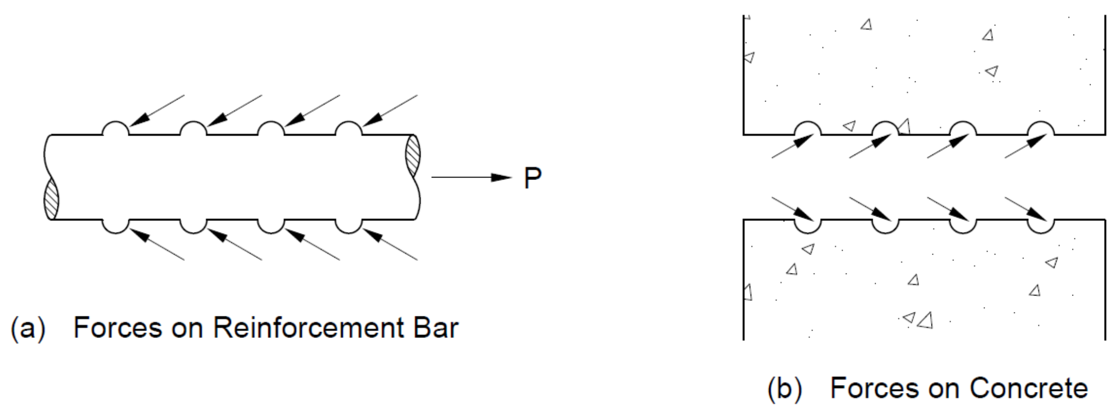

Figure 2.1 Mechanical Interlock of Reinforcement Bar with Concrete

Development length requires a fairly large length to create a sufficient amount of bond to anchor against tension caused by beam flexure and tension. The length of bond that is required to resist the tension created by flexure is called fully developed length. The American Concrete Institute's ACI 318 defines development length in Equation (2.1) (Nawy, E.G.).

$$\frac{l_b}{d_b} = \frac{3 f_y \psi_t \psi_e \psi_s}{40\sqrt{f'_c}\left(\frac{c_b + K_{tr}}{d_b}\right)} \tag{2.1}$$

Where, l_d is development length, d_b is bar diameter in inches, f'_c is the concrete compressive strength in psi, f_y is steel yield strength in psi, c_b is bar spacing factor, K_{tr} is transverse reinforcement index, ψ_t is the bar location factor, ψ_e is the coating factor, and ψ_c is the bar size factor. This equation is an empirical equation that factors to account for the bearing forces and concrete grip. Each modifying multiplier has elaborate rules for use in the ACI 318 code to make the equation include all the factors that create the concrete-rebar bond.

2.2.1 – Physical Testing of Pull-Out Strength of Rebar in Concrete

A physical test of the pull-out strength of rebar in concrete was performed by Rao G.A., et. al., 2007. The purpose of the testing was to understand the bond stress-slip response behavior between ribbed rebar and concrete. The response is linear at first where the load is transferred between the two members. But as the load increases, localized bond failure emerges. As the bond fails the concrete increasingly slips impacting the rebar's anchorage capacity.

As shown in Figure 2.2, the specimen used in work by Rao, et al. consisted of a 150 mm x 150 mm x 150 mm (5.9 inch) cube of concrete with a 16 mm (5/8 inch) diameter rebar embedded coaxially in the middle rebar protruded from the concrete 750 mm (30 inch) for pulling. Slip was measured by the bar displacement at the top of the concrete block.

Figure 2.2 Pullout Specimen Block (Rao 2007)

The specimen was hanged in a frame to pull the rebar. A steel plate of size 150 x 150 x 12mm thick (5.9 inch x 5.9 inch x 0.5 inch) with a central opening of 100 x 100 (4.0 inch x 4.0 inch) was placed on the concrete to counter the pull force. This opening allows for a free failure of concrete due to pullout.

The bond stress (τ) was calculated as the pull load was applied using Equation (2.2).

$$\tau = \frac{P}{\pi l_b d_b} \tag{2.2}$$

Where $P = pullout\ force$, $l_b = bar\ embdement\ length$, and $d_b = rebar\ diameter$. Figure 2.3 shows the bond stress versus the slip in three specimens. The specimen that is noteworthy is the “Unconfined” using 40 MPa (5800 psi) concrete compressive strength because it isolates the bond behavior without confinement.

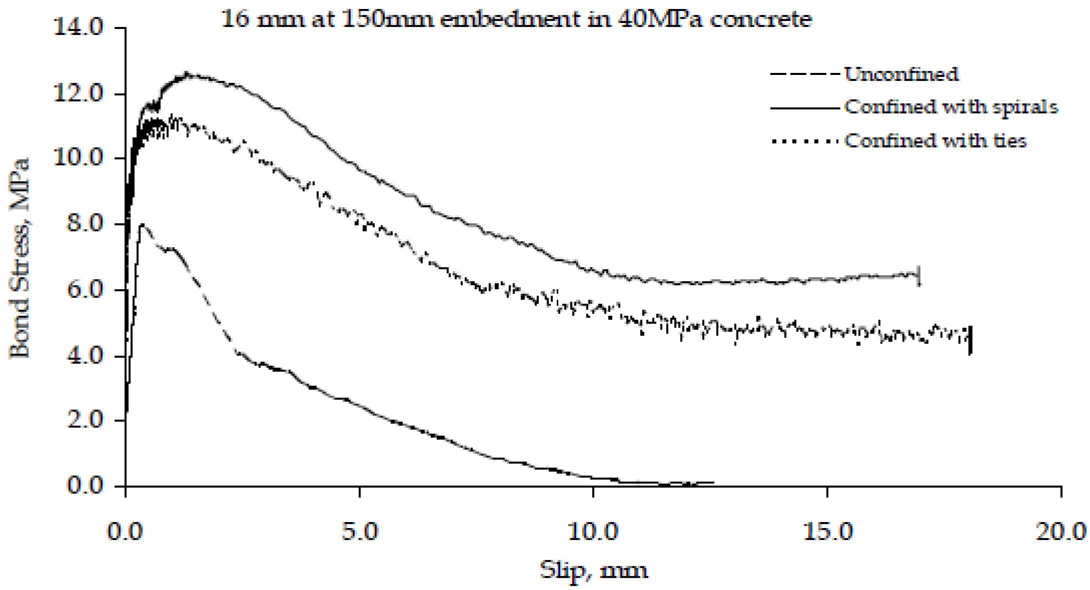

Figure 2.3 Bond Stress vs. Slip (Rao 2007)

The bond stress-slip behavior is linear until an ultimate limit is reached. At this point concrete crushing/cracking begins and rebar slipping ensues. The bond stress is greatly reduced as well. This is not completely accurate method of measurement because in all reality the bond length is also becoming smaller. There is no method for measuring this loss of bond area and so it is assumed to be constant. If this was measured, the resultant graph would remain horizontal after the ultimate anchorage strength peak.

2.2 – Bends/Hooks

When sufficient development length is not available for tensile reinforcing bars, 90° bends or a 180° hooks may be used as shown in Figure 2.4.

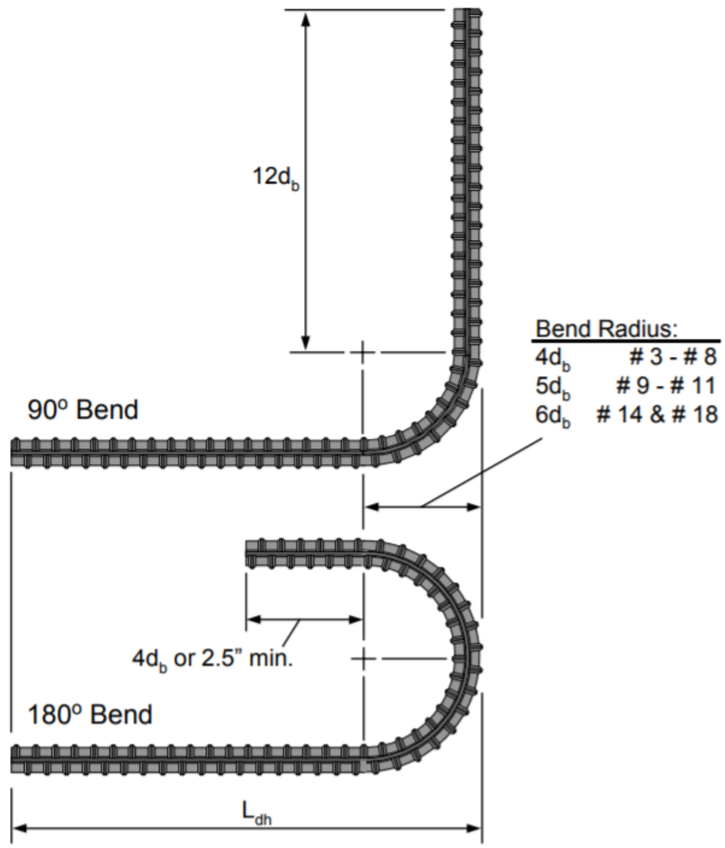

Figure 2.4 Bend and Hook Dimensions (Thompson 2000)

Bends and hooks provide adequate tension anchorage in a much smaller confined space than the standard straight development length. This is done with a combination of development length and direct bearing of the bend or hook with the concrete.

The ACI 318 code specifies the development length as the minimum dimensions shown in Figure 2.4 and in Equation (2.3).

$$l_{dh} = \frac{38 d_b f_y}{60\sqrt{f_c'}} \tag{2.3}$$

Where, l_{dh}=development length, d_b=bar diameter, f_c'= concrete compressive strength in psi, and it is assumed that the steel yield strength is 60 ksi.

There are less modification factors to the bend and hook equation than the straight development length equation because most of the anchorage is provided from the direct bearing from the steel to the concrete rather than from the mechanical bond. However, bends and hooks can cause rebar congestion in the ends of beams and when connecting precast elements.

2.3 Headed Reinforcement Bar

Headed reinforcing bars are used in construction in recent years. Headed bars are becoming a more popular way of terminating reinforcing bar because they can be used in very confined spaces such as bridge deck connections. Headed bars require significantly less space than the bend/hook anchors because a long development length or large bar radii are not required. Headed reinforcement requires less complicated joints and thus faster construction.

Heads are either round, square, or rectangular in shape. Heads are attached to the end of the rebar by a number of joining methods as shown in Figure 2.5.

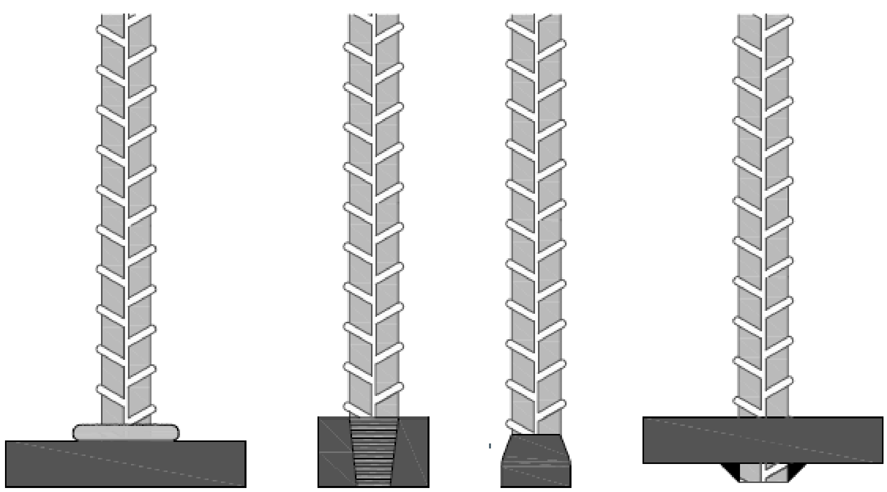

Figure 2.5 Mechanical Anchor Types. From left to right: Friction-Welding, Threaded Connection, Forging, Traditional Weld (Marchetto 2015)

The pictures of the threaded heads and welded heads are shown in Figure 2.6 and Figure 2.7, respectively. The threaded heads have a conical thread for a better transmission of forces. The threaded type allows for easy assembly in the field. Welded heads require very little manufacturing but require more work to be done in the field and not ideal for quick construction (Marchetto 2015).

Figure 2.6 Round/Threaded Reinforcement Bars (ERICO Lenton Terminator 2017)

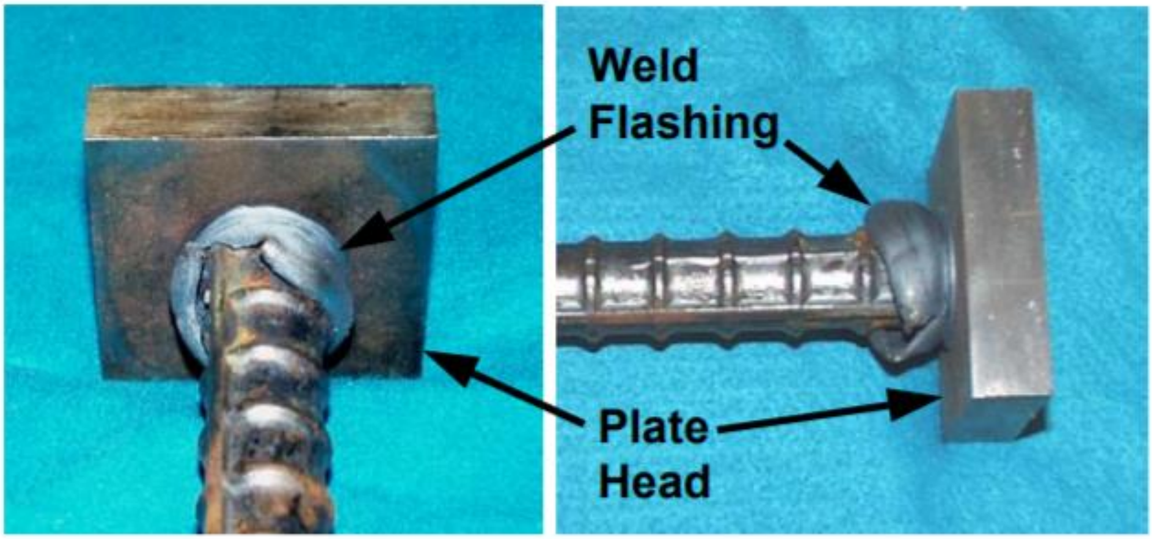

Figure 2.7 Square/Welded Headed Reinforcement (Thompson 2000.)

Headed bars are straight development length bars with a head that is attached to the end. The headed anchor performs similarly to the hook/bend joint where the straight section is bonded with the concrete and the head provides a bearing surface. The forces of a headed anchor are shown in Figure 2.8. The forces are the mechanical grip of the rebar/head along the shaft and the bearing forces provided from the head itself. The bearing forces are similar to the forces that the bend and hook provide.

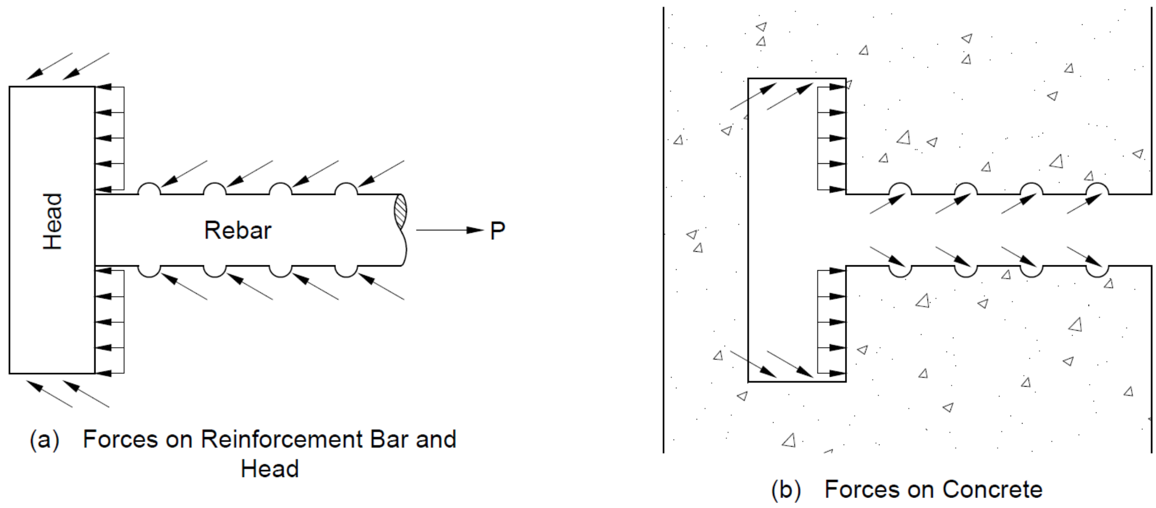

Figure 2.8 Forces on Headed Rebar and Concrete

2.4 Research and Testing of Headed Reinforcement Bar

Many studies have been performed on headed reinforcement bar. The initial work was done by three Ph.D. students from the University of Texas at Austin. The three students, DeVries in 1996, Bashanday in 1996, and Thompson in 2002 each studied and tested headed reinforcement. DeVries' focus was on pullout tests of headed rebar to determine the ratio of embedment depth and clear cover. This ratio is the head depth in the concrete vs. the distance from the edge of concrete to the reinforcement bar. His research was aimed at producing equations that could predict the strength of headed rebar. Bashanday's focus was to add to DeVries' research where studies and testing was done on plate-anchored bars as shear reinforcement, cyclic loading, and exterior beam-column joints with headed rebar. Thompson's work also continued on DeVries' research. With the focus being on testing headed rebar in beam-columns and refining DeVries' design equations. The work of these students has resulted largely in the data and empirical equations used today in designing headed rebar (Marchetto 2015).

More recently, research was done on headed rebar applications in bridge design. The experimental testing was performed by Casanova in 2018 on the behavior of headed rebar with high-early strength concrete.

2.4.1 Experimental Work by DeVries

This study was done to provide design recommendations for using headed reinforcement bar in concrete. The goal was to establish empirical equations that could be used to predict the behavior of headed reinforcement. The test consisted of two main categories, pullout-cone capacity of headed reinforcement and blowout capacity of headed reinforcement. Each category varied parameters such as embedment depth, bond length, and edge location, Figure 2.11 and Figure 2.12.

The ultimate pullout capacity is defined when a complete failure where a cone of concrete and reinforcement bar completely detach from the base component. The pullout cone is defined where a failure cone of concrete appears around headed reinforcement fails as one unit. It represents the maximum strength of the headed reinforcement. A simple figure of a pullout-cone is shown in Figure 2.9. The pullout-cone test were done with low ratios of embedment depth to edge distance also known as clear cover. This is done to ensure that the strength of the assembly is lower than the strength of the reinforcement so that the failure is witnessed in the concrete. The critical variables of these tests are embedment depth, bar bond length, concrete strength, edge distance, and perimeter of the head.

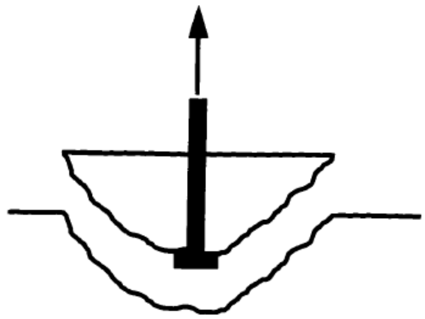

Figure 2.9 Pullout-Cone Failure (DeVries 1996)

Blowout of headed reinforcement is where spalling of the cover concrete happens and subsequently a complete failure of the anchor. Blowouts can happen perpendicular to the bar as depicted in Figure 2.10 where the anchor is not near an edge. Side-blowout happens with a high ratio of embedment depth to edge distance. These tests were done as deep-embedment tests to test side-blowout failures. Some of the critical variables of this test were edge distance, clear cover, concrete strength, and net bearing area on the head. Edge Distance is the distance from the edge to the center line of the reinforcement bar and clear cover is the distance from the edge to the surface of the reinforcement bar.

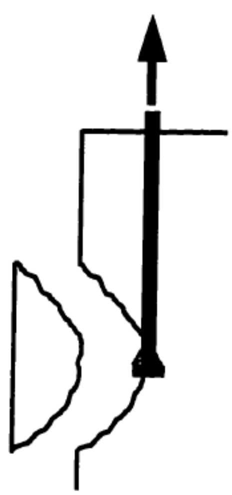

Figure 2.10 Side-Blowout Failure (DeVries 1996)

It is also worth noting two definitions of the critical variables, embedment depth and bonded length. Embedment depth is the total distance from the top surface of the concrete to the top of the head on the reinforcement. Embedment depth is noted as h_d and is shown in Figure 2.11.

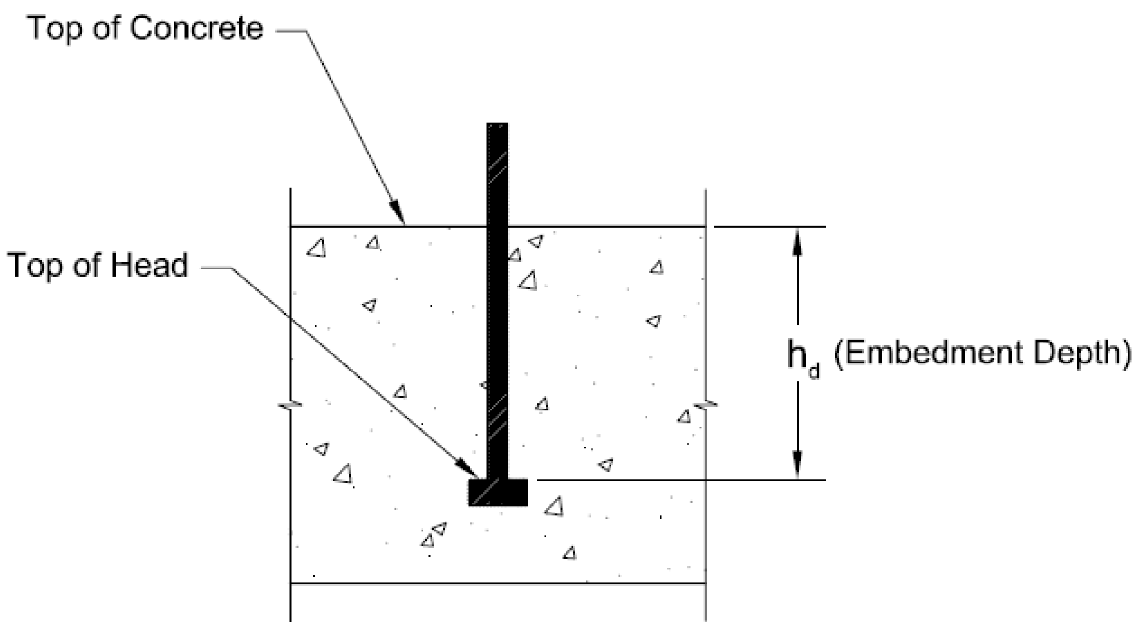

Figure 2.11 Embedment Depth

Bonded length is the length along the reinforcement bar that is bonded to the concrete from the head to the top of the concrete. DeVries provides this example "If a smooth reinforcing bar or bolt is attached to a head, then the bond length is zero." The development length is usually the same as the embedment depth. However, for the purpose of evaluating the impact of critical variables, many of the tests were performed by varying the bonded length or eliminating it entirely. DeVries controlled the bonded length by placing a PVC pipe around the reinforcement bar. The PVC was sealed with silicon caulk so that no concrete could come into contact with the reinforcement bar and creating a bond. Bonded length is noted as l_b and is shown in Figure 2.12.

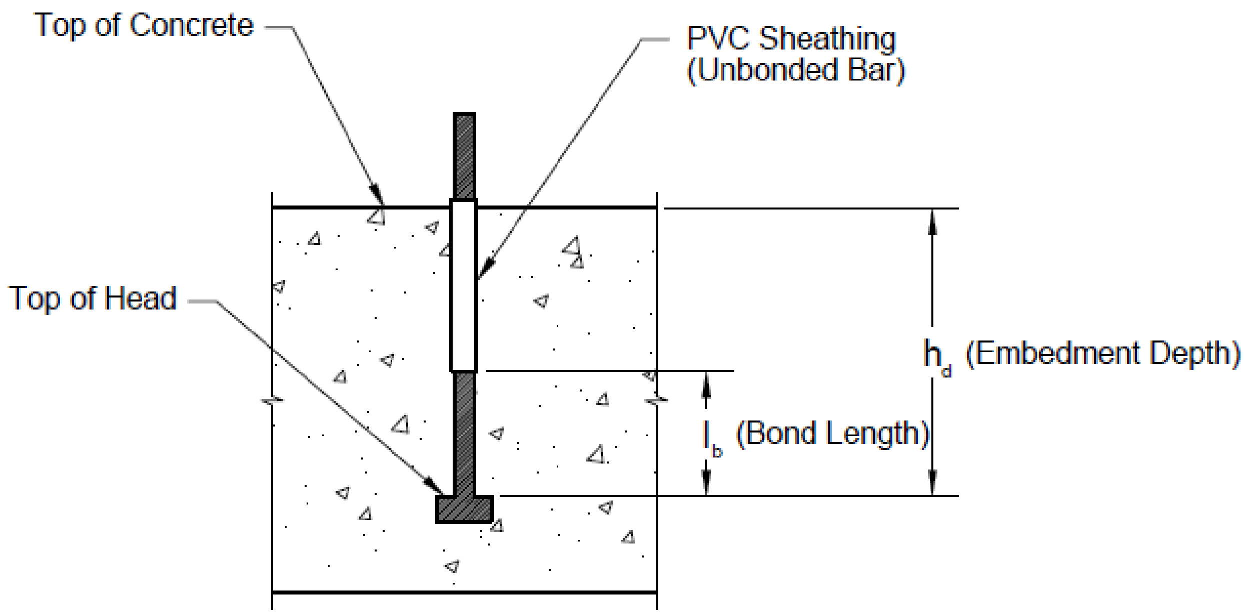

Figure 2.12 Comparison of Embedment Depth vs. Bond Length

2.4.1.1 DeVries Test Setup

The test setup for the pullout cone / shallow-embedment test is shown in Figure 2.13. The test specimens (headed bars) were cast in rows in a large concrete block 9.5’ x 5’ x 21” deep. The bars were spaced far enough apart to ensure that each individual specimen failure cone would not impact the adjacent specimen failure cone. The shallow-embedment specimens were setup with an embedment depth to clear cover of less than five. The shallow embedment reduced the confining of the concrete to allow for the anchorage strength measurement to be pure without being affected by confined concrete. The test was setup so that the anchorage was pulled in tension with the concrete block with the counter force applied at least $2h_d$ away from the loading zone. This was done to allow for the failure cone to present itself without interference from the loading fixture.

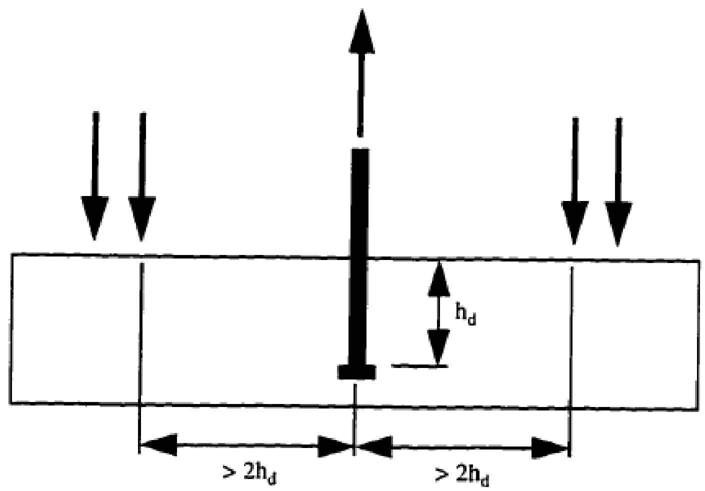

Figure 2.13 Test Setup for Pullout Cone Capacity Test (DeVries 1996)

The test setup for the side blowout tests are shown in Figure 2.14. Embedment depth to clear cover ratios greater than five were used. Because of the deep embedment specimen tests, the confinement had little impact on the anchorage strength. Therefore, the loading ram could be placed directly on the concrete block above the pullout bar.

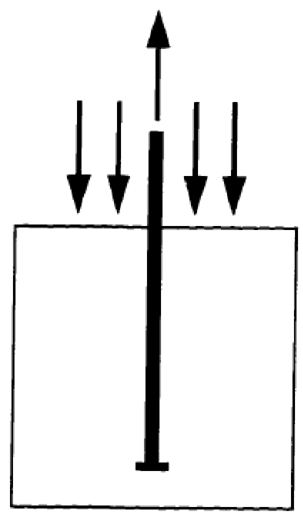

Figure 2.14 Test Setup of Side Blowout Test (DeVries 1996)

The DeVries tests used nominal yield strength of 496 MPa (72 ksi) steel reinforcing bars. Three different bar sizes were used #6, #8, and #11 for testing. Several different sizes of square and rectangular heads were used with a nominal yield strength of 496 MPa (72 ksi). Five different types of concrete were used with compressive strengths ranging from 27 MPa to 83 MPa (3,000 psi to 10,000 psi). The design parameters are listed in Table 2.1. These are standard mix designs. The purpose for varying the concrete strengths was to verify that anchorage strength did indeed increase as the compressive concrete strength increased. The parameters in this table are $d_b = bar\ diameter$, $C_1 = edge\ distance$[1] 1, $C_2 = edge\ distance\ 2$, $h_d =$

[1] Edge distance C_1 is defined as the distance from the edge of the concrete to the center line of the reinforcement bar. C_2 is the same only it is measured perpendicular to C_1.

$head\ depth$, $l_b = bond\ length$, $f'_C = 28 - day\ compressive\ strength$, $P_U =$

$ultimate\ pullout\ capacity$.

2.4.1.2 DeVries Results

The results of DeVries testing are shown in the Table 2.1. The table lists the critical variables – bar diameter, head size, anchorage edge distance, head depth, usage of transvers reinforcement, and concrete compressive strength – as well as listing the ultimate load at failure and failure mode.

Table 2.1 DeVries Test Results (DeVries 1996)

Test ID	d_b, mm	Nominal head, mm	C_1, mm	C_2, mm	h_d, mm	l_b, mm	Transverse reinforcement	f'_C, MPa	P_U, kN	Failure Mode
T1B1	20	50 × 50 × 12	457	457	36	0	None	83	77	Pullout
T1B2	20	70 × 35 × 16	457	457	36	0	None	83	62	Pullout
T1B3	20	50 × 50 × 12	457	457	113	0	None	83	205	Bar fracture
T1B4	20	70 × 35 × 16	457	457	113	0	None	83	208	Bar fracture
T1B5	35	90 × 90 × 20	457	457	80	0	None	83	215	Pullout
T1B6	35	100 × 55 × 25	457	457	80	0	None	83	225	Pullout
T1B7	35	90 × 90 × 20	457	457	209	0	None	83	490	Pullout
T2B1	20	50 × 50 × 12	51	457	229	0	None	33	184	Pullout*
T2B2	20	50 × 50 × 12	51	457	229	229	None	33	148	Pullout
T2B3	20	50 × 50 × 12	51	457	229	0	STE-1	33	160	Pullout
T2B4	20	50 × 50 × 12	51	457	229	229	STE-1	33	172	Pullout*
T2B5	20	50 × 50 × 12	51	51	229	0	None	33	88	Pullout
T2B6	20	50 × 50 × 12	51	51	229	229	None	33	122	Pullout
T2B7	20	50 × 50 × 12	51	51	229	0	STC-1	33	89	Pullout
T2B8	20	50 × 50 × 12	51	51	229	229	STC-1	33	125	Pullout
T3B4	20	50 × 50 × 12	51	457	229	0	None	27	149	Pullout
T3B8	20	50 × 50 × 12	51	51	229	0	None	27	57	Pullout
T3B11	20	50 × 50 × 12	457	457	229	0	None	27	212	Bar fracture

The results shown in Table 2.1 are better shown and compared when placed into a load-displacement response. Responses of three headed bars in terms of load versus displacement of the heads are shown in Figure 2.15. The load is measured as the force pulling on the bar and the displacement is measured from the bottom of the head.

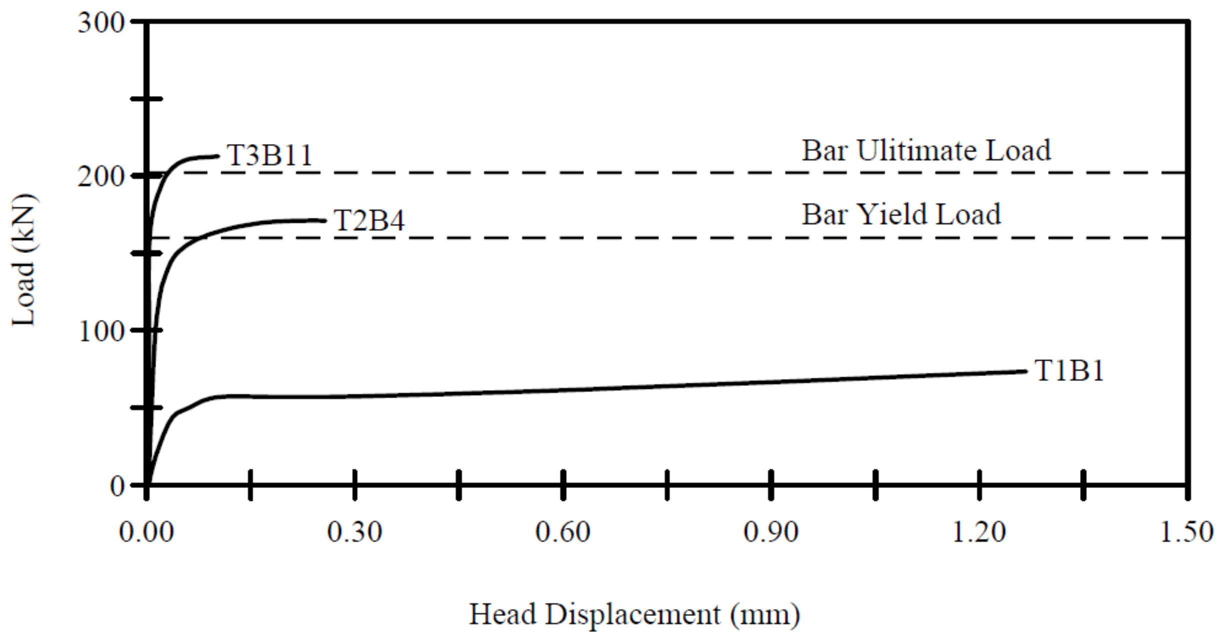

Figure 2.15 Typical Load-Displacement Behavior (DeVries 1996)

The results for force versus displacement of the head of the bar (measured directly below the head) have approximately bilinear behavior. Once the load capacity reaches the ultimate capacity of the anchorage, the curve flattens in an almost horizontal line. Where a small increase in load generates a large increase in head displacement. When the concrete fails, the cone pullout failure happens suddenly, and no cracking was observed before failure.

One aspect of the testing that is of great interest is the impact of embedment depth onto the strength of the anchor. The test numbers that depict this the best are T1B1 and T3B11 as shown above in Figure 2.15. Test number T1B1 uses a 20 mm diameter bar, 50 x 50 x 12 mm thick square head, a large edge distance, a shallow embedment depth of 36 mm, no bond on the rebar, no transverse reinforcement, and 83 MPa (12,000 psi) concrete compressive strength. T3B11 has the exact test parameters except that it is embedded into the concrete much deeper at 229 mm and has a different compressive strength of 27 MPa (3916 psi). The comparison of the two tests is dramatic as T1B1 has large displacements and T3B11 has a much greater capacity- approximately 150 kN (33.7 kip) more - with very little displacement. DeVries conducted many tests with embedment depth while varying anchorage edge distance. The results of varying edge distance are seen on Figure 2.16. In all cases, the capacity increases linearly as head embedment increases. Clearly, head embedment depth has a great impact on anchorage strength.

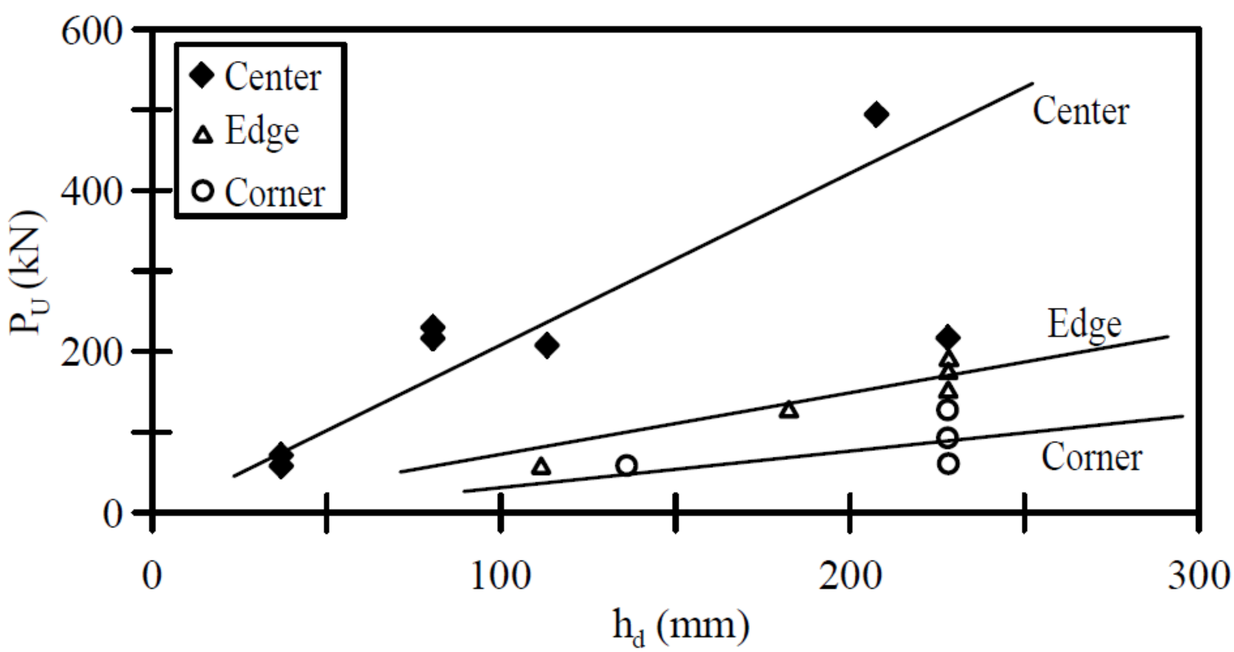

Figure 2.16 Embedment Depth vs Capacity on Varying Edge Distance (DeVries 1996)

Another test variable that DeVries examined is the effect of the bond length on the capacity. The bond length correlates with the area around the bar where the concrete grips the bar providing anchorage strength and adds to the overall anchorage capacity. The total bond strength is dependent on the surface area of the bond. Thus, the longer the bond length, the more anchorage capacity. DeVries varied the bond length in testing of headed rebar. The bond lengths tested were varied from zero mm to 229 mm (0 to 9 inches). The embedment length stayed consistent at 229 mm (9 inches). As expected, the bond length increased the capacity. The results of the typical bond length behavior are shown in Figure 2.17. This figure compares two tests, T2B5 and T2B6, which have the exact same parameters – i.e. embedment of 229 mm (9 inches) and concrete compressive strength of 33 MPa (4786 psi) – with the exception of bond length. T2B5 was covered with the PVC pipe to ensure a slip behavior with the bar and concrete while T2B6 has direct bond between the two materials for the entire length.

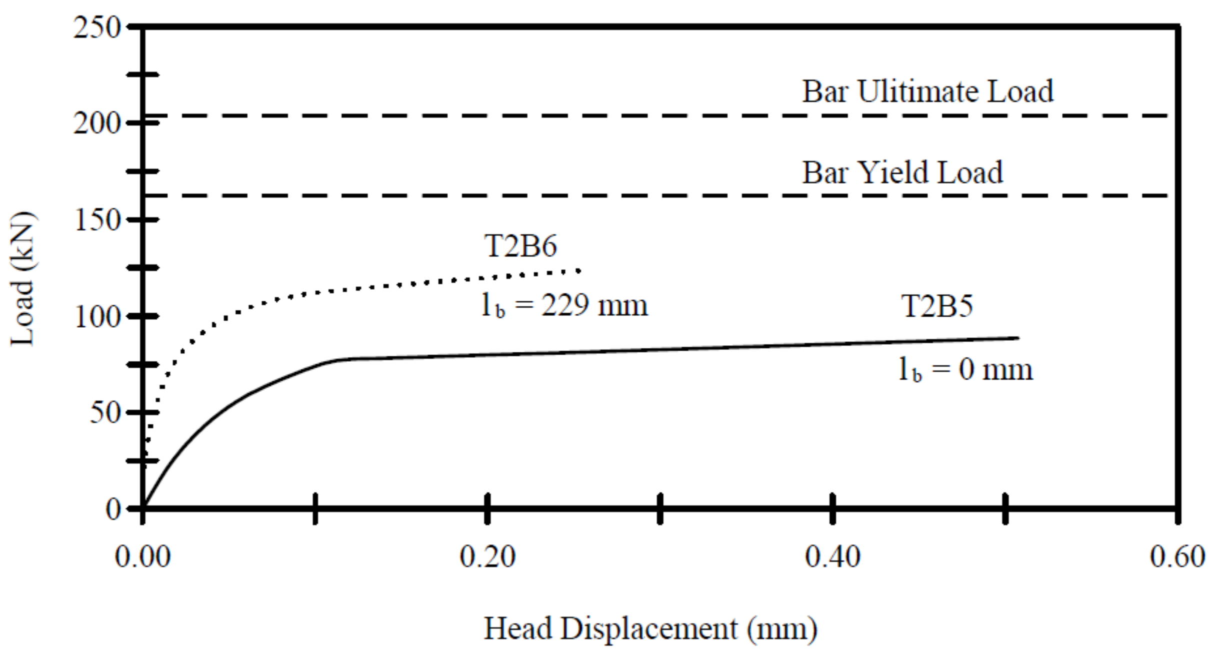

Figure 2.17 Effect of Bond Length on Capacity-Displacement (DeVries 1996)

The results of bond length are very interesting. The difference in anchorage capacity in these two tests show that the bond length can add as much as 30-40 kN (7-9 kips). These results show that bond length does have a noticeable effect on anchorage capacity. It is not as prominent as the embedment depth but it does affect the results.

The rest of the variables - concrete compressive strength, head size, head thickness, transverse reinforcement, and bar size - do not have much of an impact on the anchorage capacity as embedment length and bond length. The effect of these parameters on the anchorage capacity are shown in Table 2.1.

2.4.2 Experimental Work by Casanova

This study was done to provide an alternative connection design to be used in Accelerated Bridge Construction (ABC). ABC methods currently use precast deck elements and join them together using headed rebar and Ultra-High Performance Concrete (UHPC) or high-strength grout as a closure pour. This method is used reduce the cost and time of bridge construction. UHPC has excellent compressive strength of 17-22 ksi (120-150 MPa) but has disadvantages in ABC in certain applications. UHPC is mixed on site using small portable mixers and requires a larger construction crew. This adds to the time and cost of the bridge construction. Additionally, since UHPC is a proprietary material, the material itself is also much more expensive than the High-Early Strength (HES) with Polypropylene fibers concrete preferred by ITD.

The goal of Casanova's research was to study using (HES) concrete in lieu of UHPC as a closure pour in ABC. HES concrete can be mixed and poured in a similar method as conventional concrete. The forms can be removed after 24 hours of curing time. The mix can achieve 3,000 psi in compressive strength in 24 hours. This yields a large cost savings in bridge construction.

Casanova studied six HES concrete mixes to determine the optimum mix. The optimum closure pour mix and another on (selected by the ITD Technical Advisory Committee) were selected to test. This mix was then poured next to a precast element to test the interface bond strength. The mix was then used in a beam specimens with closure pour connecting two precast segments containing headed rebar.

2.4.2.1 Mix Design

Six mix designs were studied to determine the optimum HES mix. The mixes varied polypropylene fiber dosage, shrinkage reducing admixture, and bonding admixture. Each was tested for compressive strength, tensile split strength, and length change. Additional testing was performed on HES-D included modulus of elasticity and Poisson's ratio. The test mix labeled HES-D was determined to be the ideal alternate to UHPC because of its comparable interface bond strength and low shrinkage. It is noteworthy to mention that HES-D had the highest compressive and tensile split strength of the mixes tested. A summary of HES-D versus UHPC material properties is shown in Table 2.2.

Table 2.2 HES-D vs UHPC Material Property Comparison

	HES-D	UHPC[a]	Precast
Compressive Strength (ASTM C39), *psi*	8,864	24,000	5,041
Tensile Strength (ASTM C496), *psi*	837	1,300	600
Interface Bond Strength with Precast Concrete (ASTM C78)[b], *psi*	612	712[c]	-
Shrinkage (ASTM C157), *micro-strain*	522	555	-
Modulus of Elasticity (ASTM 469), *psi*	4,390,000	7,000,000	3,230,000
Poisson's Ratio (ASTM C469)	0.18	-	0.16
Material Cost	$200	$2,000	-

Note: HES-D = High early strength concrete Mix D; UHPC = Ultra High Performance Concrete.

[a]Average values from Table 1 of FHWA Publication No: FHWA-HRT-14-084 (Graybeal, B., 2014).

[b]28-days and precast concrete had exposed aggregate (EA) surface preparation.

[c]Value from De la Varga, Haber, and Graybeal, 2016.

2.4.2.2 Interface Bond Strength Testing

Interface bond test were performed to measure the bond strength between a precast concrete and a closure pour mix per ASTM C78, 2018. The test was set up by casting 9” x 6” x 6” sample of precast concrete which cured for approximately 28 days. Then another pour of HES-D was cast to make the beam 18” x 6” x 6” with the interface bond in the middle. A typical beam specimen and test set-up is shown in Figure 2.18.

(a) Beam Specimen

(b) Alignment marks for support and loading locations

Figure 2.18 Interface Beam Test Set-Up ASTM C78, 2018 (Casanova 2018)

All of the beams failed at the interface joint with a sudden failure. The bond strength was calculated based on the applied load and beam geometry. The average bond strength tested for mix HES-D was 612 psi with a standard deviation of 78 psi. A typical before and after picture of the test is shown Figure 2.19.

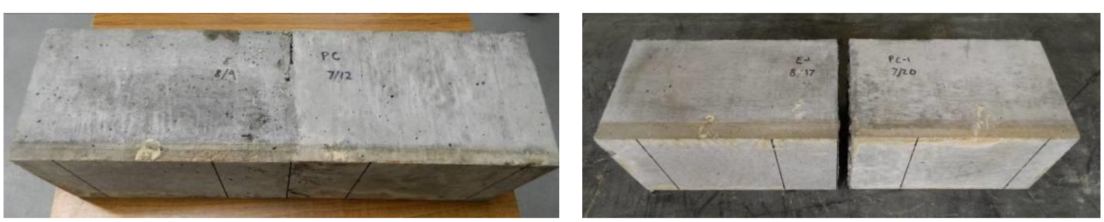

Figure 2.19 Interface Before and After the Test (Casanova 2018)

2.4.2.3 Flexural Large Beam Testing

Casanova concluded his research by testing large beams in flexure. The beams were designed to represent a 1’-0” wide section of bridge deck where two Bulb-T girders are connected. They were tested under three-point and four-point flexural bending. The three-point loading had a loaded area of 20 in. by 10 in. in the middle to represent the footprint of a set of side-by-side tires of a tandem axle truck. The four-point loading was also considered since the middle portion of the beam has a constant bending moment and was assumed to be easier to model in finite element analysis.

Figure 2.20 Typical Three-Point Flexural Beam Test (Casanova 2018)

Sample material used in the test was also collected to obtain the material properties. Average compressive strength, splitting tensile strength, modulus and Poisson’s ratio were tested on the samples. The summary of those material properties are listed in Table 2.3.

Table 2.3 Beam Concrete Material Properties Summary

	Compression strength (psi)	Split tension strength (psi)	Modulus, E (psi)	Poisson's ratio, μ	Age (days)
Closure	8,354	773	4.425×10^6	0.176	28
Precast	4,969	596	3.181×10^6	0.154	119-123

The large beams, shown in Figure 2.21, were created to produce an 8" thick x 12" wide x 72" long beam that includes precast concrete components, rebars, and closure pour. The precast ends were initially poured and cured, each containing two layers of rebar, #5 bars on the upper layer and #5 bars with heads on the lower layer. The precast ends and rebar are shown in Figure 2.22 (a) and (b) staged and ready for the closure pour to join them together.

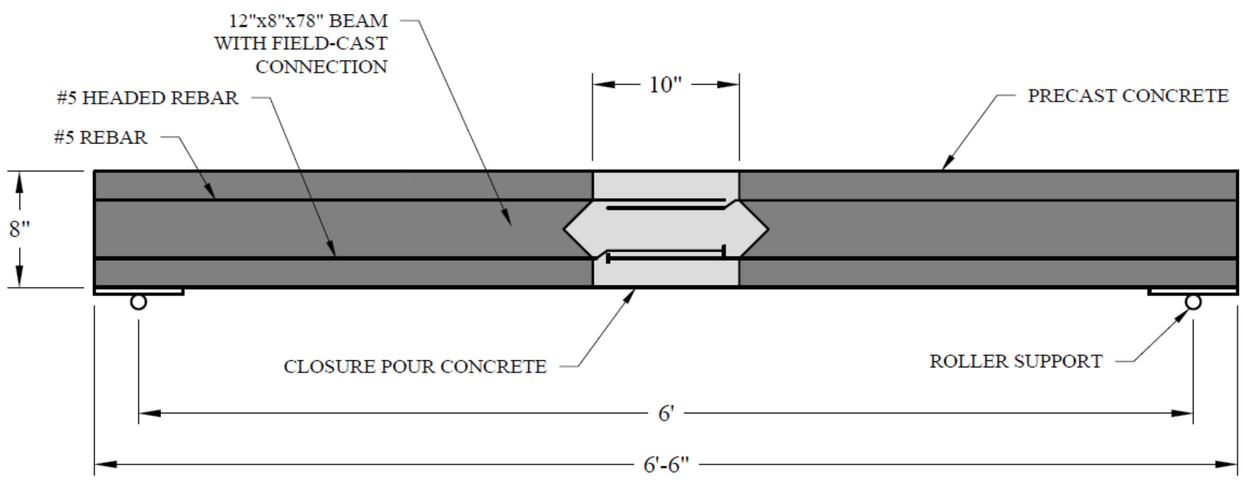

Figure 2.21 Large Beam Components and Dimensions (Casanova 2018)

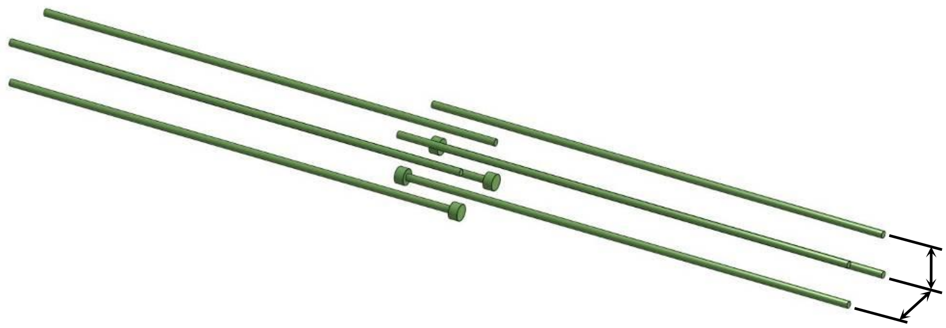

(a) Rebars

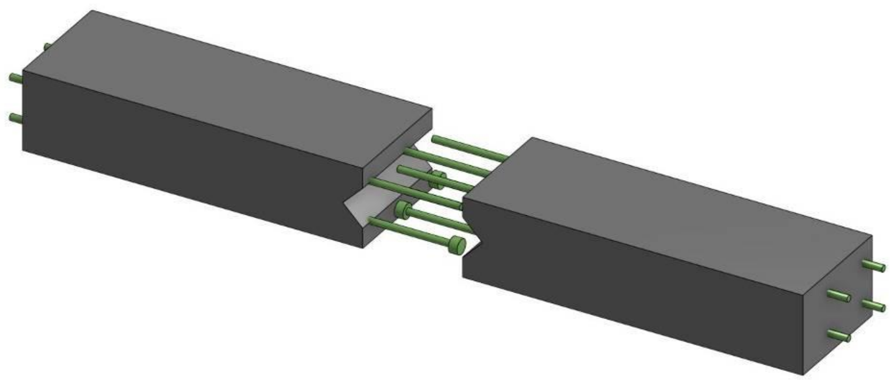

(b) Precast concrete segments cast

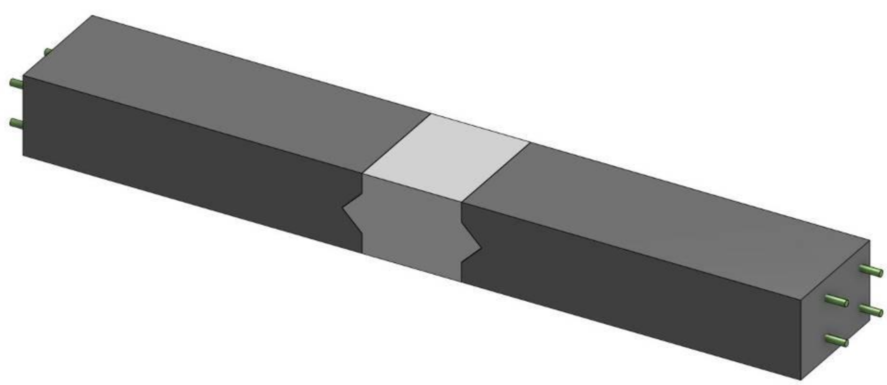

(c) Closure concrete cast

Figure 2.22 Large Beam Assembly Steps (Casanova 2018)

Instrumentation was added in the form of two 0.25 in. long strain gage attached to each of the two headed rebars and strain gages at the bottom of the beam. These gages allow for measurements near the headed rebar as well as the maximum bending point in the beam.

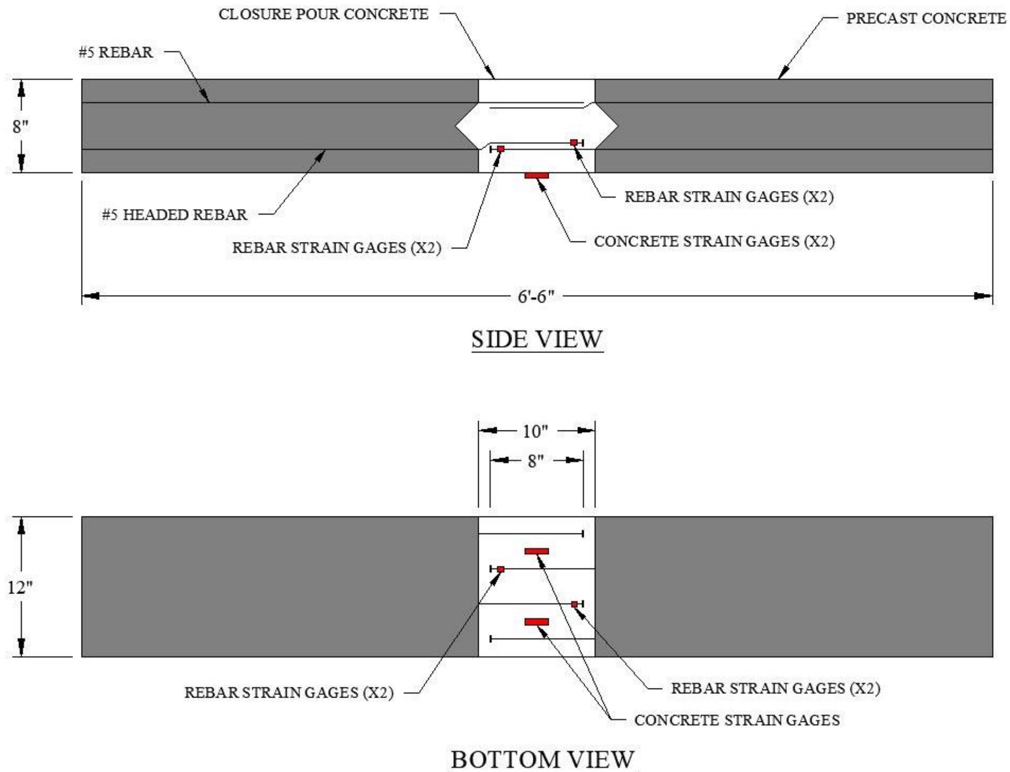

Figure 2.23 Instrumentation Plan for Large Beams (Casanova 2018)

(a) Rebar gauges

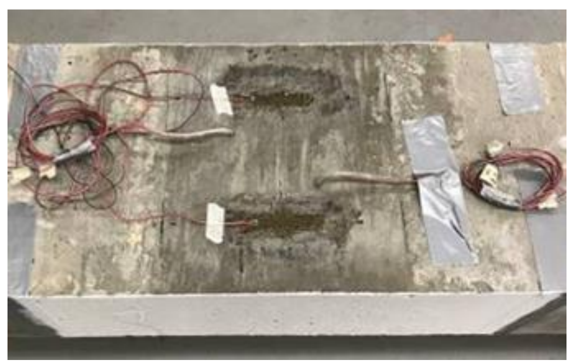

(b) Concrete gauges

Figure 2.24 Large Beam Strain Gauges Installed (Casanova 2018)

The void, see Figure 2.24 (a) between the precast beams was then filled with mix HES-D as the closure pour. The closure pour bonds each precast by bonding with the rebar and the open faces of the precast. The closure pour was allowed to cure for 28 days. Both sides of the beam were painted white with black lined drawing locating the interface surface. The painted surfaces allow for easy identification of crack and the lines at the interface served as references where the cracks initiated; in all cases, the cracks started at the interface.

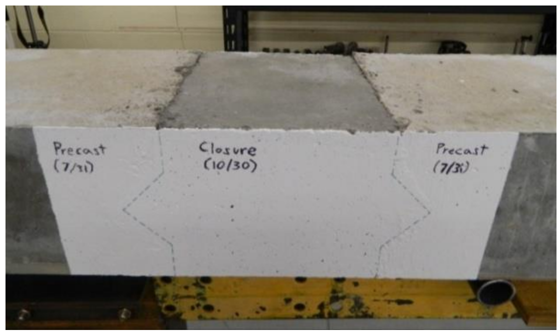

Figure 2.25 Completed Beam Specimen with White Paint (Casanova 2018)

The beam tests were conducted under two styles of loading: three-point loading and four-point loading. The three-point loading setup used a 20” x 10” x 1” thick steel plate to create a distributed load across the closure pour simulating a truck tire footprint. Variances in the beam top surface and the plate created gaps. To reduce the gaps, a rubber mat was placed between the plate and beam for most of the specimens. Details of three-point bending setup are shown on Figure 2.26. A image of the loading fixture is shown in Figure 2.27 with a compression load cell (CLC) measuring the applied force.

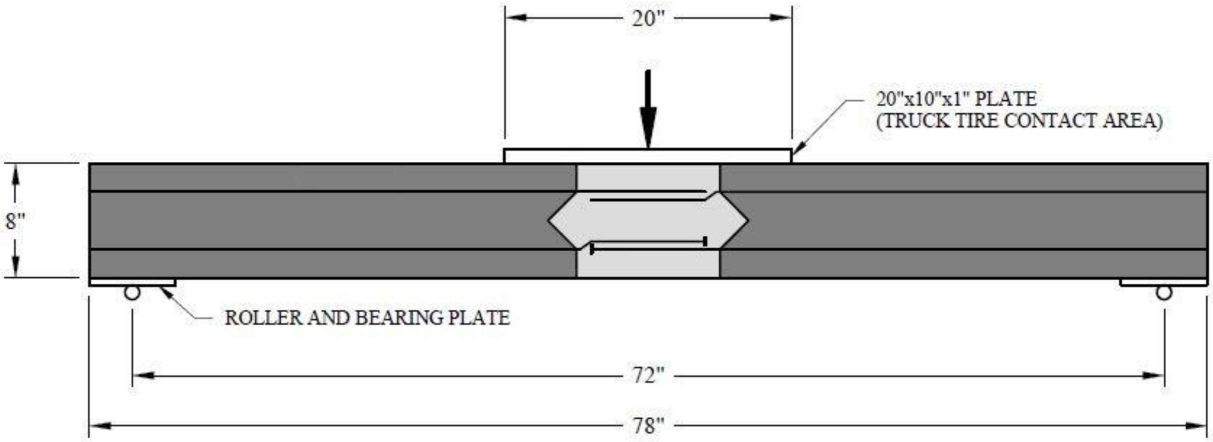

Figure 2.26 Three-Point Flexural Test Diagram (Casanova 2018)

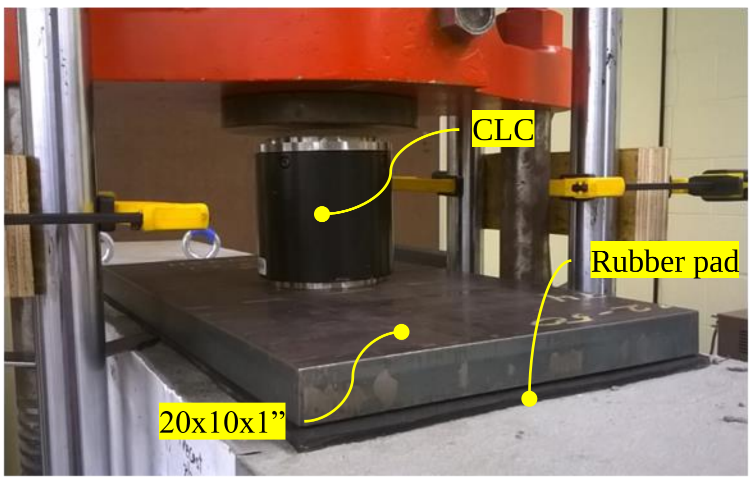

Figure 2.27 Three-Point Loading Set-Up (Casanova 2018)

The four-point loading consisted of top loading the beam in two locations 24” apart. This is far enough apart to span the closure pour and create a constant moment across the area of interest. Details of four-point bending setup are shown on Figure 2.28 and Figure 2.29.

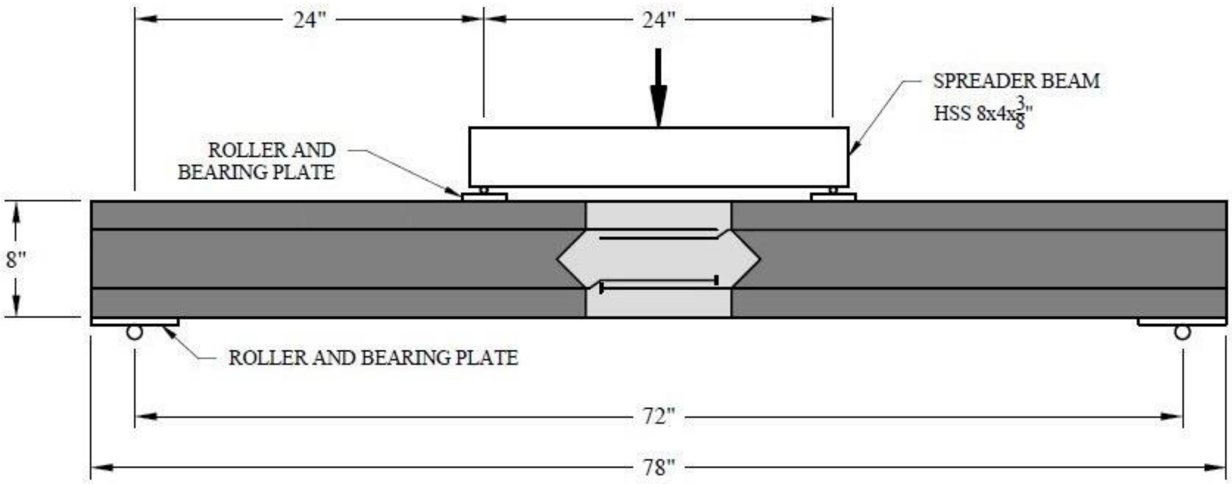

Figure 2.28 Four Point Flexural Test Diagram (Casanova 2018)

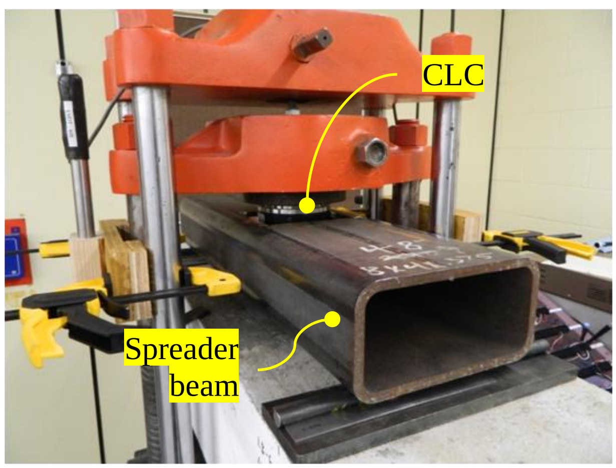

Figure 2.29 Four-Point Loading Setup (Casanova 2018)

The results from the three-point loading specimens were not ideal. This is due to the gaps between the plate and the concrete. The load was also not a perfect distributed load because the steel plate has some elasticity and bends with the specimen.

A force-deflection graph, Figure 2.30, depicts the behavior and ultimate load for each beam specimen. The solid lines represent the beams under three-point loading and the dashed lines for the four-point loading. Average ultimate loads for the three-point was 9,492 lb and for the four-point was 12,209 lb.

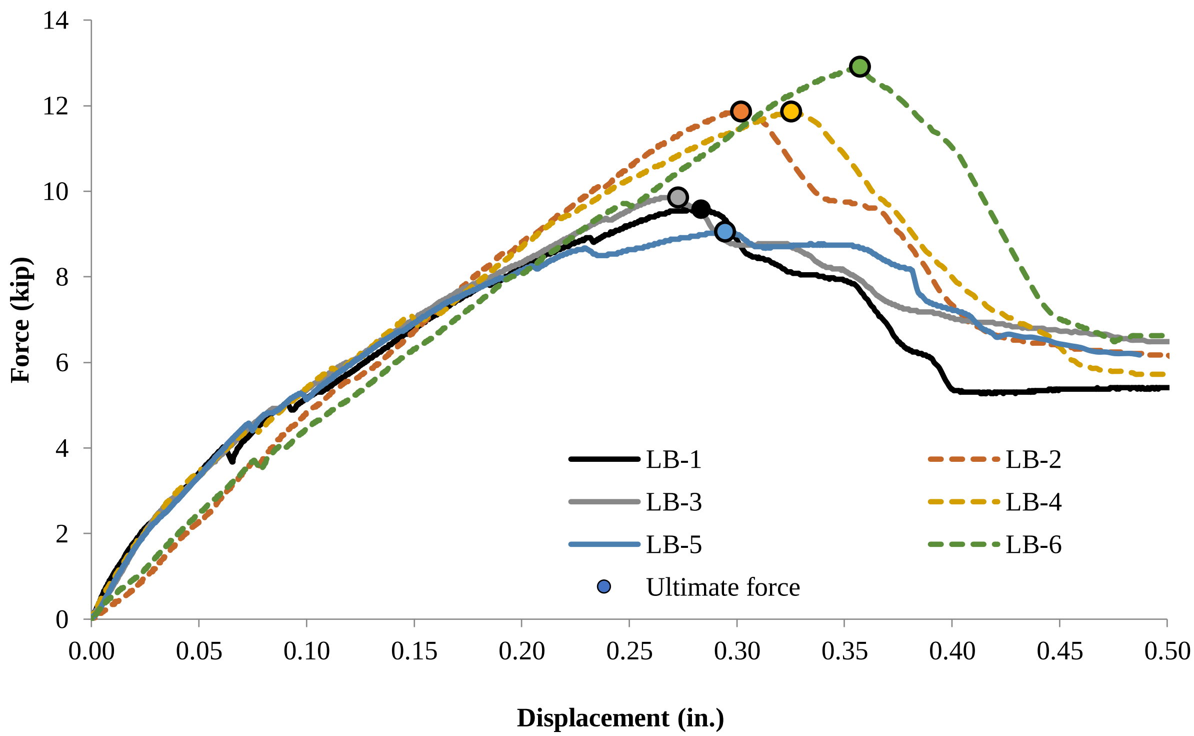

Figure 2.30 Beam Force vs. Deflection (Casanova 2018)

The specimen was observed to crack in four distinct phases. Actual cracks from specimen LB-2 are photographed in Figure 2.31. The first cracks were observed mainly on the interface surfaces during loading up to the ultimate load at an approximate load of 3 kip. All other cracks were observed after the ultimate load and on the failure of the beam. A typical cracking map was produced on the beam specimen LB-2 and shown in order of appearance in Figure 2.32.

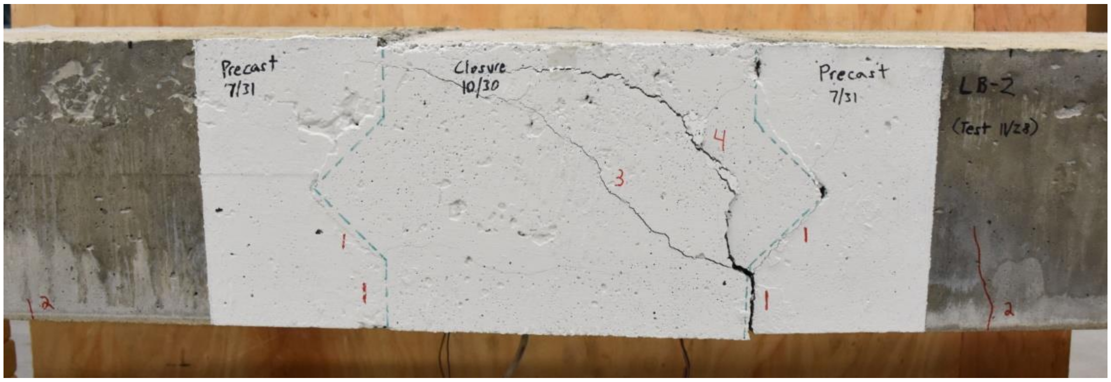

Figure 2.31 Beam Cracking - Specimen LB-2 (Casanova 2018)

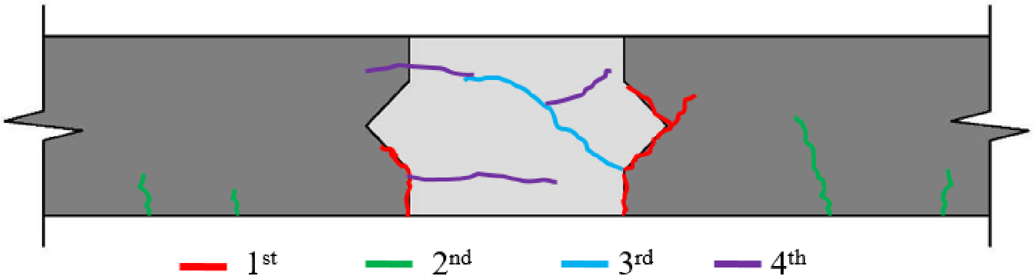

Figure 2.32 Typical Beam Cracking Diagram (Casanova 2018)

Stress near the head of the rebar was plotted with the beam moment, Figure 2.33. The average ultimate moments for three-point and four-point bending were 147.1 kip-in. and 146.5 kip-in., respectively. Again, primary cracking was observed at a moment loading of 35-44 kip-in. It is noteworthy that all the beams performed in a linear fashion for approximately the first 60% of the loading.

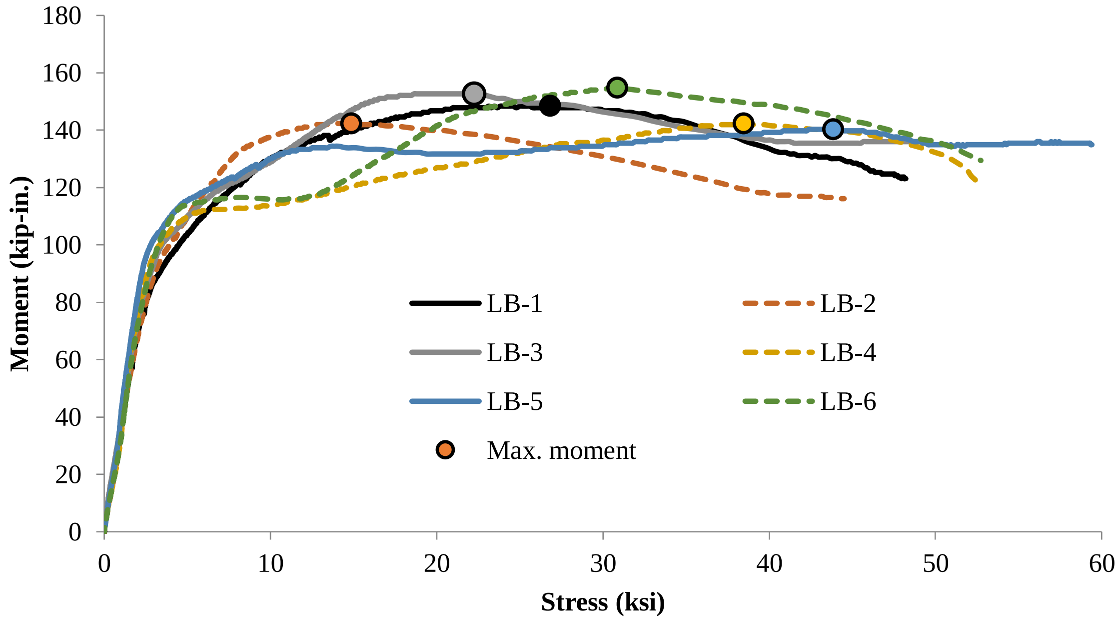

Figure 2.33 Moment vs. Rebar Stress (Casanova 2018)

CHAPTER 3 LITERATURE REVIEW OF FINITE ELEMENT MODELING OF CONCRETE

3.1 General Concrete Properties

Several material mechanical properties are needed to create an accurate material model when only compressive strength is given. General properties can be identified easily when normal weight concrete is used. Normal weight concrete is defined as concrete typically has a density (unit weight) between 135 and 160 lb/ft^3, and is normally taken as 145 to 150 lb/ft^3. The main properties are those typically found on a concrete stress-strain diagram. These include 28-day concrete compressive strength f'_c, initial tangent modulus (modulus of elasticity) E_{IT}, 28-day compressive strain ε'_c, 28-day tension strength f'_t, and 28-day tension strain ε'_t. These variables are shown on the general concrete stress-strain diagram in Figure 3.1 (Nawy 2009).

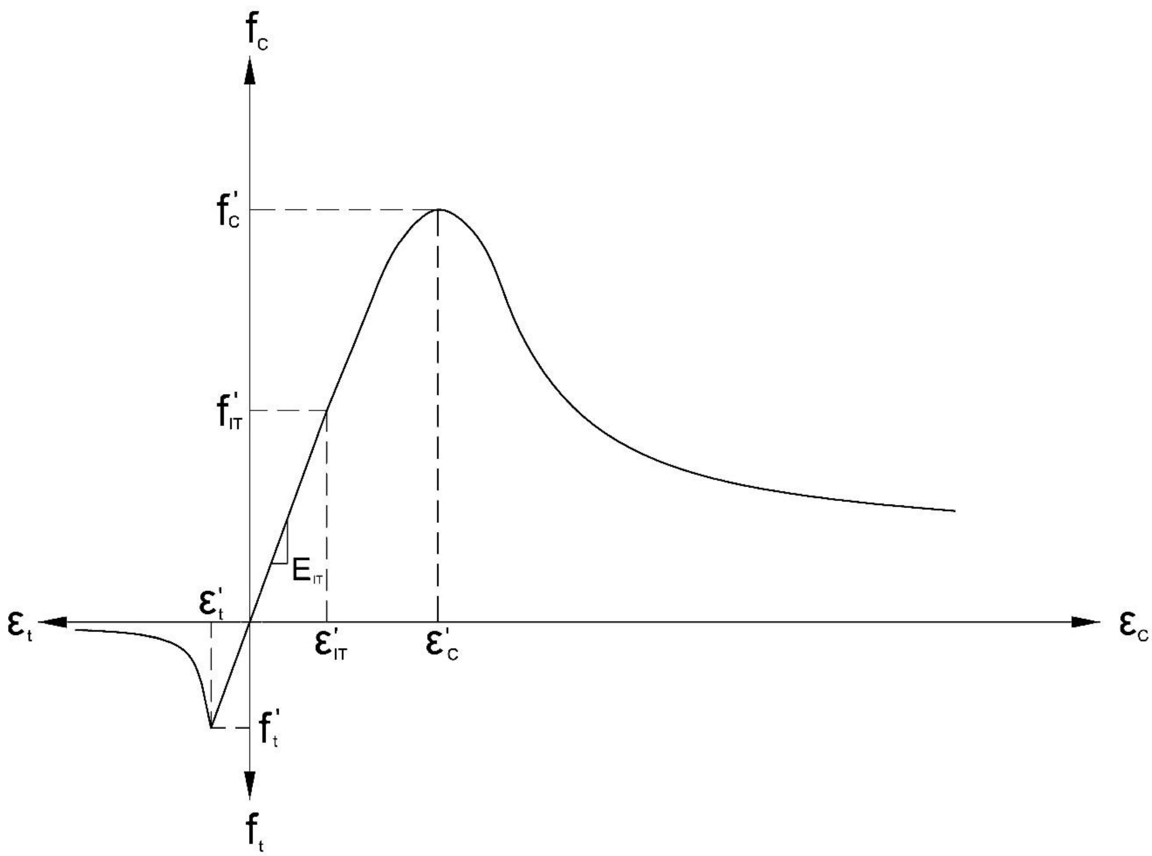

Figure 3.1 Concrete Stress-Stain Typical Properties

Other general concrete properties also needed for a finite element model are Poisson's ratio, ν. For normal weight concrete, Poisson's ratio is taken as 0.2 (Nawy 2009).

3.1.1 Stress-strain Relationship for Plain Concrete in Compression

Carreira and Chu, developed an equation that represents the stress-strain curve for concrete in compression (Carreira and Chu 1985). The serpentine shaped equation is shown as Equation (3.3) with the variables f_c and ε represent the stress and strain, respectively, at any given point.

$$\frac{f_c}{f_c'} = \frac{\beta(\varepsilon/\varepsilon_c')}{\beta - 1 + (\varepsilon/\varepsilon_c')^{\beta}} \tag{3.3}$$

$$\beta = \frac{1}{1 - \frac{f_c'}{\varepsilon_c' E_{IT}}} \tag{3.4}$$

Where, f_c' is the 28-day concrete compressive strength in ksi, ε_c' is the 28-day compressive strain, β is the material parameter, and E_{IT} is the modulus at initial tangent (modulus of elasticity in ksi). f_c' is typically given as the material strength of concrete and is determined directly through experimentation. Carreira and Chu state that the 28-day compressive strain, ε_c' can be estimated with Equation (3.5) where f_c' is in units of ksi.

$$\varepsilon_c' = (4.88\, f_c' + 168) * \ 10^{-5} \tag{3.5}$$

Initial tangent modulus is determined as a factor of f_c' in units of psi. ACI allows the modulus of normal weight concrete to be defined as Equation (3.6) (ACI 318-08). The actual tangent modulus is lower than Equation (3.6). ACI 318-08 acknowledges that modulus equation is an approximation and can vary as much as +/- 20%. However, without testing on the actual material, Equation (3.6) is a good approximation of concrete modulus of elasticity.

$$E_{IT} = \ 57{,}000\sqrt{f_c'} \tag{3.6}$$

Through compression testing, Carreira and Chu showed that these parameters can adequately represent concrete compressive behavior. It should be noted that the Equations (3.3) through (3.6) represent normal weight concrete conditions but may not be applicable to every concrete.

3.1.2 Stress-strain Relationship for Plain Concrete in Tension

Concrete in tension stress-strain behaves in a linear fashion along the initial tangent modulus until it reaches the ultimate tensile strength. At that point, concrete cracking ensues. The tensile strength capacity of the concrete rapidly decreases. Kim and Taha (2104) developed a method for approximating the ultimate tensile strength in concrete. Their method was developed by performing experimental tests and then used that to develop an equation for an ultimate tensile strength in concrete. Equation (3.7) is used for tensile strength with units of MPa. (Kim and Taha 2014). It is important to enter the 28-day concrete compressive strength in MPa and, if needed, convert the calculated tensile strength to psi for usage in US customary units.

$$f'_t = 0.34\sqrt{f'_c}\,(MPa) \tag{3.7}$$

3.2 Abaqus Concrete Materials

Reinforced concrete is a complicated material to be modelled using finite element methods. A complete material model of reinforced concrete should be capable of representing both linear and non-linear, behavior of concrete in compression and tension. Therefore, the development of a finite element model requires physical material testing to incorporate into the material model in the finite element software. Abaqus has two concrete material models to choose from. The first is the Smeared Cracking Material (SCM) which doesn't create large discontinuities in the form of cracks. Instead, cracks are "smeared" or disturbed into the material properties. Smeared cracking material is designed as a general application to model plain concrete and reinforced concrete. It allows the user to input linear-elastic and nonlinear parameters in both tension and compression (Abaqus Users Guide).

The second material model is Concrete Damaged Plasticity (CDP). Concrete damaged plasticity also allows the user to input linear-elastic and nonlinear parameters in both tension and compression. This material model is designed to be used in the analysis of reinforced concrete. It has many advanced capabilities that can be used for cyclic loading or damaged concrete. It requires many input parameters to successfully define the material properties. The input parameters are initial tangent modulus of elasticity, Poisson's ratio, dilation angle, eccentricity, fb0/fc0 (ratio of initial equibiaxial compressive yield stress to initial uniaxial compressive yield stress), K, viscosity parameter, tensile yield stress, inelastic tensile strain, compressive yield stress, and inelastic compressive strain. CDP material model also has the capability to input damage properties which are useful for modeling materials under cyclic loading.

Methods for calculating material inputs for modulus, Poisson's ratio, tensile, and compression values are discussed previously in this section based from concrete's 28-day compressive strength. The dilation angle, eccentricity, fb0/fc0 (ratio of initial equibiaxial compressive yield stress to initial uniaxial compressive yield stress), K, and viscosity parameter are more difficult to obtain without extensive laboratory testing. It is for this reason that a Simplified Concrete Damaged Plasticity (SCDP) material model is used to obtain these inputs (Hafezolghorani, et. al. 2017). SCDP is useful for simple models where the complexity of CDP is not needed. The simplified values are listed in Table 3.1.

Table 3.1 SCDP Plasticity Values

Parameter	Value
Dilation Angle	20-40°, 31° is recommended
Eccentricity	0.1
fb0/fc0	1.16
K	0.67
Viscosity parameter	0

3.3 Maximum Principal Stress Failure Theory

Maximum principal stress failure theory is a failure criterion generally applied in predicting failure in brittle materials. It combines tension, compression, and shear stresses on an element and orients the element such that shear stresses are zero. Only principal stresses remain which represent the maximum and minimum normal stresses at the point. One of the principal stresses is positive and the other negative representing tension and compression, respectively. In a material such as concrete, failure occurs when the positive principal stress exceeds the tensile strength in a simple uniaxial tensile test of the same material. This theory is unlike other failure theories because the strength of the material depends upon only one of the principal stresses and is entirely independent of the other two.

The Mohr's circle for a brittle material is shown in Figure 3.2. Each of the circles is a principal circle for the state of stress which it represents. Failure will typically occur when only the stress exceeds past the vertical line S_{yt} (tensile yield strength).

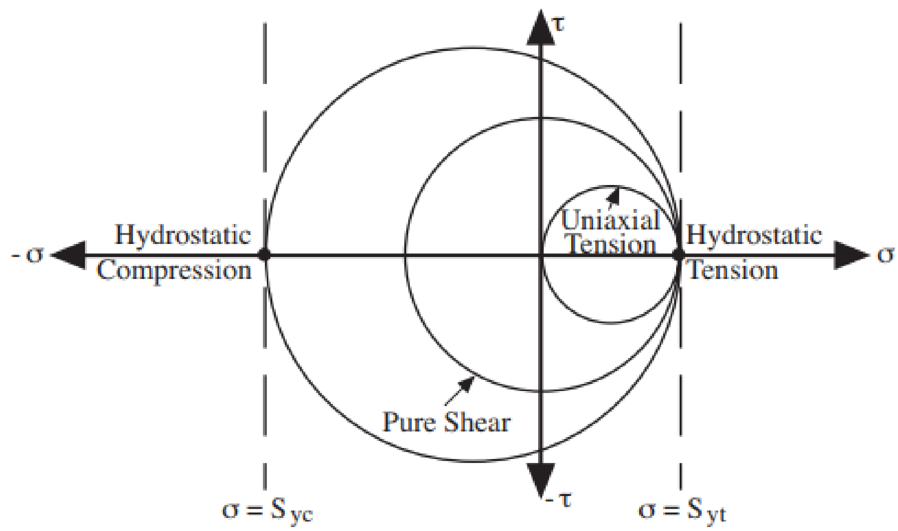

Figure 3.2 Principal Mohr's Circles for Several Stress States Representing Incipient Yielding According to Maximum Normal Stress Theory (Wolf 2001)

The failure locus for maximum normal-stress theory is shown in Figure 3.3. The principal stresses are σ_1 and σ_2. Failure will occur if either of the principal stresses exceed the yield strength of the material in compression or tension. For concrete, failure is often almost always in tension or the maximum positive principal stress.

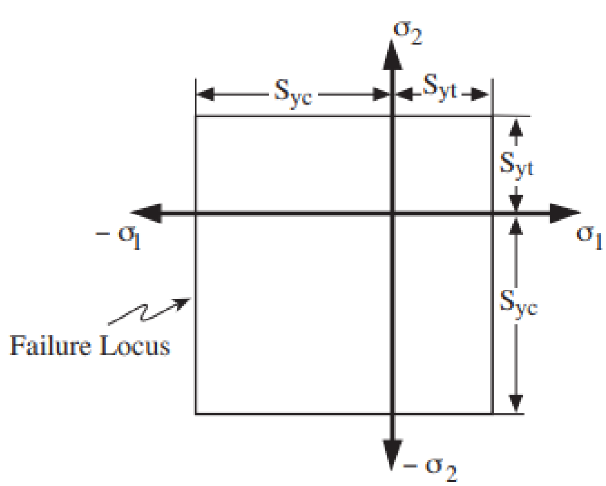

Figure 3.3 Failure Locus for the Biaxial Stress State for the Maximum Normal-Stress Theory (Wolf 2001)

CHAPTER 4 METHODOLOGY

In this chapter, the results obtained from known experimental tests found in the literature test are compared to finite element modeling in Abaqus in order to develop methodology for finite element modeling of beam tests carried out by Casanova (2018). Model calibration is an important step to ensure that computational results replicate physical results. This section details the process of modeling known physical tests of headed rebar and comparing the results. Experimental tests were selected for the separate effects from each test to compare with model results. Complex models can be difficult to troubleshoot where smaller testing can validate each variable individually. Also, this chapter presents a brief description on the procedure of modeling in Abaqus. There are not many detailed tutorials available regarding modeling and analyzing headed rebar/concrete structures using Abaqus. It is the hope of the author that this tutorial will be an aid to anyone using Abaqus to perform complex analysis of composite materials such as reinforced concrete.

4.1 Abaqus Model of DeVries Head Pullout Test

The DeVries tests were selected for model comparison for the separate effects of headed rebar. A headed bar pullout test modeled in this section do not contain any bond length (i.e. $l_b = 0$ inch from Figure 2.12) of the rebar to the concrete. It only includes the anchorage capacity effects that the head provides. DeVries tests T1B1 and T3B11 are both head only tests with the differences in the head embedment depth and concrete strength.

4.1.1 Finite Element Model Setup for Head Pullout

An axisymmetric two-dimensional model was created of DeVries' T1B1 and T3B11 pullout tests. The model was dimensioned exactly as the experiment with one exception, the head was modeled as round rather than square for simplification. It is assumed that a round head and a square head perform similarly. A simple view of the model geometry is shown in Figure 4.1. The concrete block was dimensioned large enough so that the pullout would be a cone failure with no edge effects. Model geometry is created in the "Parts" module of Abaqus. Two separate parts were created; one for rebar and head and one for the concrete. The parts were assembled in the "Assembly" module by using the translation command to properly orient the parts.

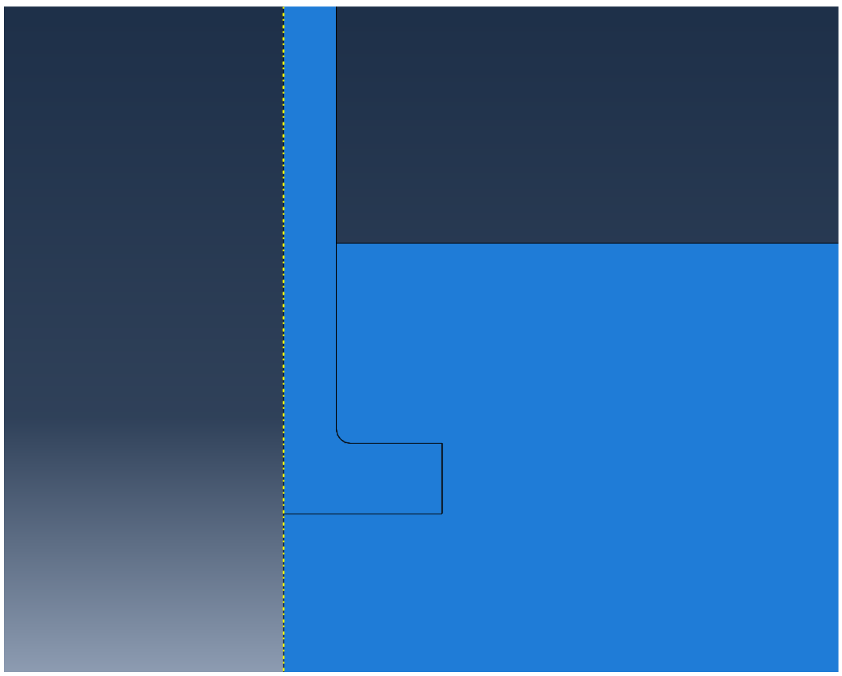

Figure 4.1 T1B1 Model Pullout Geometry

4.1.2 Defining Material Properties for Head Pullout

Material properties are simple for steel in this model. Steel is assumed to be perfectly elastic because it is expected that yielding will not occur in the steel. A Modulus of Elasticity (Young's Modulus) of $29x10^6$ psi and Poisson's Ratio of 0.3 was entered in the "Elastic" material properties of steel.

Concrete material properties are much more complex to define than the steel rebar. Only f_c' is given as a material property from the experiment. All concrete material properties were calculated from f_c'. For instance, test T1B1 has a $f_c' = 12{,}000$ psi (83 MPa) and all properties calculated using methods described in Chapter 2. A verification of concrete material properties in compression and tension are shown in Appendix A. The calculation results are shown in Table 4.1 along with the equation used.

Table 4.1 Material Properties for T1B1 Model

<table>
<tr><th colspan="4">Concrete Properties with $f_c' = 12,000\ psi$</th></tr>
<tr><th>Property</th><th colspan="2">Value</th><th>Equation</th></tr>
<tr><td>Initial Tangent Modulus</td><td colspan="2">$E_{IT} = 6.244\ x\ 10^6\ psi$</td><td>(3.6)</td></tr>
<tr><td>Tension Strength Yield Stress</td><td colspan="2">$f_t' = 822\ psi$</td><td>(3.7)</td></tr>
<tr><td rowspan="15">Compressive Stress as a function of Compressive Strain</td><td>Strain (in/in)
ε_c</td><td>Stress (psi)
f_c</td><td rowspan="15">(3.3)
using (3.4) and (3.5)</td></tr>
<tr><td>0</td><td>0</td></tr>
<tr><td>0.0005</td><td>2861</td></tr>
<tr><td>0.0012</td><td>5857</td></tr>
<tr><td>0.0018</td><td>7649</td></tr>
<tr><td>0.002</td><td>8124</td></tr>
<tr><td>0.0024</td><td>8929</td></tr>
<tr><td>0.0028</td><td>9573</td></tr>
<tr><td>0.0032</td><td>10090</td></tr>
<tr><td>0.0036</td><td>10505</td></tr>
<tr><td>0.004</td><td>10838</td></tr>
<tr><td>0.005</td><td>11412</td></tr>
<tr><td>0.006</td><td>11737</td></tr>
<tr><td>0.007</td><td>11909</td></tr>
<tr><td>0.008</td><td>11985</td></tr>
<tr><td>0.009</td><td>11999</td></tr>
</table>

4.1.3 Time Step Setup for Headed Bar Pullout

The time step is created in the Abaqus “Step” module. In the “Basic” tab a time period of 1 is imputed. “Nlgom” is turned on so that Abaqus will include the nonlinear effects of large deformations and displacements. Automatic stabilization is also turned on with a damping factor of 0.5 specified to assist Abaqus convergence on a solution. In the “Incrementation” tab the increments are left “automatic” and set to a maximum of 300. The minimum increment size is set to 1e-8 to allow Abaqus to go to a small increment, if needed, for analysis convergence.

4.1.4 Interaction Setup for Head Pullout

Abaqus’ interaction module is where constraints between parts are defined. The head pullout model requires an interaction to be defined between the head and the concrete. This interaction is defined as only a “contact” which tells Abaqus that the two parts cannot occupy the same space within the model. For the head pullout, an interaction property of “contact” with “normal behavior” was selected and the surfaces between the top of the head and the concrete were selected. The interaction property and surface selection are shown in Figure 4.2.

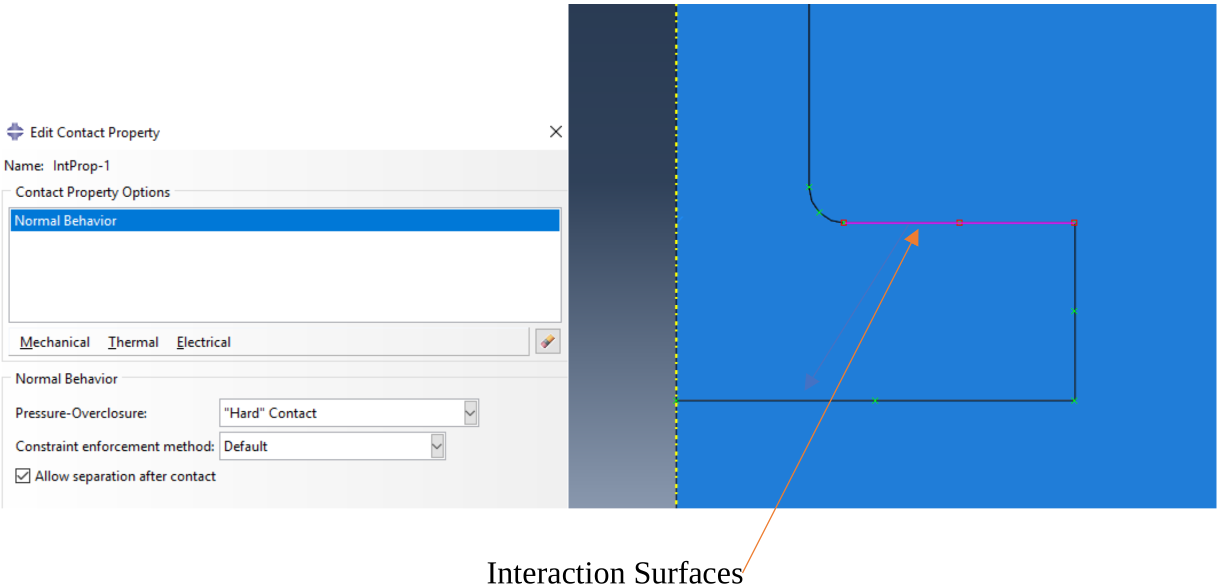

Figure 4.2 Head Pullout Interaction Property and Surfaces

4.1.5 Load and Boundary Conditions for Head Pullout

A fixed boundary condition was selected for the bottom of the slab. This ensures that the bottom of the concrete will not move in any direction. It is also far enough from the area of interest to not affect the results near the head and bar. The fixed boundary condition also helps the Abaqus solver converge on solutions. The fixed boundary selection is depicted on Figure 4.3 as blue and orange arrows.

In axisymmetric model, a boundary condition is applied as a default by Abaqus. The symmetry boundary conditions are in-place from the model creation when “Axi-symmetric” is selected as the model type. The symmetry is by default on the axis and is properly applied by creating the models on the axis. The symmetry line is shown in Figure 4.3 as a dashed yellow line.

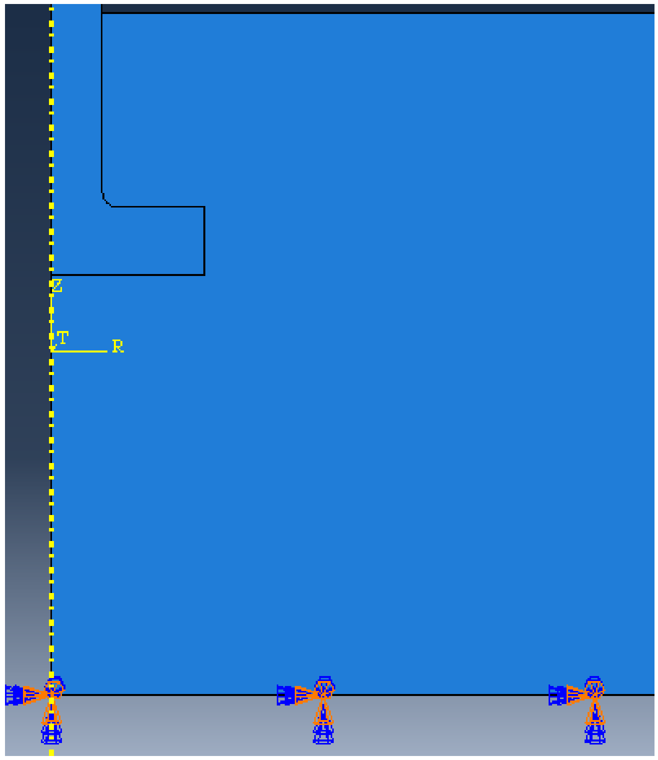

Figure 4.3 Head Pullout Boundary Conditions

The physical test had a load applied by pulling the rebar. The same load can be applied in Abaqus by one of two methods, a pressure load or a displacement. Displacement was chosen to provide a consistent pull on the rebar and aid the Abaqus solver in convergence issues. A displacement of 0.2 inches was applied to the top of the rebar pulling upward in the Y-direction (U2). This is not applied all in one increment, but rather applied proportionally at each increment. The maximum displacement occurs when the increment sum totals one time step. The displacement setting is done using a boundary condition which is shown in Figure 4.4.

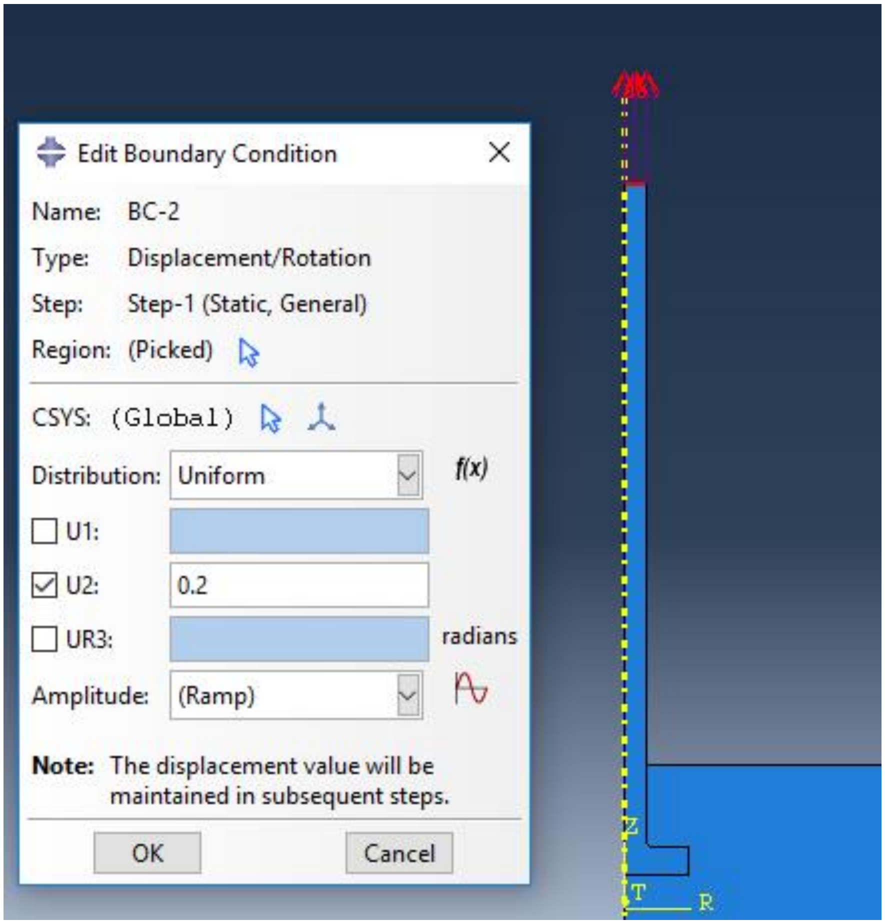

Figure 4.4 Head Pullout Load and Boundary Conditions

4.1.6 Selection of Element Types and Mesh for Headed Bar Pullout

Because the analysis is axisymmetric, the default element is a CAX4. Which is a 4-node bilinear axisymmetric quadrilateral element. This element type was assigned to both the rebar and concrete block. Element settings are shown in Figure 4.5. The mesh was applied on nodes at approximately every 0.10 inches as a quad element. This element size is small enough to capture the behavior in the area of interest but large enough to not cause computation challenges. The final mesh for the model is shown in Figure 4.6.

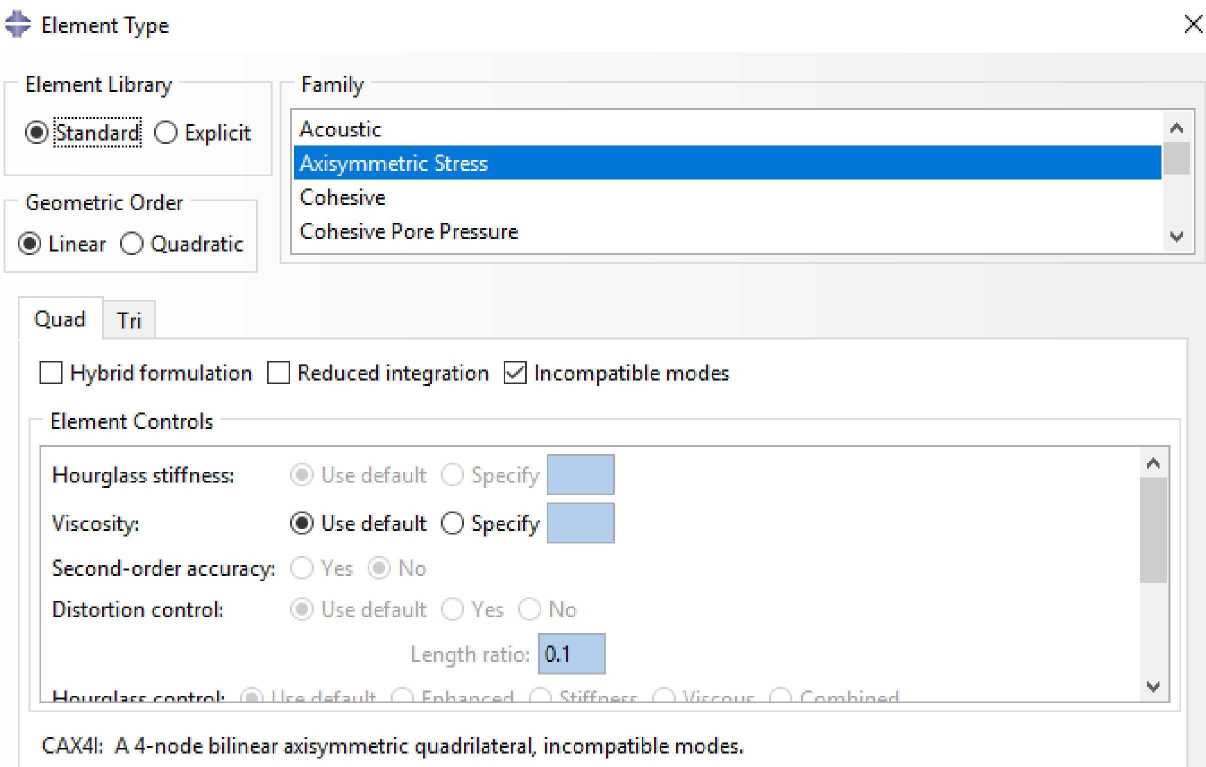

Figure 4.5 Head Pullout Element Type

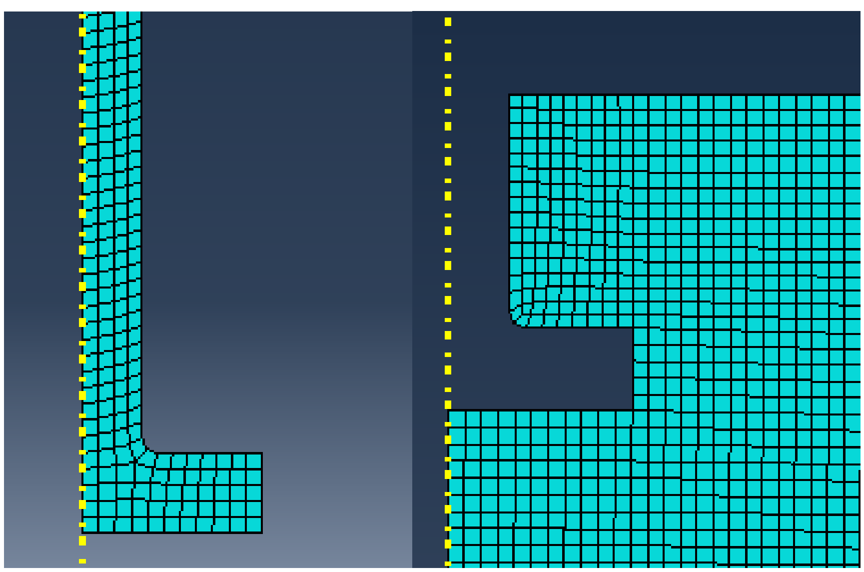

Figure 4.6 Head Pullout Mesh

4.1.7 Results and Comparison of the Pullout Tests

A job was then created in Abaqus/CAE and submitted to for processing. Four processors were used in parallel. The analysis results are shown graphically in Figure 4.7. The graph shows a slight crack forming in the concrete near the head. Abaqus will default to showing von Mises stresses which is the maximum distortion strain energy for homogenous material. This is not useful when evaluating material such as concrete because of its low tensile strength. Concrete that is loaded in bi-axial directions will begin to damage once the tensile strength is exceeded. Abaqus allows the user to view stresses in at the maximum principal stresses. Principal stress theory determines the orientation of an element such that the normal stresses are at a maximum and has no shear stress. This is an excellent method for evaluating a brittle material such as concrete because the maximum positive principal stress is the stress in tension. When it exceeds the tensile strength of the material, a crack will form. Looking at the maximum positive principal stress gradient forms in the concrete showing the location of high stress. All negative stress values are shown as a black color and all high stresses in the bar were limited at 20,000 psi and shown as a light grey color. The high stress area in the concrete is at approximately 30° angle off horizontal, which is consistent with the pullout cone shape that DeVries observed.

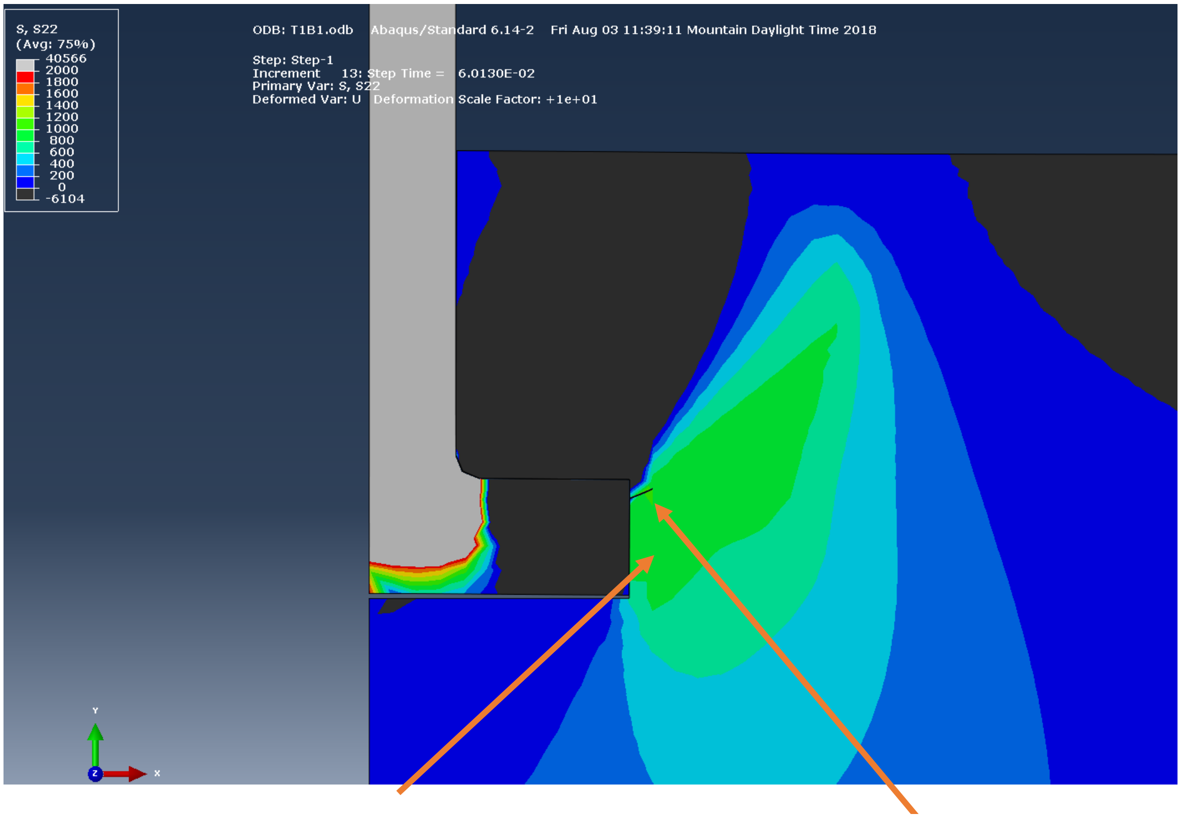

Figure 4.7 Head Pullout T1B1 Results

Upon completion of the analysis, the field output request was queried, and head displacement and bar stress were copied. From there, the data in the XY report was exported to Microsoft Excel. The result data was plotted and overlaid with the DeVries results for comparison in Figure 4.8. The DeVries test labeled T1B1 is shown as a gray line where the anchor capacity is linear up to approximately 11,000 lb and then undergoes large displacement. The Abaqus results of T1B1 are similar to the DeVries results in the elastic region and begins to undergo the large displacement as the concrete cracks and crushes. The Abaqus solver had difficulty converging on a solution and was stopped at a 0.005 inch head displacement.

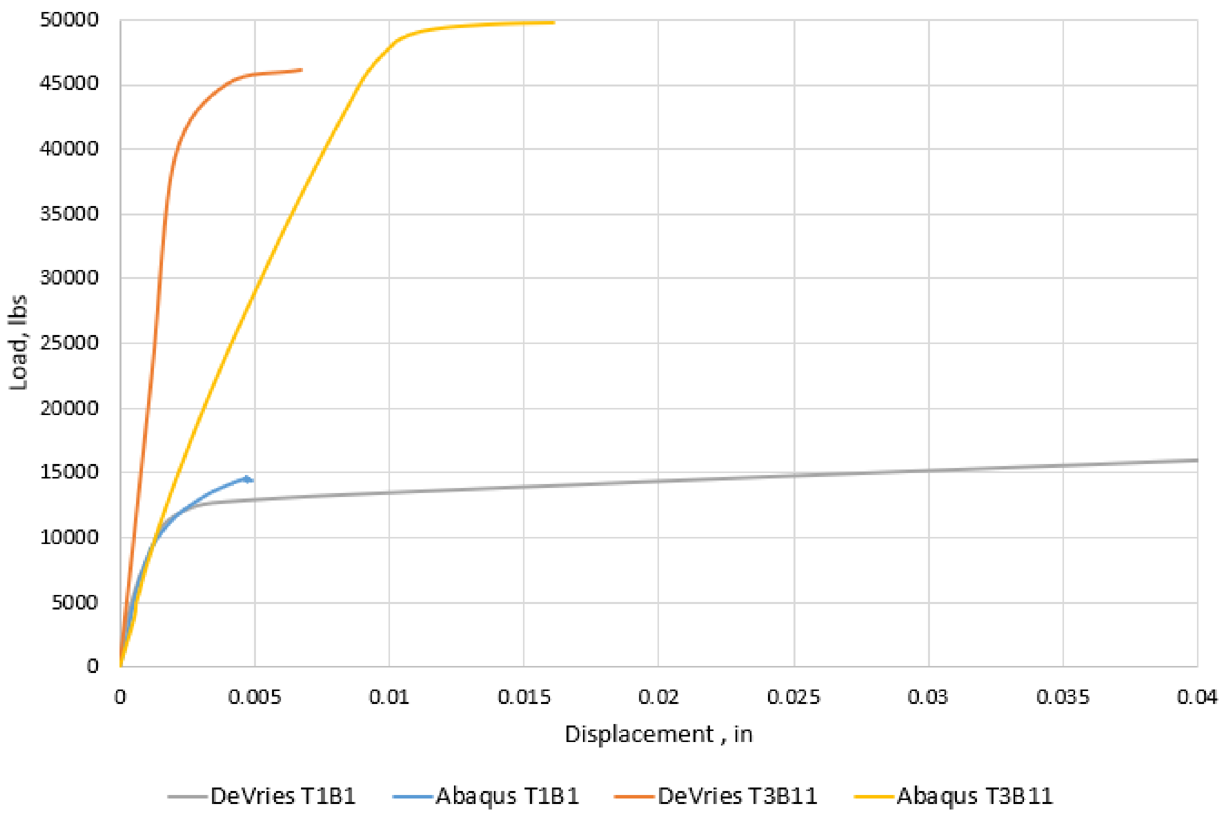

Figure 4.8 Head Pullout Result Comparison

An Abaqus model was created for T3B11 similar to the T1B1 model. It should be noted that the concrete strength for T3B11 is lower than T1B1, 27 MPa and 83 MPa respectively. The Abaqus results of T3B11 exhibit a similar behavior to the DeVries test. Both the Abaqus and DeVries tests have a large load capacity at larger than 40,000 lb. However, the DeVries test is slightly stiffer in that it has less head displacement. The disparity between the physical and Abaqus model appears to be large, however it is a displacement difference of 0.005 inches which is less than the diameter of a human hair. It is encouraging that both Abaqus models exhibit near the same anchorage capacity as their physical tests. These tests confirm that Abaqus can adequately model the anchorage of capacity that a head placed on the end of a rebar. Section 4.2 compares tests that include the supplementary capacity which includes the addition of the rebar-concrete bond.

4.2 Abaqus Model of Head/Bar Bond Tests

The DeVries tests were selected for model comparison for the total anchorage effects of head and the addition of rebar to concrete bond anchorage. The purpose of this comparison is to verify that an Abaqus model can approximate the anchorage capacity of a complete headed rebar with a full bond length (i.e., headed bars with bond length equal to embedment length $l_b = h_d$ from Figure 2.12.) DeVries' T2B5 and T2B6 are ideal test to use for a model comparison. These two tests are the exact same parameters, i.e. $f_C' = 33\ MPa, h_d = 229\ mm, and\ C_1 = C_2 = 51\ mm$. The only difference is that one allows a bond on the reinforcement bar, T2B6, and the other, T2B5, does not. This section compares both physical tests to Abaqus results and utilizes the bar bond-slip method described in Appendix B.

4.2.1 Finite Element Model Setup and Materials for Head/Bar Bond Tests

Models of test T2B5 and T2B6 were created similarly to the model of T1B1 in the previous section. One dimensional difference is that the head was set 229 mm deep into the concrete. Material properties for the steel remain the same and the concrete properties were changed for the 33 MPa compressive strength. All other parameters remained the same, i.e. mesh, element type time step, head interaction, loading, and boundary conditions.

4.2.2 Interaction Setup for Head/Bar Bond Tests

One variation between the two tests, T2B5 and T2B6, is that an interaction (aka bond) was placed on T2B6. Figure 4.9 shows that the bond is placed along the surface of the reinforcement bar and connects the bar and the concrete the entire length of the embedment, T2B6 only.

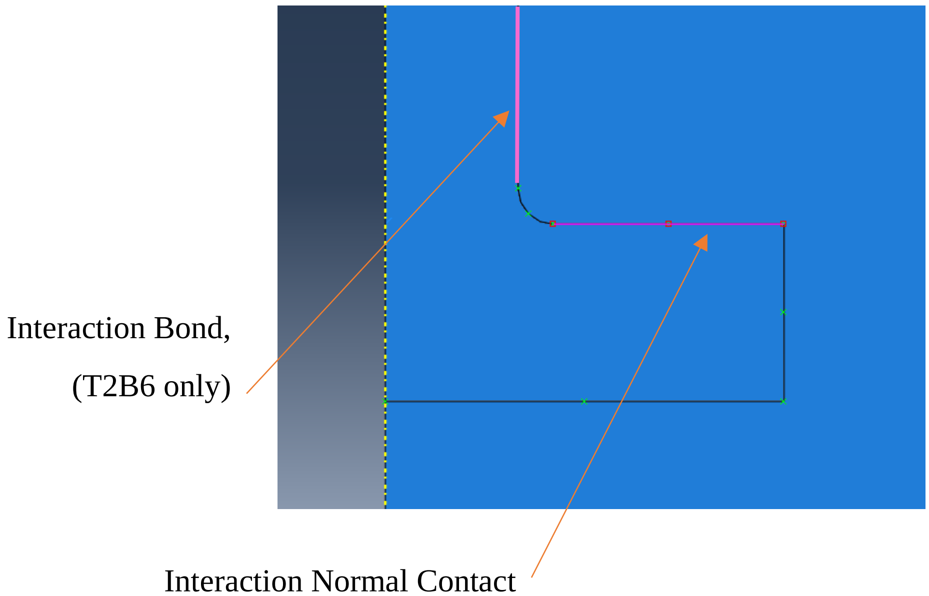

Figure 4.9 Head/Bar Bond Pullout Interaction Surfaces

The bond, for T2B6, is modeled with a cohesive contact. **Error! Reference source not found.** shows the contact settings that are entered to achieve a proper reinforcement bar to concrete bond. This method is discussed and verified in Appendix B. A maximum shear must be specified as a damage parameter that will begin to fail the bond when the value is exceeded. That damage parameter is calculated using Equation (B.2). A concrete compressive strength of $f_C' = 33\ MPa$ is entered and then a plot of the results is shown in Figure 4.10 with units converted to inches and psi. It can be seen that the maximum shear/bond stress is 1063 psi. This is the value that is entered into Abaqus as the shear damage parameter for the interaction. Figure 4.11 shows where the 1063 psi is entered into Abaqus as the contact property.

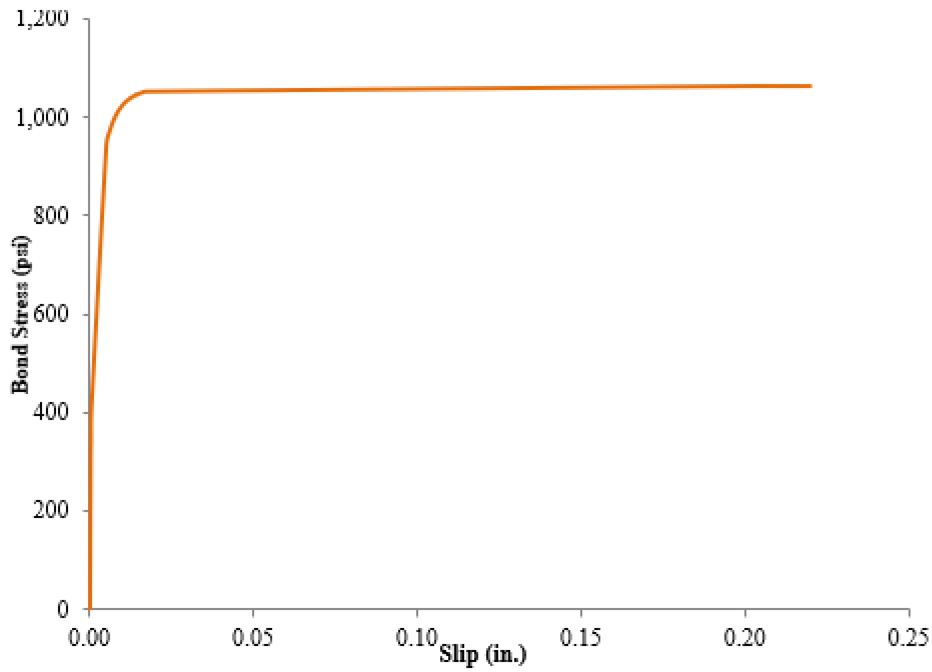

Figure 4.10 Bond-Slip Relationship for DeVries Test T2B6

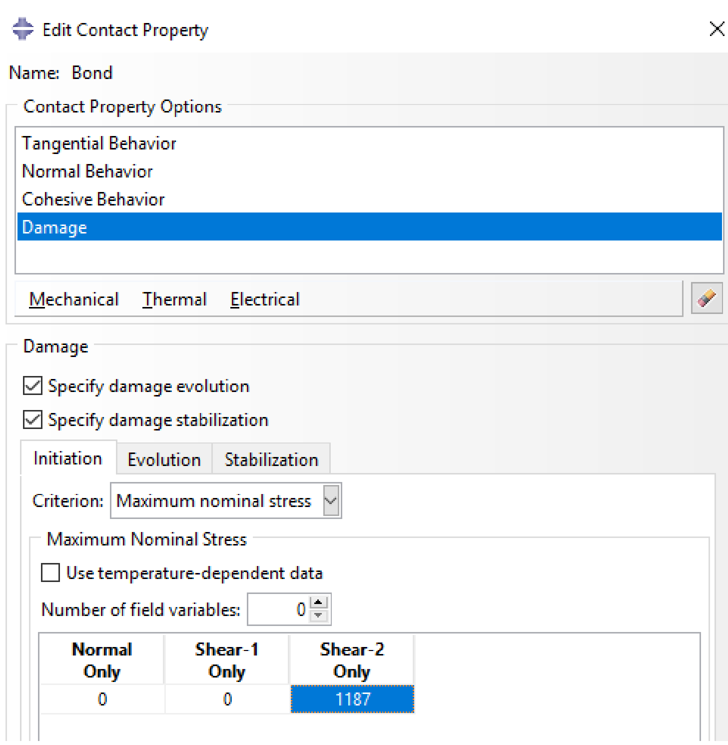

Figure 4.11 Abaqus Contact Property for Bond-Slip

4.2.3 Results and Comparison of Head/Bar Bond Tests

A job was then created in Abaqus/CAE and submitted to for processing. Measurements, within Abaqus, were taken similar to the T1B1 tests in the previous section. These measurements results were then plotted in Figure 4.12. The results from the Abaqus FEA models are shown as a dotted line and compared to DeVries' physical testing results which are show as a solid line. The blue represents the T2B5 test which is an anchorage of head only. The orange lines represent the T2B6 test that is an anchorage of the head and bar bond combined. It can be seen that the bar bond increased anchorage capacity. The Abaqus results are similar to DeVries' physical tests. There is some variation in through the linear-elastic region which is likely due to the influence of using tangent slope for initial modulus of elasticity for concrete. The results begin to diverge when large displacements occur.

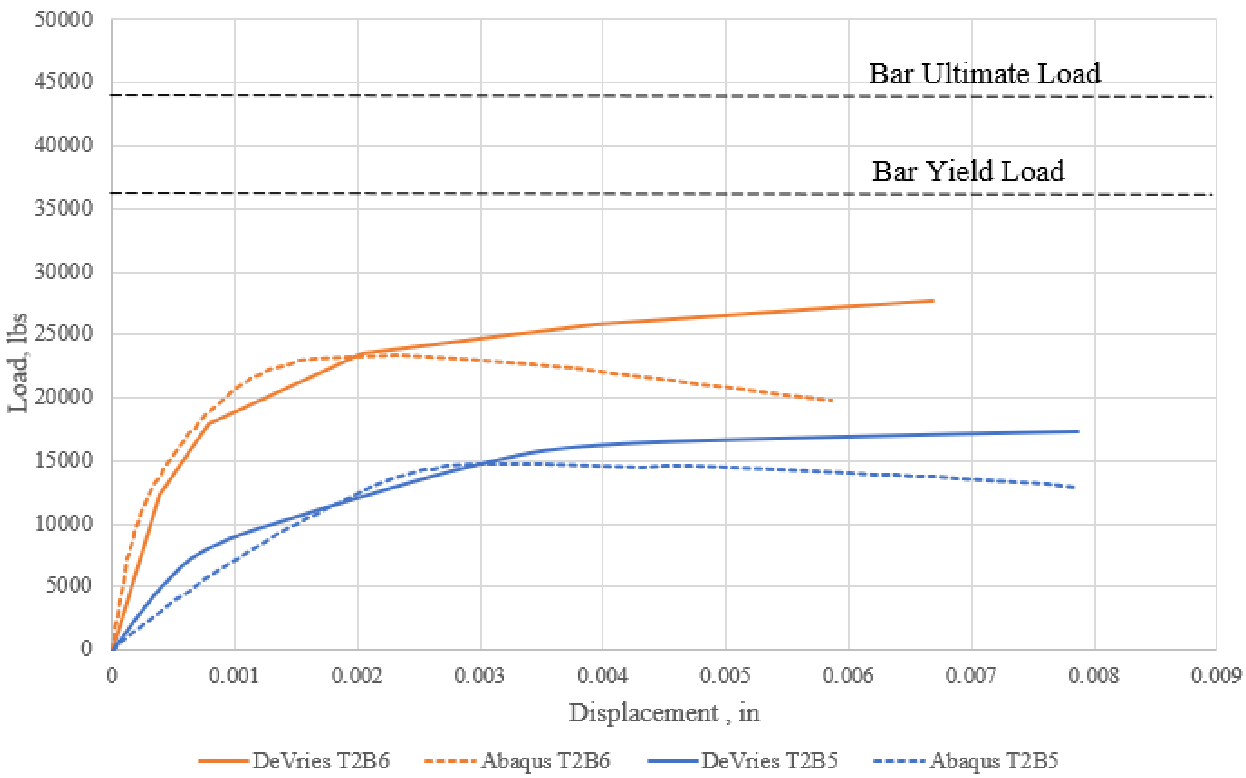

Figure 4.12 Head/Bar Pullout Result Comparison

CHAPTER 5 FINITE ELEMENT MODELING BEAM TESTS

The physical test, performed by Casanova (Section 2.4.2.3), of a beam in flexure under four-point bending represent a 1'-0" wide section of a bridge deck connection. The work of Casanova provides excellent measurement and results of the connection behavior using Mix D closure pour. However, there is a limitation to physical testing in that measurements cannot be taken everywhere. Especially on the interior of the beam where stresses fields cannot be visually seen. For example, in the large beam experiments, the headed bars were instrumented with strain gages next to the head. However, it is very likely that the bars right above the interface between the closure pour concrete and precast segment (i.e., where the maor cracks will first initiate) will experience more stress. FEM has the capability of performing measurements at any location to provide additional results.

Another benefit of FEM is that once a model has been verified to be correct, some parameters can be modified to analyze the effects. This chapter provides the FEM results of Casanova's four-point flexural beam tests (using Mix D closure pour) and provides additional insight into the beam's performance. This chapter also contains a similar four-point flexural beam test using UHPC closure pour to provide a comparison of the two closure pour configurations.

5.1 Abaqus Model of the Beam Specimen with Mix D Closure Pour Concrete

Casanova's 2018 beam test, using Mix D for the closure pour, under four-point bending as shown in Figure 2.8 and Figure 2.9, is an ideal physical test that can be modeled using Abaqus. The four-point bending allows for a constant bending moment across the entire closure pour. Figure 5.1 shows the shear and moment diagram of a beam under four-point bending. The maximum moment occurs between the two point loads and is constant value between them.

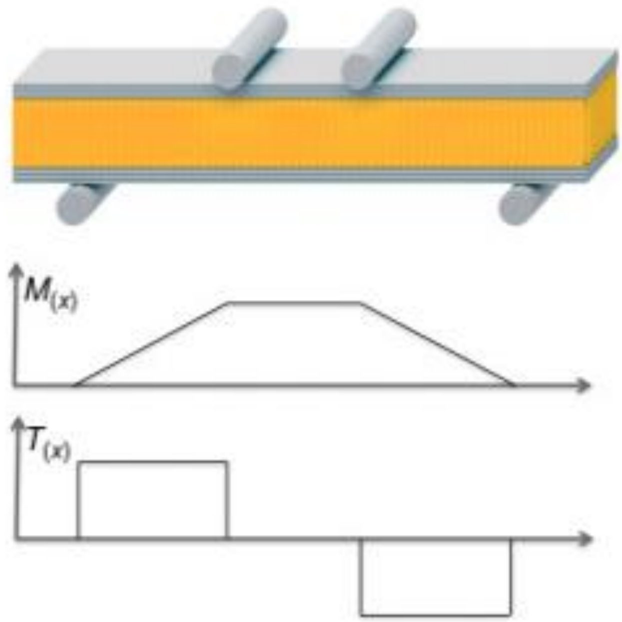

Figure 5.1 Four-Point Bending Moment and Shear Diagram

Image source: https://www.sciencedirect.com/topics/engineering/bending-tests

Casanova measurements included a strain gauge on the inner reinforcement bars near the head to estimate bar stresses as shown in Figure 2.24 (a). Another measurement was made by measuring the force loading placed on top of the beam. Using the same parameters from the physical testing and the methodology defined in Chapter 4, a finite model was created in Abaqus. If the Abaqus model recreates the similar results of bar stress versus force compared to the physical testing, then other internal measurements can be measured from the finite element model. One such measurement is the stress in the reinforcement bar at the concrete interface. The stress in the bar should be at a maximum in the location of the interface and key parameter in the bridge joint performance.

5.1.1 Finite Element Model Geometry for Mix D Closure Beam Test

Finite element modeling in Abaqus with multiple component begins with creating the correct part geometry. The beam test consists of five unique parts: closure pour, precast left, precast right, headed rebars, and top rebar.

The closure pour geometry begins with a two-dimensional profile as shown in Figure 5.2. It is best practice to model this profile around a fixed center point to allow the user to take advantage of mirroring commands in Abaqus. Thus, a center point was placed at the origin point in the model. This point was locked in place using the fixed constraint. Figure 5.3 shows the two-dimensional profile that is created and dimensioned in the Abaqus sketch editor. The profile is then extruded 12 inches to create a three-dimensional shape. Figure 5.4 shows where the blind holes are then added to remove material that will be occupied by the reinforcement bars.

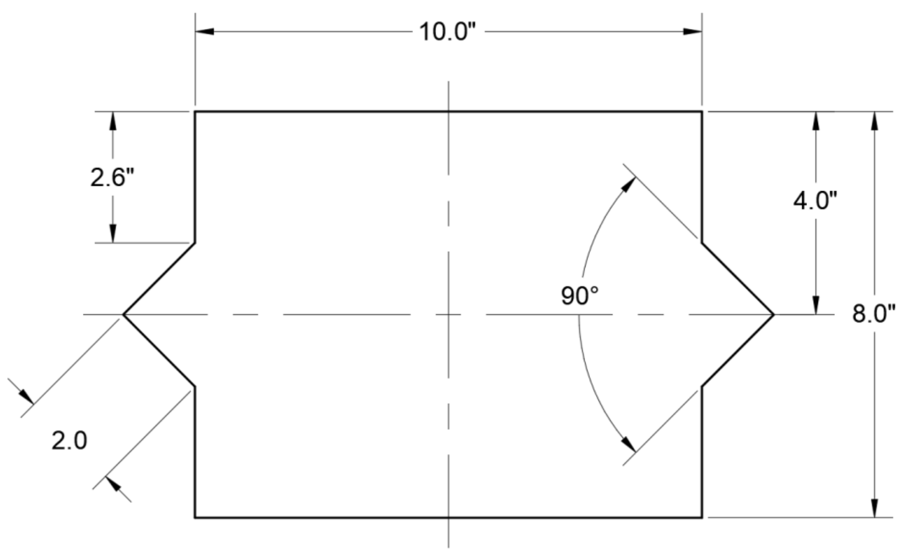

Figure 5.2 Mix-D Closure Pour Two-Dimensional Profile

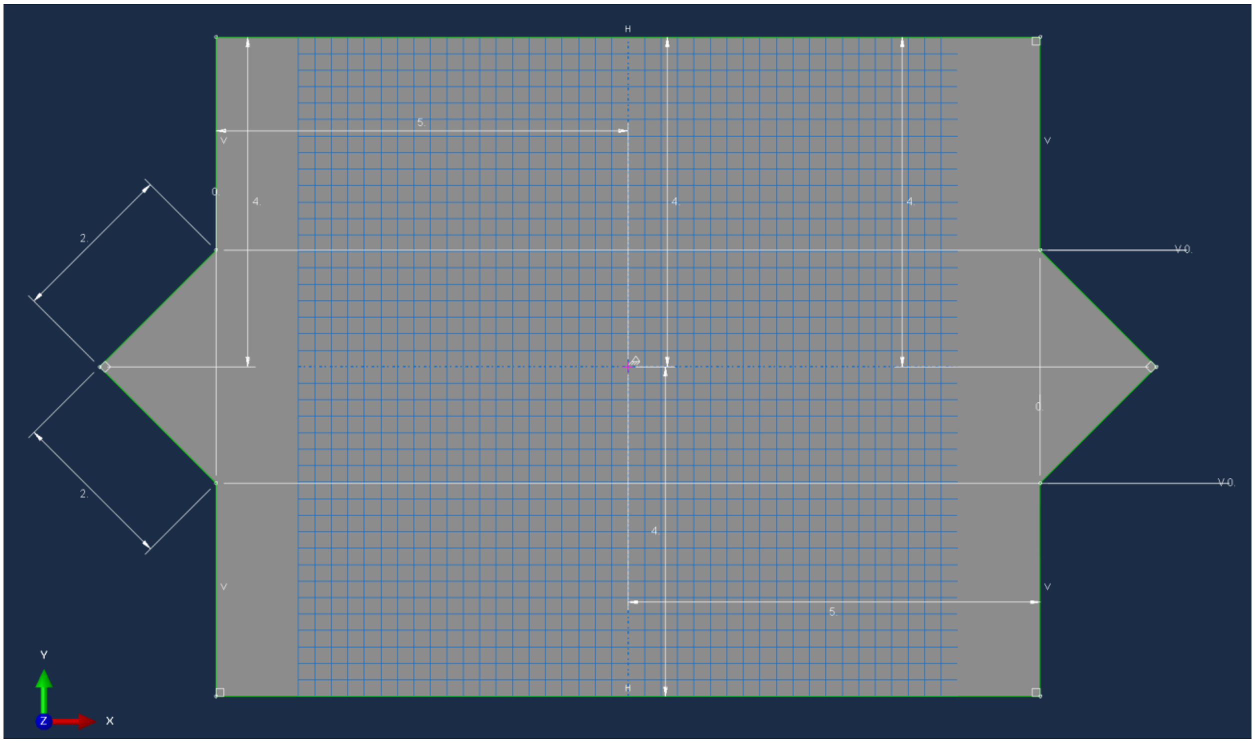

Figure 5.3 Mix-D Closure Pour Profile Sketch

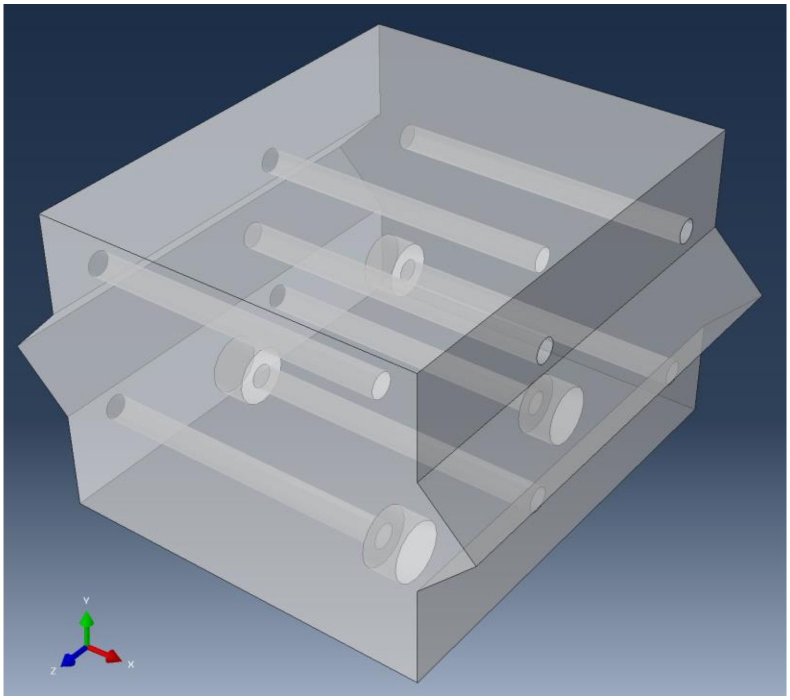

Figure 5.4 Mix-D Closure Pour Three-Dimensional Shape

Next, the left and right precast parts are created. These parts are exactly the same which allows for the left to be modeled and then the right is a duplicate copy. The left precast begins with a two-dimensional profile as shown in Figure 5.5. Again, it is best practice to model this profile around a fixed center point to allow the user to take advantage of mirroring commands in Abaqus. Thus, a center point was placed at the origin point in the model. This point was locked in place using the fixed constraint. This point will be the center point in the assembly thus the model profile is dimensioned 5 inches to the left of the origin point. Figure 5.6 the two-dimensional profile was created and dimensioned in the Abaqus sketch editor. The profile is then extruded 12 inches to create a three-dimensional shape. A zone must be created on the top surface of the precast shape so that a load can be applied similarly to the actual physical loading that used a round bar and rubber bearing pad. Figure 5.7 shows the loading area that is created using Abaqus' partition command and is dimensioned as a 1 inch wide strip that is 23.5 inches from the beam end. Figure 5.8 shows the blind holes are then added to remove material that will be occupied by the reinforcement bars.

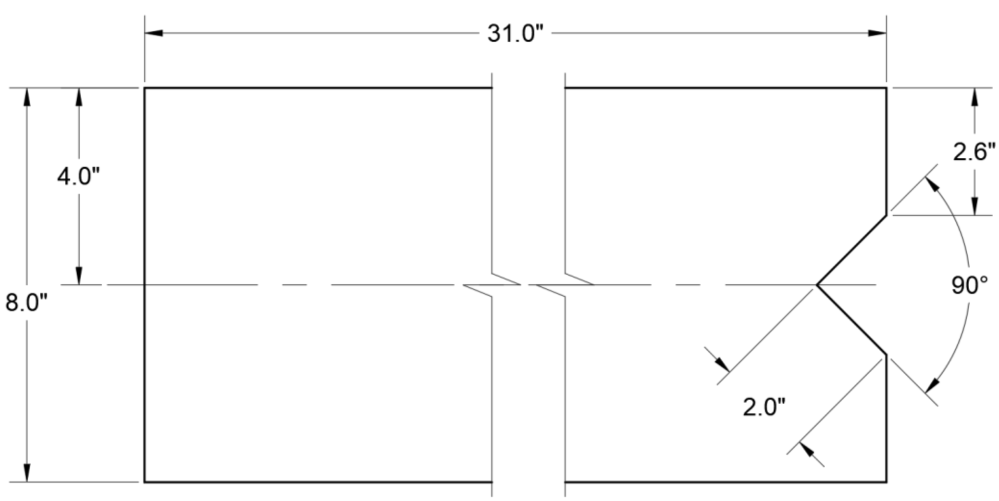

Figure 5.5 Precast Two-Dimensional Profile

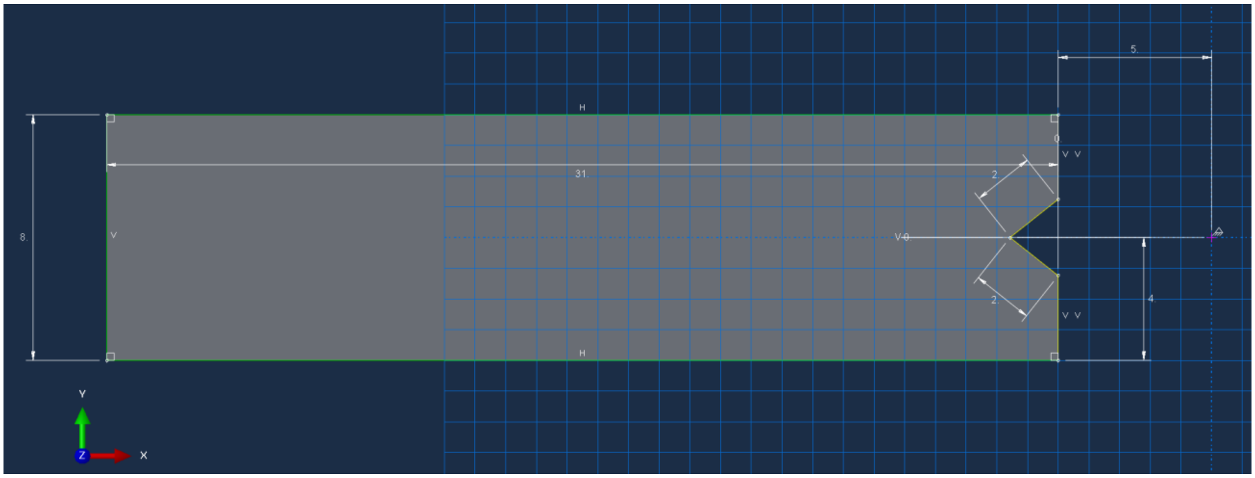

Figure 5.6 Closure Beam Precast Profile Sketch

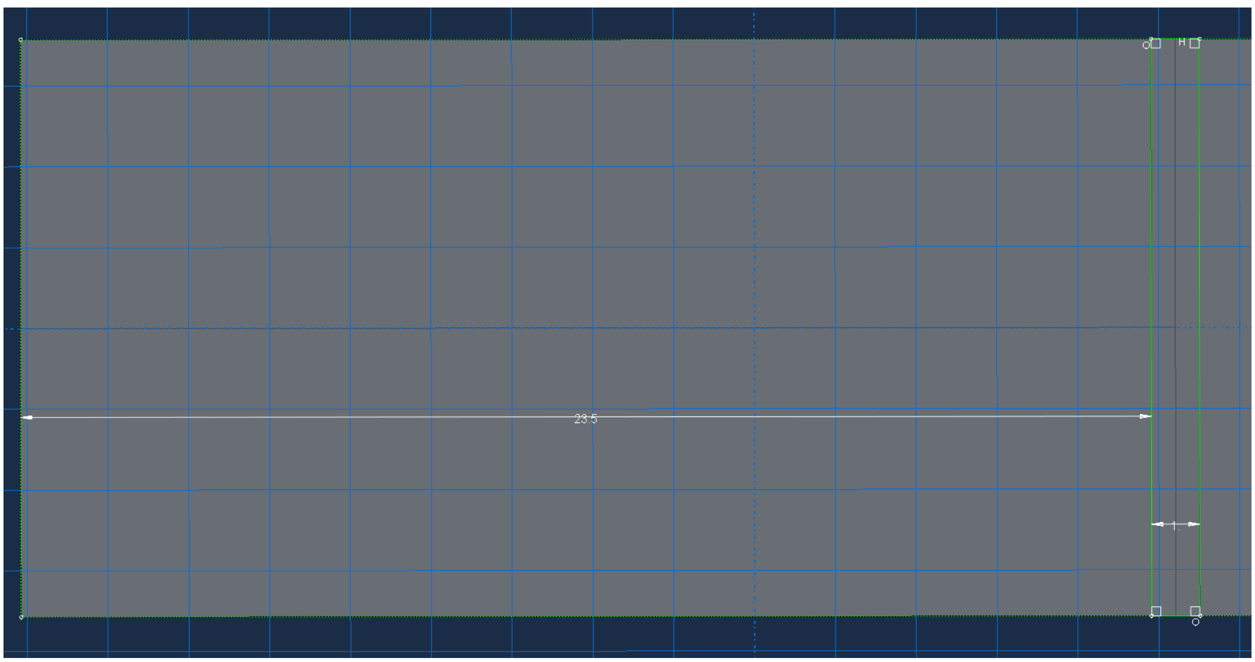

Figure 5.7 Precast Top Partition Area

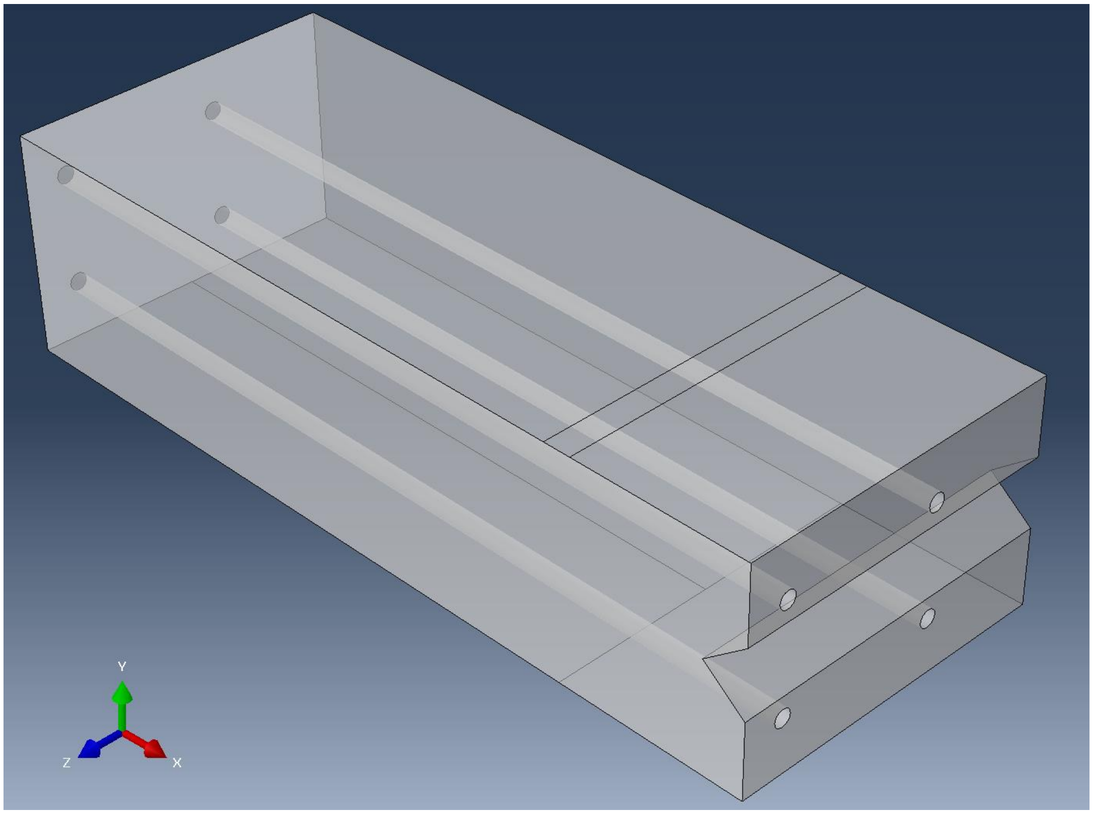

Figure 5.8 Precast Three-Dimensional Shape

Headed rebar is typically two parts, a head and rebar, joined together with a weld or a threaded connection. Because connection between the head and rebar do not separate in any of the testing presented in chapter 2, it is assumed that these components can be modeled as just one part. Figure 5.9 shows the headed two-dimensional profile was created and dimensioned in the Abaqus sketch editor. The profile is then extruded 0.875 inches to create a three-dimensional shape. Similarly, another circular profile was created with a 0.625 inch diameter circle, to represent a No. 5 bar, and extruded 38.55 inches for a three-dimensional shape show in Figure 5.10.

The top rebar is created in a similar fashion. A two-dimensional profile is created with a 0.625 inch diameter circle and extruded 38.5 inches long.

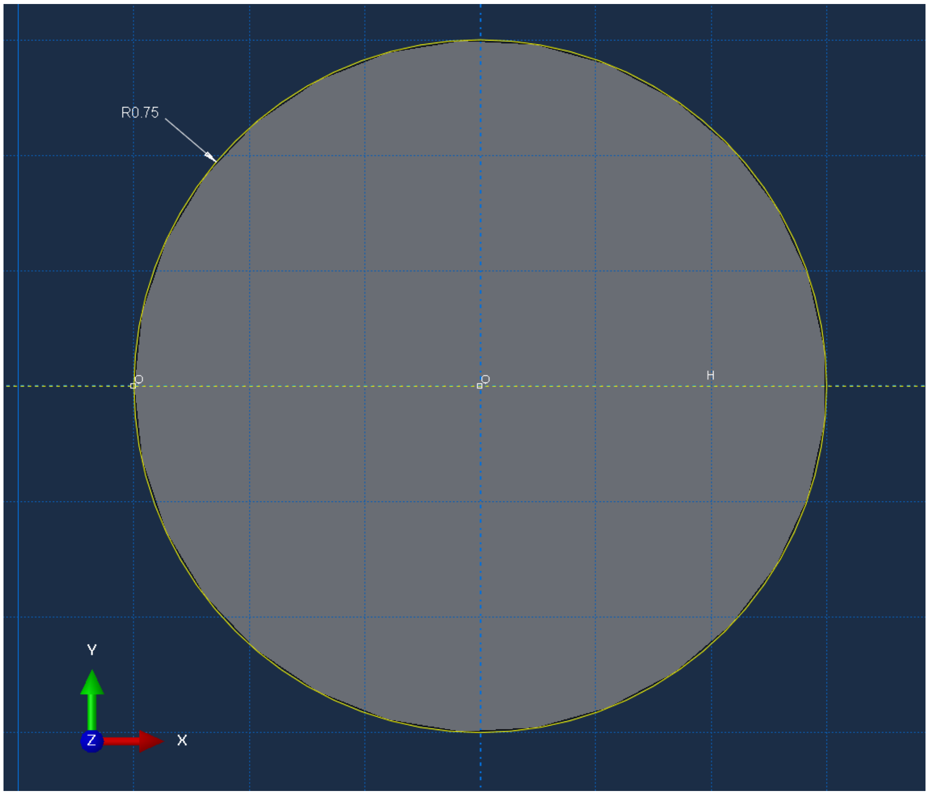

Figure 5.9 Headed Rebar Two-Dimensional Profile

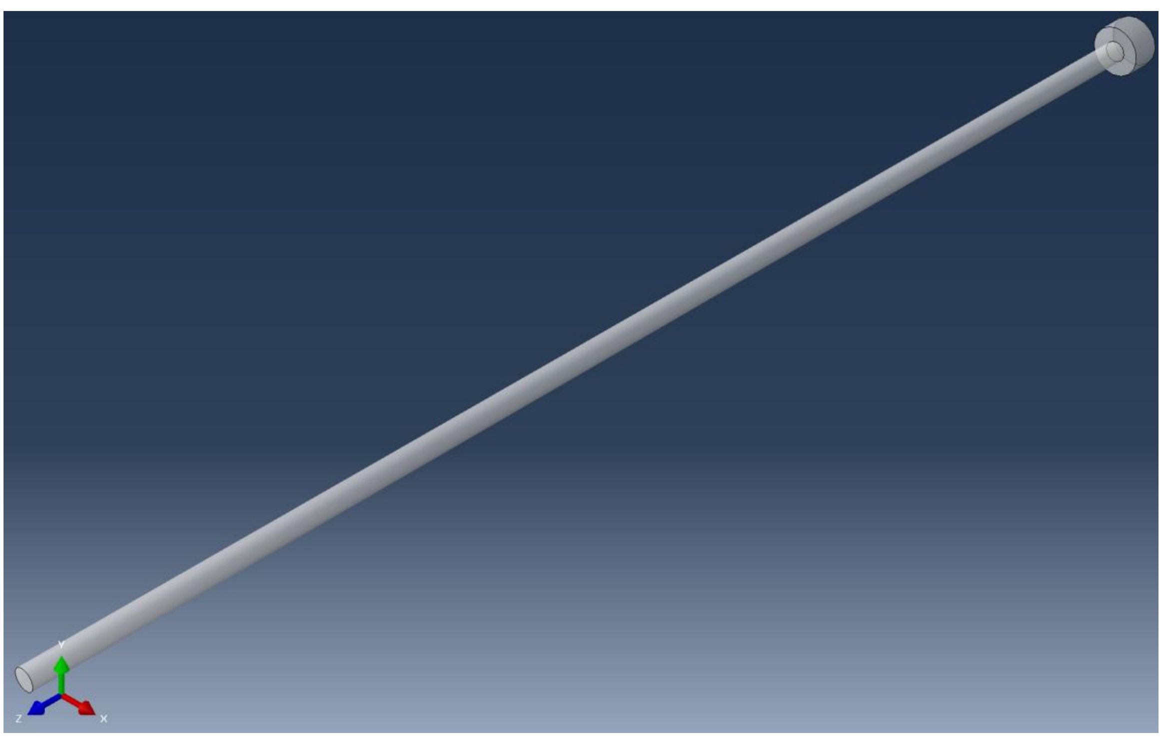

Figure 5.10 Headed Rebar Three-Dimensional Shape

5.1.2 Finite Element Model Materials for Mix D Closure Beam Test

Material properties for the rebar and headed rebar are for steel. Steel is assumed to be perfectly elastic because it is expected that yielding will not occur in the steel. A Modulus of Elasticity (Young's Modulus) of 29×10^6 psi and Poisson's Ratio of 0.3 was entered in the "Elastic" material properties of steel.

Concrete material properties are provided by the information given in Table 2.3 and Table 3.1 are much more complex to define than the steel rebar. Using f_c', tensile and compressive strength were determined with the methods defined in Chapter 3. The calculation results are shown in Table 5.1 and Table 5.2 along with the equation entered into Abaqus using the "Concrete Damage Plasticity" material.

Table 5.1 Closure Beam Test Mix-D Closure Material Properties

Closure Pour Properties with $f'_c = 8,354\ psi$			
Property	**Value**		**Equation / Source**
Initial Tangent	$E_{IT} = 4.425\ x\ 10^6\ psi$		Table 2.3
Tension Strength	$f'_t = 374\ psi$		(3.7)
Poisson's Ratio	$\mu = 0.176$		Table 2.3
Compressive Stress as a function of Compressive Strain	Strain (in/in)	Stress (psi)	(3.3) using (3.4) and (3.5)
	0	0	
	0.0005	2301	
	0.0012	4505	
	0.0018	5724	
	0.002	6035	
	0.0024	6550	
	0.0028	6951	
	0.0032	7265	
	0.0036	7513	
	0.004	7709	
	0.005	8039	
	0.006	8219	
	0.007	8311	
	0.008	8349	
	0.009	8352	

Table 5.2 Mix-D Closure Beam Test Precast Material Properties

Precast Properties with $f'_c = 4,969\ psi$			
Property	**Value**		**Equation / Source**
Initial Tangent	$E_{IT} = 3.181 \text{ x } 10^6\ psi$		Table 2.3
Tension Strength	$f'_t = 290\ psi$		(3.7)
Poisson's Ratio	$\mu = 0.154$		Table 2.3
Compressive Stress as a function of Compressive Strain	Strain (in/in)	Stress (psi)	(3.3) using (3.4) and (3.5)
	0	0	
	0.0005	1657	
	0.0012	3028	
	0.0018	3704	
	0.002	3867	
	0.0024	4130	
	0.0028	4329	
	0.0032	4480	
	0.0036	4597	
	0.004	4688	
	0.005	4836	
	0.006	4915	
	0.007	4953	
	0.008	4968	
	0.009	4967	

5.1.3 Time Step Setup for the Beam Test

The time step is created in the Abaqus "Step" module. In the "Basic" tab a time period of 1 is imputed. "Nlgom" is turned on so that Abaqus will include the nonlinear effects of large deformations and displacements. Automatic stabilization is also turned on with a damping factor of 0.5 specified to assist Abaqus convergence on a solution. In the "Incrementation" tab the increments are left “automatic” and set to a maximum of 500. The minimum increment size is set to 1e-9 to allow Abaqus to go to a small increment for analysis convergence.

5.1.4 Interaction Setup for Reinforcement Bar and Concrete

Abaqus’ interaction module is where constraints between parts are defined. The head pullout model requires an interaction to be defined between the head and the concrete. This interaction is defined as only a “contact” which tells Abaqus that the two parts cannot occupy the same space within the model. For the head pullout, an interaction property of “contact” with “normal behavior” was selected and the surfaces between the top of the head and the concrete were selected.

The bond between the reinforcement bar and the concrete is modeled with a cohesive contact. This method is discussed and verified in Appendix B. A maximum shear must be specified as a damage parameter that will begin to fail the bond when the value is exceeded. That damage parameter is calculated using Equation (B.2). A concrete compressive strength of $f_C' = 34.5\ MPa\ (5{,}000\ psi)$ is entered and then a plotted to see where the shear stress where the bar begins to slip. This method produces a maximum shear/bond stress is 1378 psi. This is the value that is entered into Abaqus as the shear damage parameter for the interaction.

5.1.5 Interaction Setup between the Precast and Closure Pour

The interface is modeled with an interaction property within Abaqus. The interaction has all three Abaqus properties of “Tangential Behavior”, “Cohesive Behavior”, and “Damage” assigned. This interaction layer has no thickness and merely defines how one node from one part is to interact with its corresponding node with the adjacent part. The damage parameter must be assigned to the normal stress at which the nodes will separate. This value is obtained by using equation (5.1) from Taha, 2014. The modulus of rupture (flexural tensile strength) is from Table 2.2 as the interface bond strength from a flexural beam test.

$$f_t = \frac{f_r}{2.5} \tag{5.1}$$

This results in a direct tensile are $f_t = 245\ psi$ and is entered in the contact property between the surfaces. The interface surfaces assigned as an interaction are highlighted in pink/red on Figure 5.11.

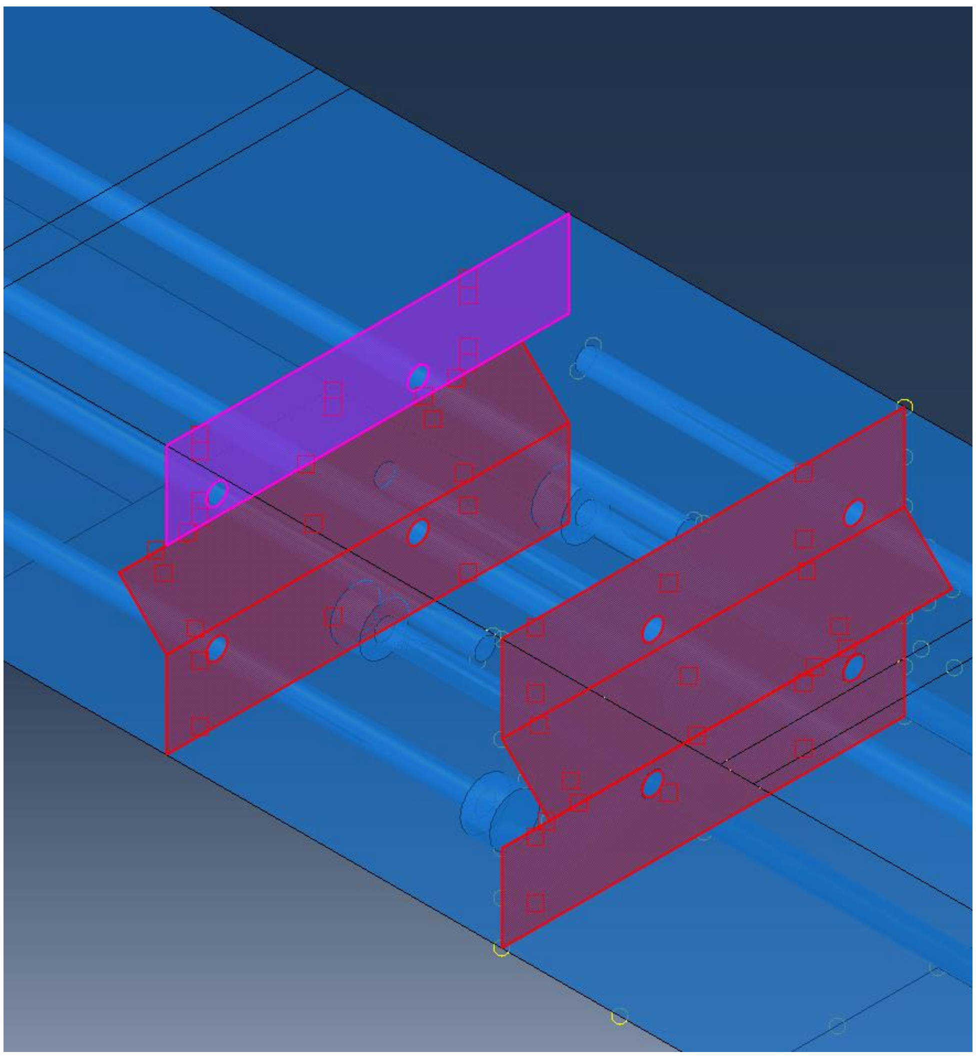

Figure 5.11 Mix-D Closure Beam Test Interaction Surfaces

5.1.6 Load and Boundary Conditions for Beam Test

Loads are applied on the beam similar to the test setup shown in Figure 2.28 with rectangular areas with a pressure load. The two rectangular areas 1” x 12” strips that simulate the load area of the physical testing apparatus. A line load could also be used in lieu of the strip, but that causes localized stress concentrations where the strip does not. The two load areas cause a constant moment across the closure pour to isolate the effects of the bond strength. The maximum magnitude of the pressure load is 2,000 psi which is enough to fail the beam at the interface.

Boundary conditions are applied as a simple beam experiment with one end pinned with no movement in the x- and y-direction and rotation allowed. The other end is set as a roller with the only restriction of no movement allowed in the y-direction. A graphic of the loads and boundary conditions is shown in Figure 5.12.

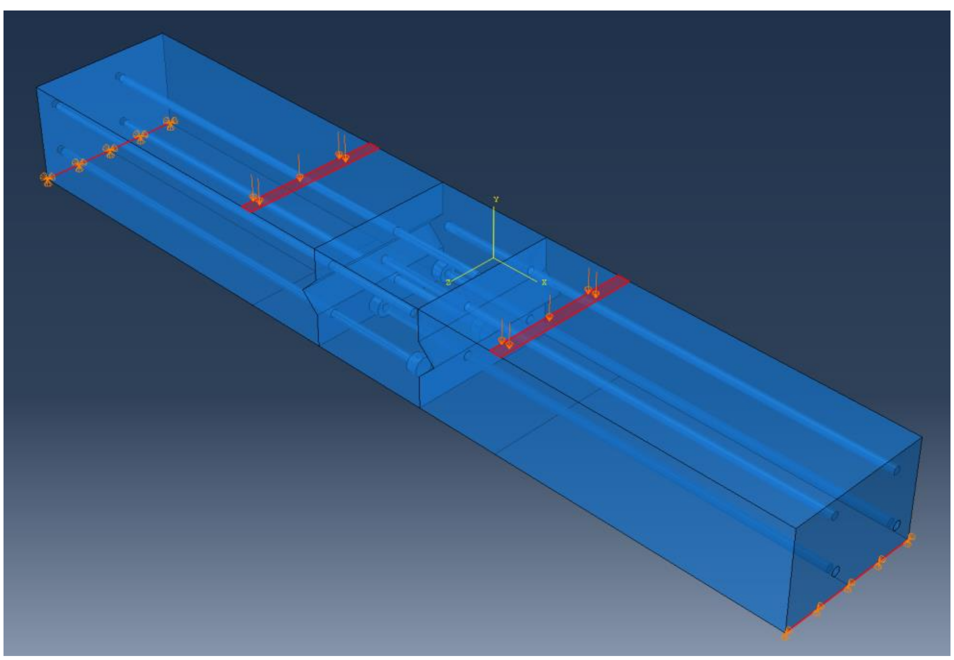

Figure 5.12 Mix-D Closure Beam Test Loads and Boundary Conditions

5.1.7 Selection of Element Types and Mesh for Headed Bar Pullout

A 3-dimensional tetrahedron (tet) mesh were used with tetrahedral element mesh shapes with linear interpolation. A mesh size of 2.0 inches between nodes was used on the concrete components (precast/closure pour) and a mesh size of 0.3 inches for the metal components (headed bar/rebar). The element type is a C3D10 which is a 10-node quadratic tetrahedron. The mesh of all the parts is shown in Figure 5.13.

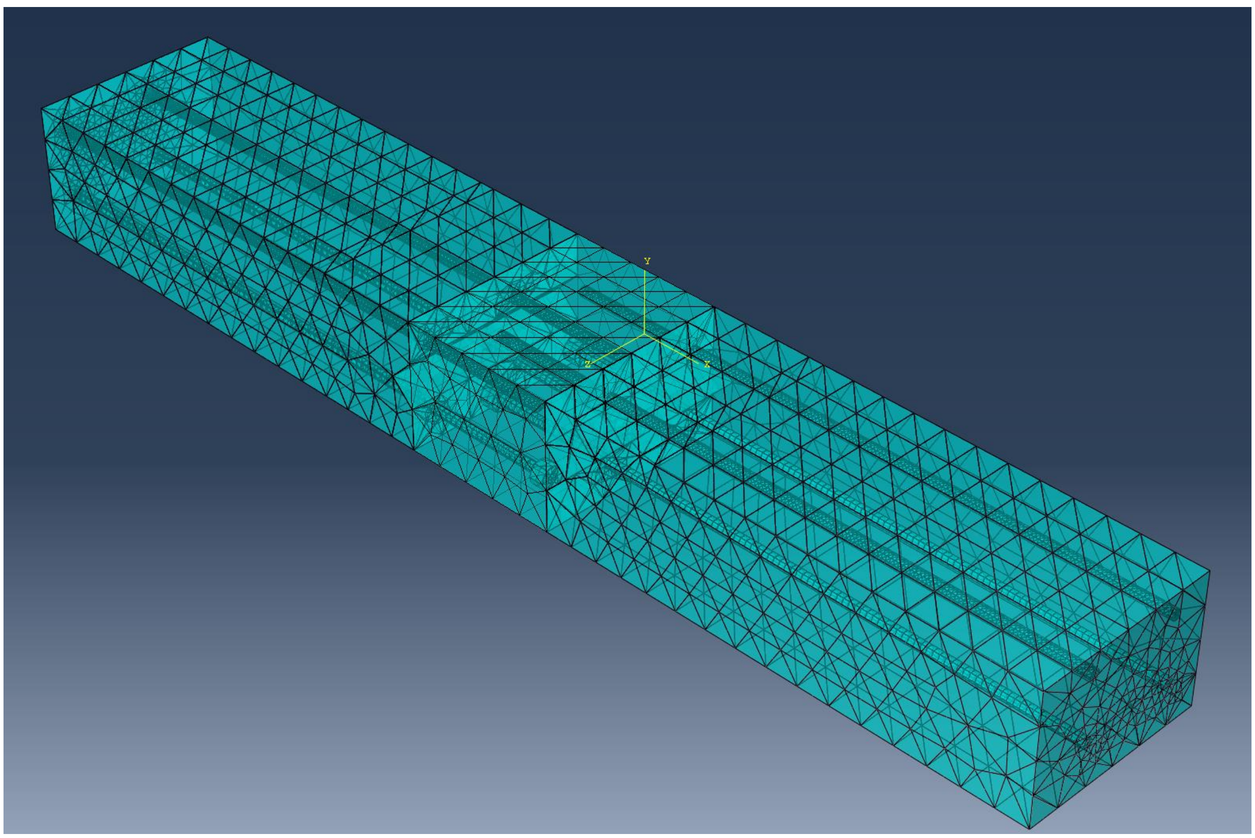

Figure 5.13 Mix-D Beam Test Mesh

5.1.8 Results and Comparison of the Mix-D Beam Test

A job was then created in Abaqus/CAE, and submitted to Abaqus/Standard for processing. Four processors were used in parallel with a total processing time of 42 hours. Figure 5.14 shows the results of the analysis can be shown looking at the stresses in the front view of the beam and Figure 5.15 shows an isometric view of the results. The stresses are viewed in the S11 (x-direction) showing only the bending stresses. It can be seen on both views that the highest stresses are in the bottom-inner reinforcement bars at the location of the interface.

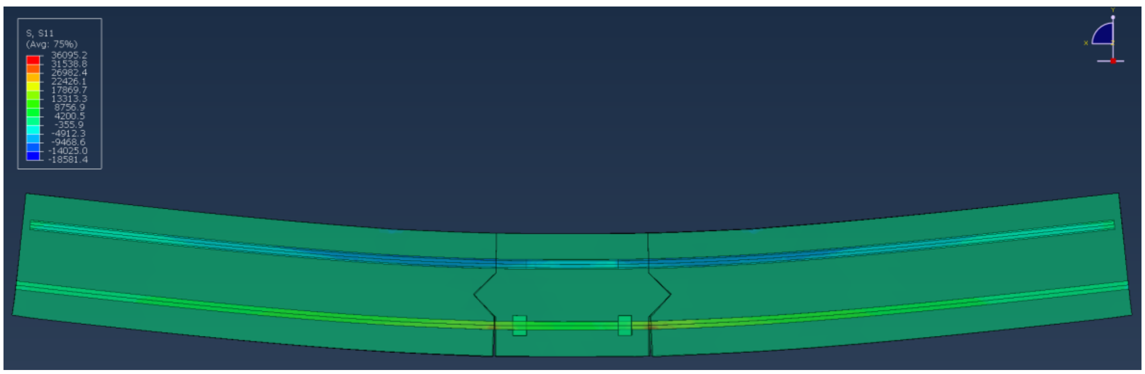

Figure 5.14 Mix-D Closure Beam Test Front View Results

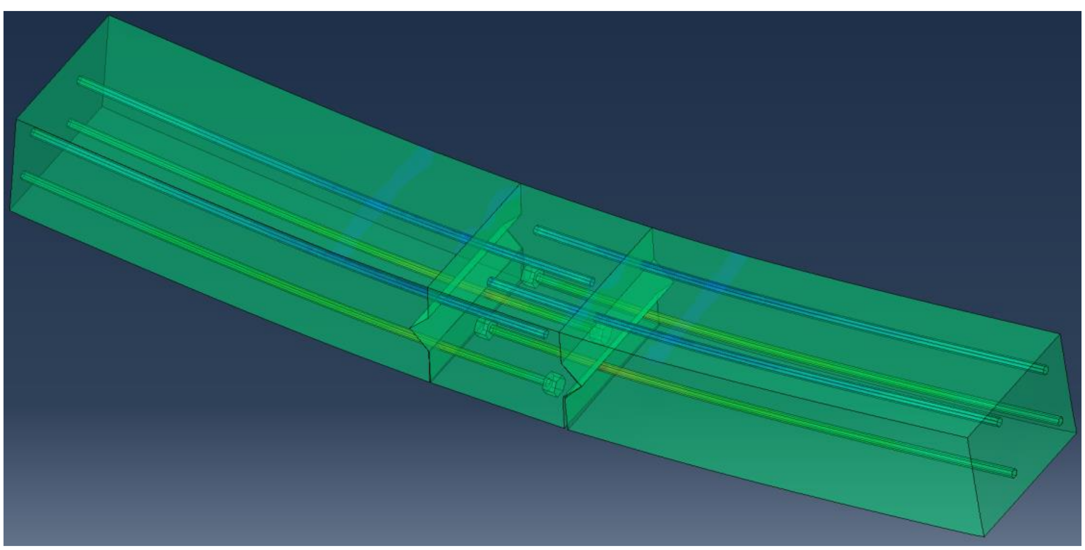

Figure 5.15 Mix-D Closure Beam Test Isometric View Results

The physical beam tests done by Casanova compared the moment versus rebar stress therefore, the same is done with the FEM model results. The moment is calculated first by calculating the point load from the applied pressure load at each given step as shown in equation (5.2). The maximum moment is then calculated at each time step using equation (5.3) from (AISC 2017), where $P = point\ load$ and $a = position$.

$$P = pressure * area \tag{5.2}$$

$$M_{max}\ (between\ loads) = P * a \tag{5.3}$$

The calculated moment is then compared to the measured stress in the rebar. The stress in the rebar is measured at two locations, one near the head (to compare to physical results) and the other at the interface. This comparison of results is show in Figure 5.16 The figure shows that the stress calculated from Abaqus near the head in within the experimental result envelope which was also for the stress near the head. These results prove that the model is accurately representative of the beam's behavior. Hence, more information can be extracted from the model, such as the stress in the bars at the interface which was not measured in the experimental work. Another area where stress can be evaluated is in the concrete. Figure 5.17 shows the bending stresses in just the concrete prior to the interface cracking.

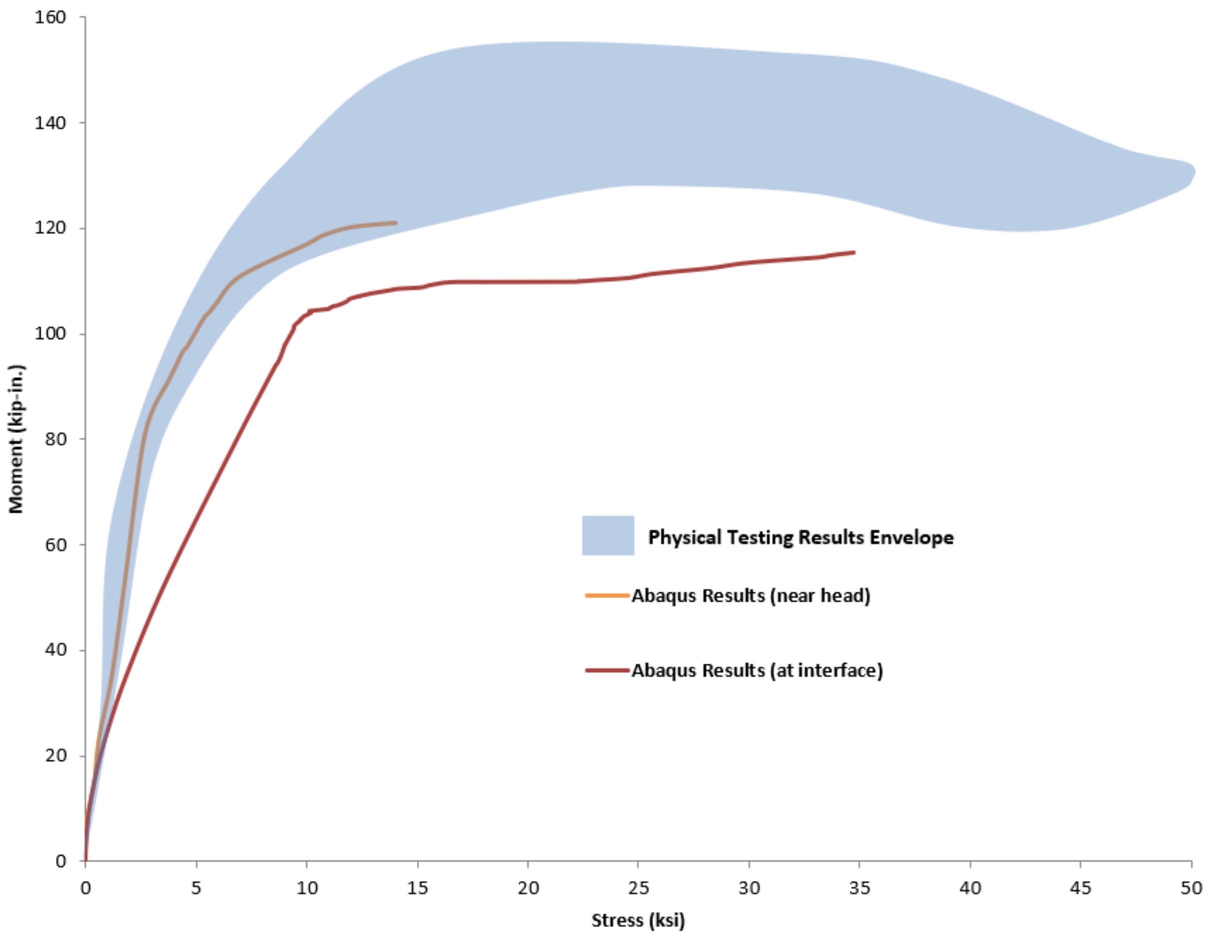

Figure 5.16 Mix-D Beam Test Results

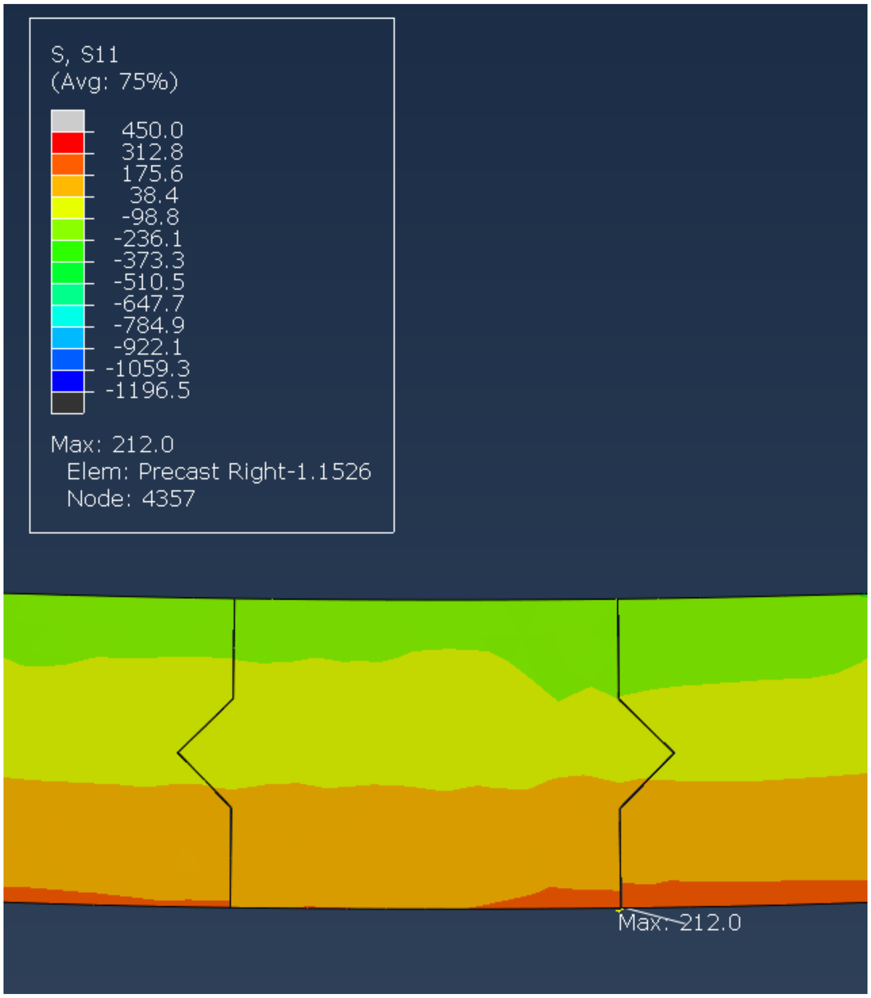

Figure 5.17 Mix-D Beam Test Concrete Stress Results

5.2 Abaqus Model of UHPC Closure Beam Test

Casanova's work included many tests of closure pour materials and identified a Mix-D as the best closure pour material. The purpose of Casanova's study was to find an alternative closure pour material to use in lieu of the costly UHPC. Because of the time and material cost of laboratory testing, Casanova did not perform a four-point beam test using UHPC for a direct comparison to Mix-D. This is an area that FEM excels because the Abaqus model in the previous section can easily be modified to UHPC dimensions and material properties. This section discusses an FEM of a UHPC four-point beam test and compares the results to the Mix-D for comparison.

5.2.1 Finite Element Model Geometry for UHPC Closure Beam Test

The UHPC closure beam test consists of five unique parts: closure pour, precast left, precast right, headed rebar, and top rebar.

The closure pour geometry begins with a two-dimensional profile as shown in Figure 5.18. The closure pour is modeled as described in the previous sections. The main difference is that the UHPC closure pour is 6” wide rather than 10” with Mix-D (Ebrahimpour, 2019).

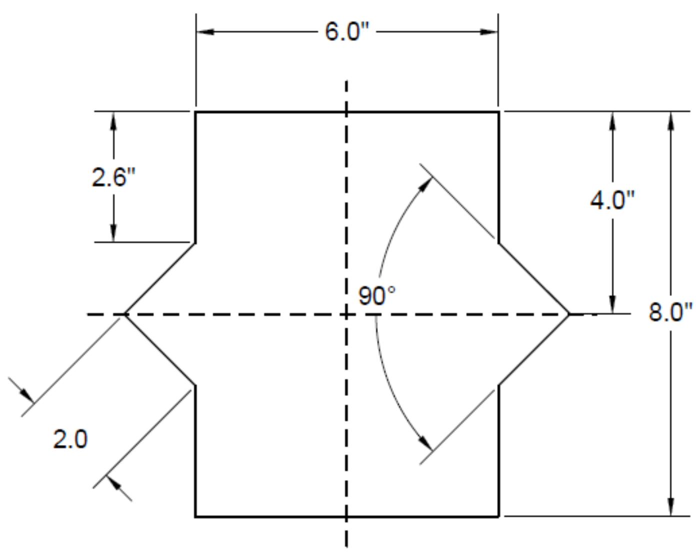

Figure 5.18 UHPC Closure Pour Two-Dimensional Profile

Next, the left and right precast parts are created. The precast geometry begins with a two-dimensional profile as shown in Figure 5.19. The main difference being the length of the precast is shortened to accommodate the wider closure pour.

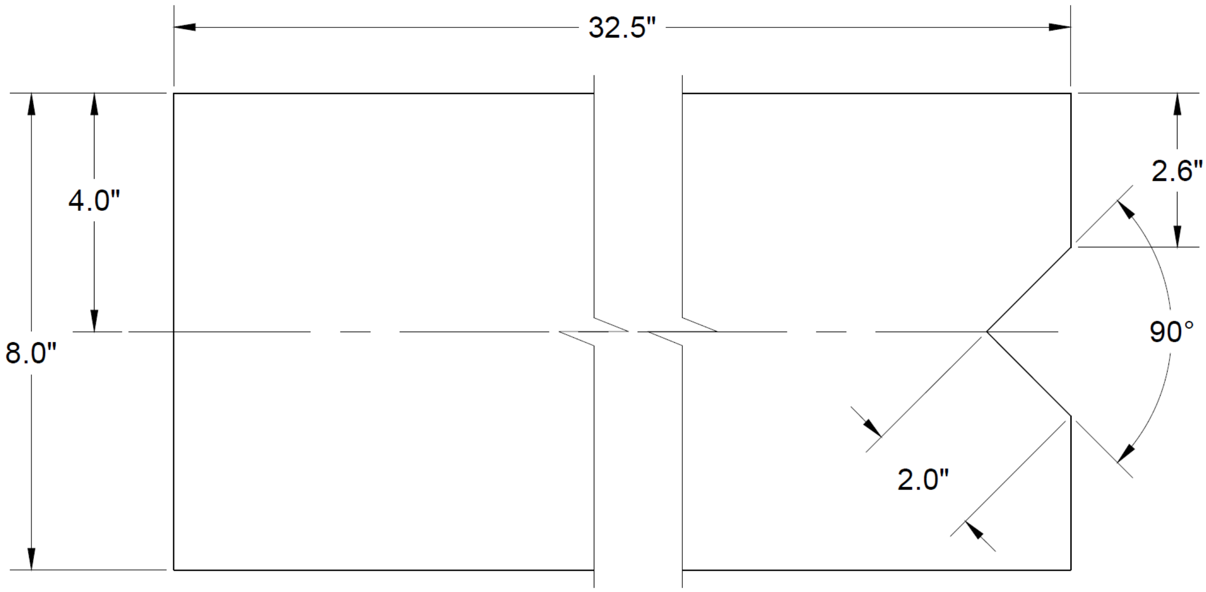

Figure 5.19 Precast Two-Dimensional Profile

The headed rebar is modeled exactly as in the previous section with the only change is the length is increased by 2” to account for the deeper embedment within the closure pour.

5.2.2 Finite Element Model Materials for UHPC Closure Beam Test

Material properties for the rebar and headed rebar are steel. Steel is assumed to be perfectly elastic because it is expected that yielding will not occur in the steel. A Modulus of Elasticity (Young’s Modulus) of $29x10^6$ psi and Poisson’s Ratio of 0.3 was entered in the “Elastic” material properties of steel.

Concrete materials are precast and UHPC. The material properties of the precast will remain the same as shown in Table 5.2. UHPC material properties are provided by the information given in Table 2.2 and Table 3.1 will again require the methods described Chapter 3. The calculation results are shown in Table 5.3 along with the equation entered into Abaqus using the “Concrete Damage Plasticity” material.

Table 5.3 UHPC Closure Material

Closure Pour Properties with $f'_c = 24,000\ psi$			
Property	**Value**		**Equation / Source**
Initial Tangent	$E_{IT} = 7.0\ x\ 10^6\ psi$		Table 2.2
Tension Yield Stress	$f'_t = 634\ psi$		(3.7)
Poisson's Ratio	$\mu = 0.2$		(Nawy 2009)
Compressive Stress as a function of Compressive Strain	Strain (in/in)	Stress (psi)	(3.3) using (3.4) and (3.5)
	0	0	
	0.0005	4248	
	0.0012	9333	
	0.0018	12822	
	0.002	13820	
	0.0024	15591	
	0.0028	17093	
	0.0032	18362	
	0.0036	19430	
	0.004	20324	
	0.005	21961	
	0.006	22973	
	0.007	23565	
	0.008	23874	
	0.009	23992	

5.2.3 Time Step / Interaction / Loads / Boundary / Mesh for UHPC Beam

Similar to previous section 5.1, the time step, interactions, and boundary conditions remain the same for the UHPC beam test. All of the parts were re-meshed because of dimensional changes but the node spacing remained the same. A view of the mesh is shown in Figure 5.20.

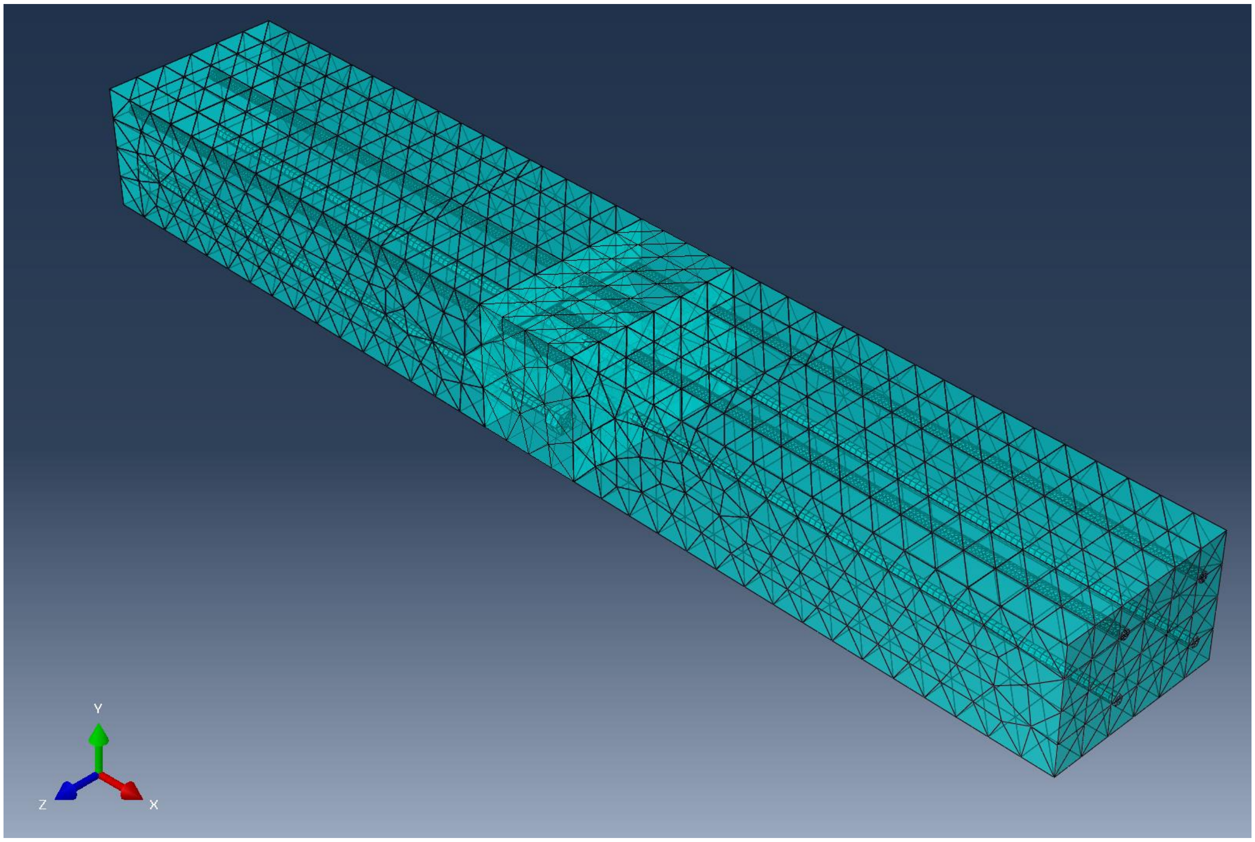

Figure 5.20 UHPC Closure Beam Test Mesh

5.2.8 Results and Comparison of the UHPC to Mix-D

A job was then created in Abaqus/CAE, and submitted to Abaqus/Standard for processing. Four processors were used in parallel with a total processing time of 42 hours. The results of the analysis can be shown looking at the stresses in the front view of the beam, Figure 5.21, and an isometric view, Figure 5.22. The stresses are viewed in the S11 (x-direction) showing only the bending stresses. It can be seen on both views that the highest stresses are in the bottom-inner reinforcement bars at the location of the interface.

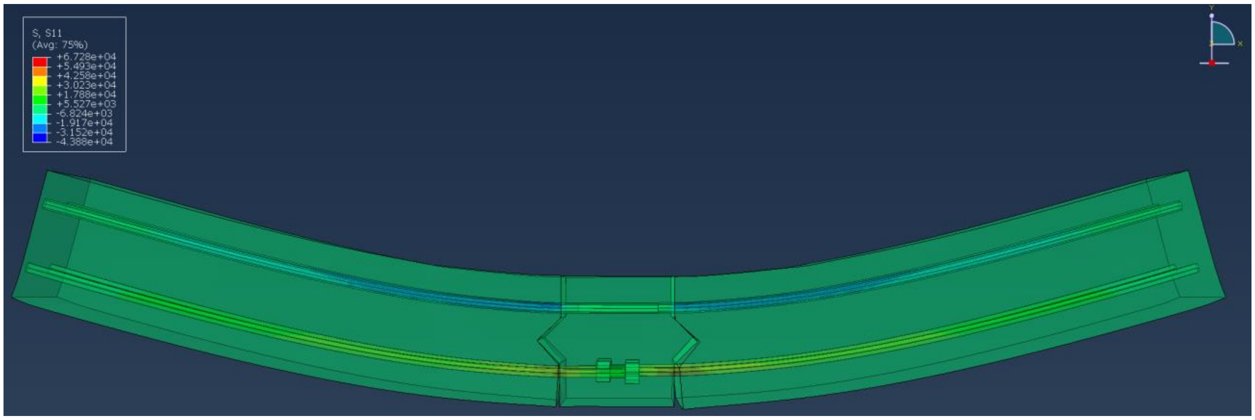

Figure 5.21 UHPC Closure Beam Test Front View Results

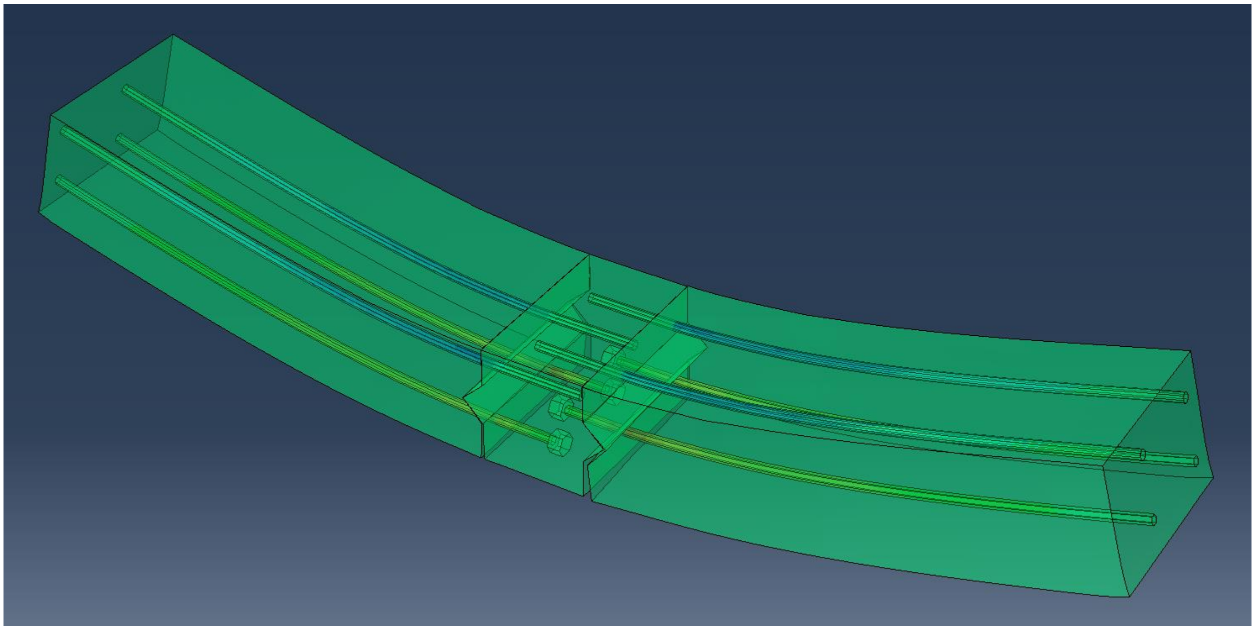

Figure 5.22 UHPC Closure Beam Test Isometric View Results

The maximum moment at each time step was calculated using equations (5.2) and (5.3).

The calculated moment is then compared to the measured stress in the rebar as was done in the previous section. The stress in the rebar is at the interface. This is compared to the same measurement from the Mix-D Beam Test and the results are shown Figure 5.23 It shows that the Mix-D and UHPC perform almost identical until the interface separates. These results depict that

Mix-D is an adequate replacement of UHPC in closure pours. That is because the limiting factor is the strength of the interface bond which is exceeded before the tensile strength of the concrete.

As the shown in Figure 5.17, the bending stresses in just the concrete prior to the interface cracking are shown in Figure 5.24. A comparison shows that the concrete stress at the bottom of each beam is about 200 psi with the next step exceeding the interface bond strength of 245 psi. However, there is a subtle difference where the maximum concrete stress in the UHPC is located at around the headed bar elevation.

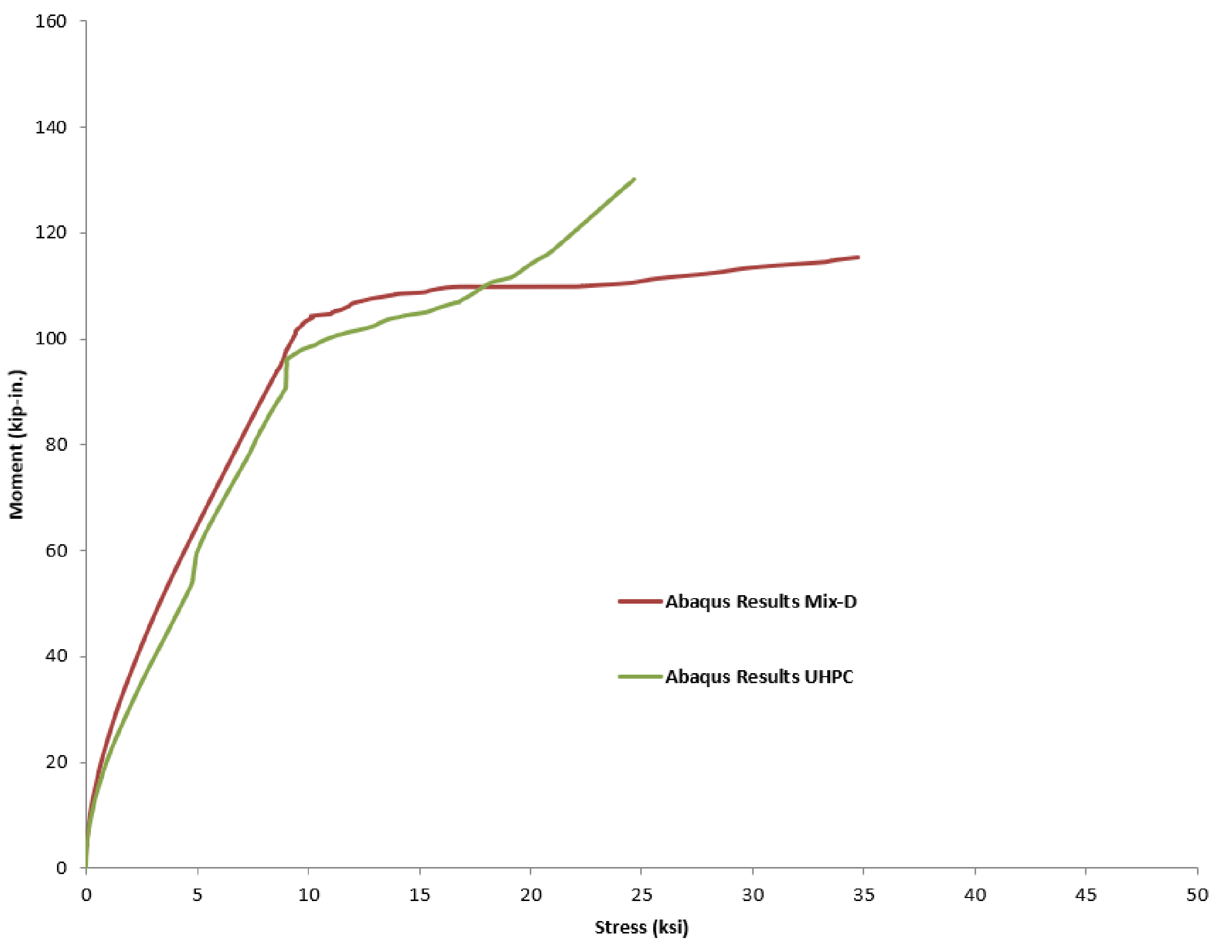

Figure 5.23 Comparison of UHPC to Mix-D Beam Test Results

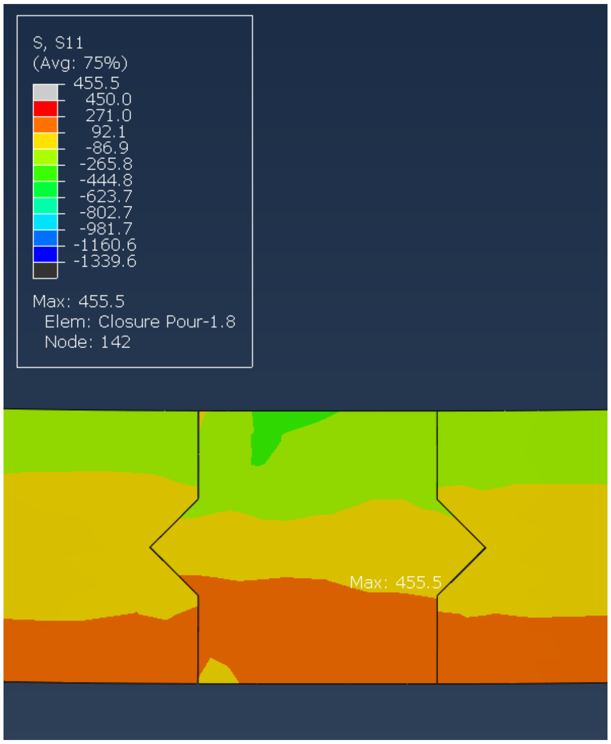

Figure 5.24 UHPC Beam Test Concrete Stress Results

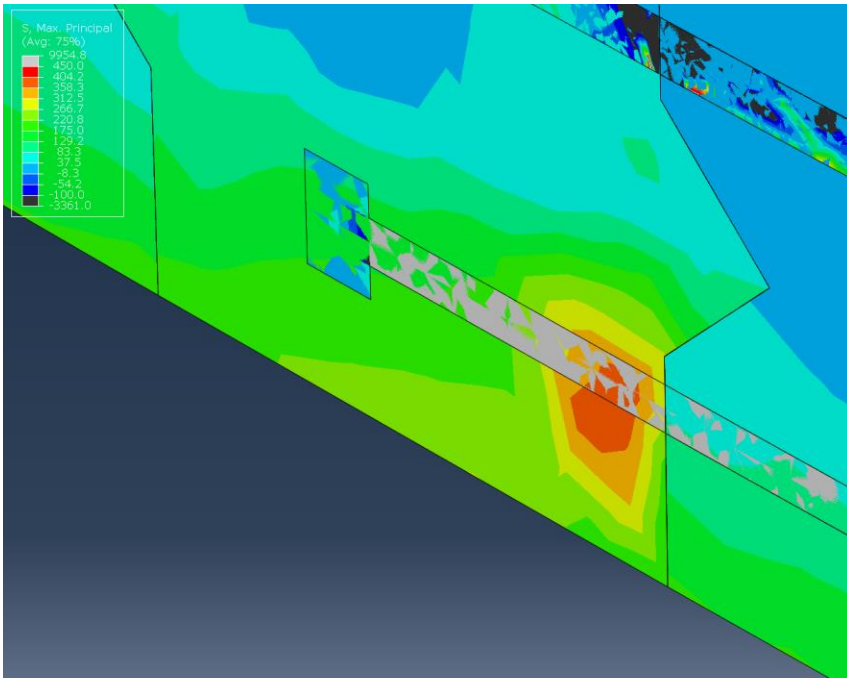

Figure 5.25 UHPC Beam Test Concrete High Stress Area

CHAPTER 6 SUMMARY, CONCLUSIONS, AND FUTURE WORK

The purpose of this chapter is to summarize the results generated from this research project. From the beginning, this research project set out to determine if a HES Mix-D could be used as an alternative for field-cast connections of precast elements in accelerated bridge construction.

6.1 Methodology Summary

Developing accurate models is paramount when using FEM. Many smaller studies are needed to that computational results replicate physical results. Methodology of mechanical phenomenon was verified to ensure the following model features worked properly:

- Material properties
- Headed reinforcement bar pullout
- Bar to concrete bond
- Interface strength (cohesive contact)[2]

6.2 FEM Beam Test Summary

Physical testing is limited in that measurements cannot be taken everywhere. Especially on the interior of the beam where stresses fields cannot be visually seen. FEM has the capability of performing measurements at any location to provide additional results. It was shown that the

[2] To date, it is unknown if interface bond tensile testing has been performed on precast concrete to UHPC. In the absence of such data, the interface bond strength is assumed to be the same as defined in section 5.1.5 of $f_t = 245\ psi$.

highest bar stress occurred at the interface rather that near the head where physical tests were measured.

Another benefit of FEM is that once a model has been verified to be correct, some parameters can be modified to analyze the effects that gives insight into the beam's performance. A similar four-point flexural beam test using UHPC closure pour was analyzed to provide a comparison of the two closure pour configurations. It was shown that there is no benefit to using UHPC over a HES Mix-D concrete as a closure pour because in both cases the beams failed with cracks in the interface.

An unexpected result was found where the highest stresses in the concrete occurred a different location between the beams. The Mix-D beam had the highest concrete stresses at the bottom of the beam where the UHPC beam had the highest concrete stresses at the same elevation as the headed rebar.

6.3 Conclusion

In this research project, it was determined that the material behavior of a HES Mix-D concrete was an effective alternative for field-cast connections of precast elements in accelerated bridge construction. In both cases, the tensile strength of the concrete was not exceeded and thus, not the limiting factor. In both cases the weakest factor is the interface bond.

Because UHPC requires a special labor force and processes, it can be very expensive as compared to a HES Mix-D for field-cast connections of precast elements in accelerated bridge construction. UHPC also requires a longer curing time than HES Mix-D which adds additional time to a bridge constructions schedule (Ebrahimpour, 2019.)

6.4 Future Work

There is no testing data on interface bond strength between the UHPC closure pour and the precast element. Therefore, an assumption was made in the UHPC beam test that the interface bond strength is the same a Mix-D/precast bond. Because the bond is the limiting feature of a closure pour, it is recommended that physical testing be performed on the bond strength of UHPC.

An additional recommendation for future work would be a cyclic loading study. The work in this research project focused on one constant load of the beam until failure. This is not a realistic loading of a bridge. It is recommended that a more typical bridge loading be placed on the beam model and analyzed under a cyclic loading to determine the effect of concrete and steel fatigue in the closure pour/headed bar area.

REFERENCES

ACI, 318-08 (2008), "Building Code Requirements for Structural Concrete and Commentary." *American Concrete Institute ACI 318-0,8* Detroit, Michigan.

AISC, (2017), *Manual of Steel Construction*, 15th Ed., AISC, Chicago, IL.

ASTM, (2018), "Standard test method for flexural strength of concrete (Using simple beam with third-point loading)." *ASTM C78-18*, West Conshohocken, PA.

Carreira, D.J. and Chu, K. (1985*)*. "Stress-Strain Relationship for Plain Concrete in Compression." Title No. 82-72. ACI Journal.

Casanova, M. (2018). *Mechanical Behavior of High Early Strength Concrete with Polypropylene Fibers for Field-Cast Connections of Bridge Precast Elements.* Master's Thesis. Idaho State University.

De la Varga, I., and Graybeal, B. (2016). "Dimensional stability of grout-type materials used as connections for prefabricated bridge elements." *FHWA-HRT-16-008*, FHWA, McLean, VA.

De la Varga, I., Haber, Z. B., and Graybeal, B. (2016). "Performance of grouted connections for prefabricated bridge elements-part I: material-level investigation on shrinkage and bond." *2016 PCI National Bridge Conference*, PCI, Nashville, TN.

DeVries, R.A. (1996). *Anchorage of Headed Reinforcement in Concrete.* Ph. D. Dissertation. University of Texas at Austin.

Ebrahimpour, A., Ruminski, L., Mashal, M. (2019). "Use of High Early Strength Concrete Class 50AF with Polypropylene Fibers as a Cost-Effective Alternative for Connecting Precast Bridge Girders in the Field." *Western Bridge Engineers' Seminar*. Boise, ID.

ERICO Lenton Terminator Mechanical Anchors. (2017). "Mechanical Anchor Catalog." www.erico.com/catalog/categories/R2072?pdf=1&language=en&country=US (2017 July 07).

Graybeal, B. (2014). "Design and construction of field-cast UHPC connections." FHWA-HRT-14-084, FHWA, McLean, Virginia.

Hafezolghorani, M., Hejazi, F., et. al. (2017). "Simplified Damage Plasticity Model for Concrete." *Structural Engineering International*

Hong, S. (2008). "Bond Stress-Slip Relationship In Reinforced Concrete: New Relationship And Comparative Study." *Our World In Concrete & Structures.* 33rd Conference. Singapore.

Kim, J.J. and Taha, M.R. (2014). "Experimental and Numerical Evaluation of Direct Tension Test for Cylindrical Concrete Specimens." Advances in Civil Engineering. Volume 2014. Article ID 156926. Hindawi Publishing Corporation.

Logan, D.L. (2012). *A First Course in the Finite Element Method.* Fifth Ed. Cengage Learning. Stamford, Connecticut.

Marchetto, F. (2015). “Use Of Headed Reinforcement Bars in Construction.” Ph.D. Dissertation. Technical University of Madrid.

Nawy, E.G. (2009). *Reinforced Concrete a Fundamental Approach*. Sixth Ed. Pearson Education, Inc. New Jersey.

Nilson, A.H., et. al. (1991). *Design of Concrete Structures.* Eleventh Ed. McGraw-Hill, Inc. New York.

Rao, G.A., et. al. (2007). “Studies On The Pull-Out Strength Of Ribbed Bars In High-Strength Concrete.” *Indian Institute of Technology Madras,* University of Stuttgart, Stuttgart 70569, Germany.

Shima, H. (1986). “Micro and macro models for bond behavior in reinforced concrete.” University of Tokyo, Tokyo, Japan.

Thompson, M.K., Jirsa, J.O., Breen, J.E., and Klingner, R.E. (2000). “Anchorage Behavior of Headed Reinforcement Literature Review.” Research Report 1855-1. *Center for Transportation Research Bureau of Engineering Research.* University of Texas at Austin.

Wolf, L., et. al. (2001). “Introduction To Structural Mechanics.” 22.312 Engineering Of Nuclear Reactors Online Course Notes. Massachusetts Institute of Technology. https://ocw.mit.edu/courses/nuclear-engineering/22-312-engineering-of-nuclear-reactors-fall-2015/readings-and-assignments/MIT22_312F15_note_L4.pdf

APPENDIX A Abaqus Material Verification of Nonlinear FEA

Introduction:

Nonlinear analysis is important to analyzing complex engineering structural analysis. It can be used to as a tool to model mechanical phenomena such as buckling, extreme loading, plastic deformations, and seismic loadings. Nonlinear analysis is used more and more as time goes on due to the demand for accurate analysis and the continuing advancements in computing capabilities.

Elastic and Plastic Behavior:

An understanding of elastic and plastic material characteristics is the key to nonlinear analysis. A linear-elastic material response is characterized by a linear-elastic equilibrium path. The elastic region is shown in Figure A.1 where the linear-elastic regions are represented by a line. When a load is applied in this region and then subsequently removed, the strain returns back to its original state.

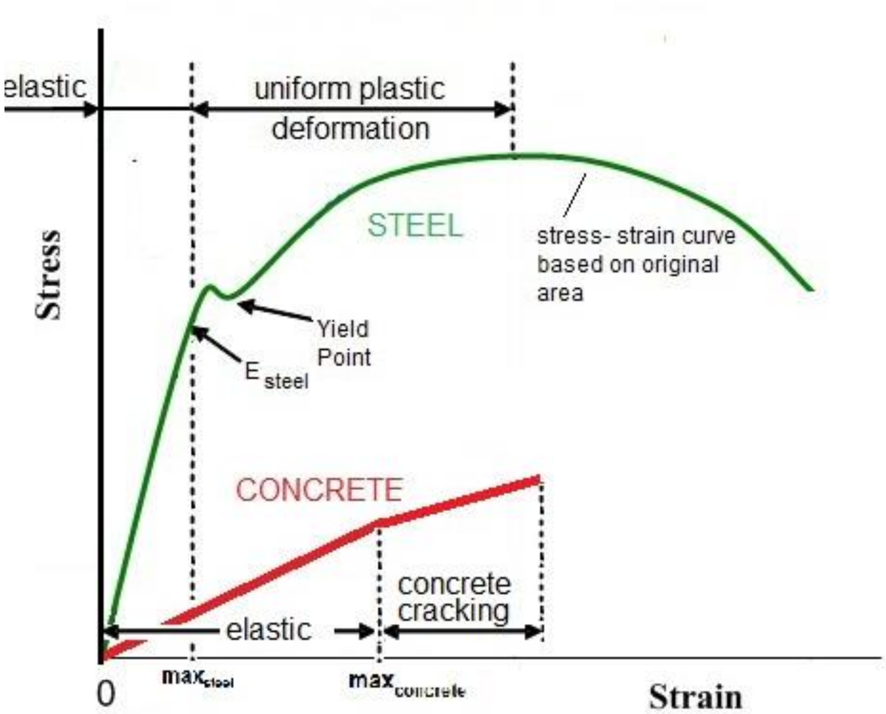

Figure A.1 Stress-Strain Diagram for Steel and Concrete

Image source: http://www.o-lay.net/innovative/elastic-bending

Plastic behavior occurs as the stress increases past the elastic zone. This point is known as the yield point. Plastic behavior differs from elastic behavior in that permanent distortion occurs.

Concrete Material Model:

Several material mechanical properties are needed to create an accurate material model. These include 28-day concrete compressive strength f_c', modulus initial tangent (modulus of elasticity) E_{IT}, 28-day compressive strain ε_c', tension strength f_t', and tension strain ε_t'. These variables are shown on the general concrete stress-strain diagram in Figure 3.1. The equations and methodology for calculating all parameters needed as inputs into the Abaqus material model can be found in Chapters 3 and 4.

Linear Analysis Verification:

Linear analysis is best when defining elastic behavior because it is a good approximation up until material yielding. Linear analysis is very useful in design calculations because designs generally do not want material yielding or large displacements. The stress-strain diagram of a linear analysis is shown in Figure B.2

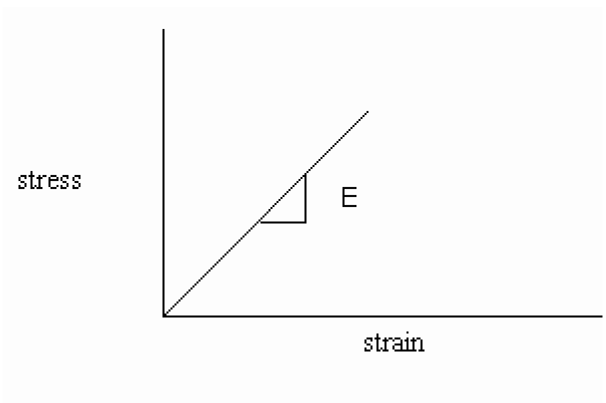

Figure A.2 Stress-Strain Diagram of a Linear Analysis

A typical linear analysis in a finite element software such as Abaqus requires the Young's modulus and Poisson's ratio as inputs. This is not realistic because it does not contain a yield point which means the material has infinite strength.

A simple example in Abaqus depicts the exact nature of a linear analysis. A 1" x 1" x 1" block was modeled. The purpose of selecting a 1" block allows for the deformation to equal the strain for easy comparison to an analytical solution. The block was fixed in the y-direction on the bottom surface and a pressure load of 50 ksi was applied on the opposite side. Figure A.3 shows a material input of $29x10^6$Young's modulus and 0.3 Poisson's ratio into an elastic material behavior which are the only material parameters needed for a linear analysis.

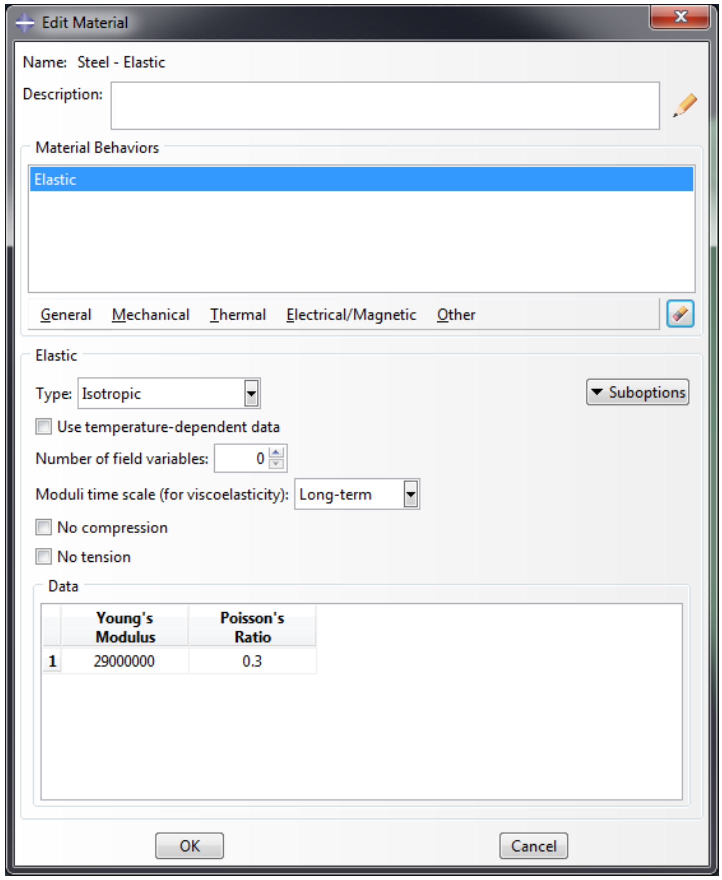

Figure A.3 Abaqus Elastic Material Input for Linear Analysis

Figure A.4 shows the base of the block fixed in the y-direction and a displacement on the top of the block to provide a uniform pressure load.

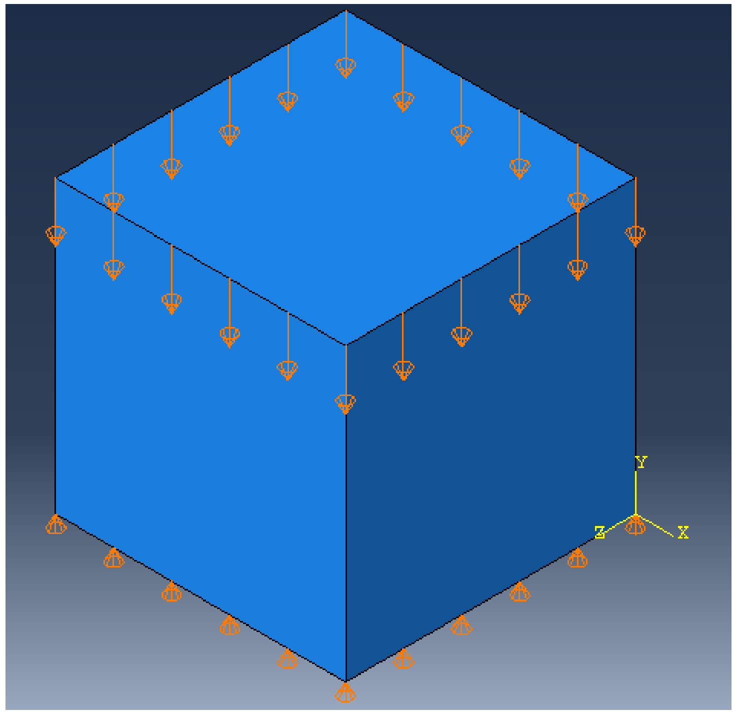

Figure A.4 Load and Boundary Conditions for Linear Analysis

A view of the displacement results in the U2 (y-direction) displays that the maximum displacement in the Abacus model is 0.172”. This displacement is shown in Figure A.5.

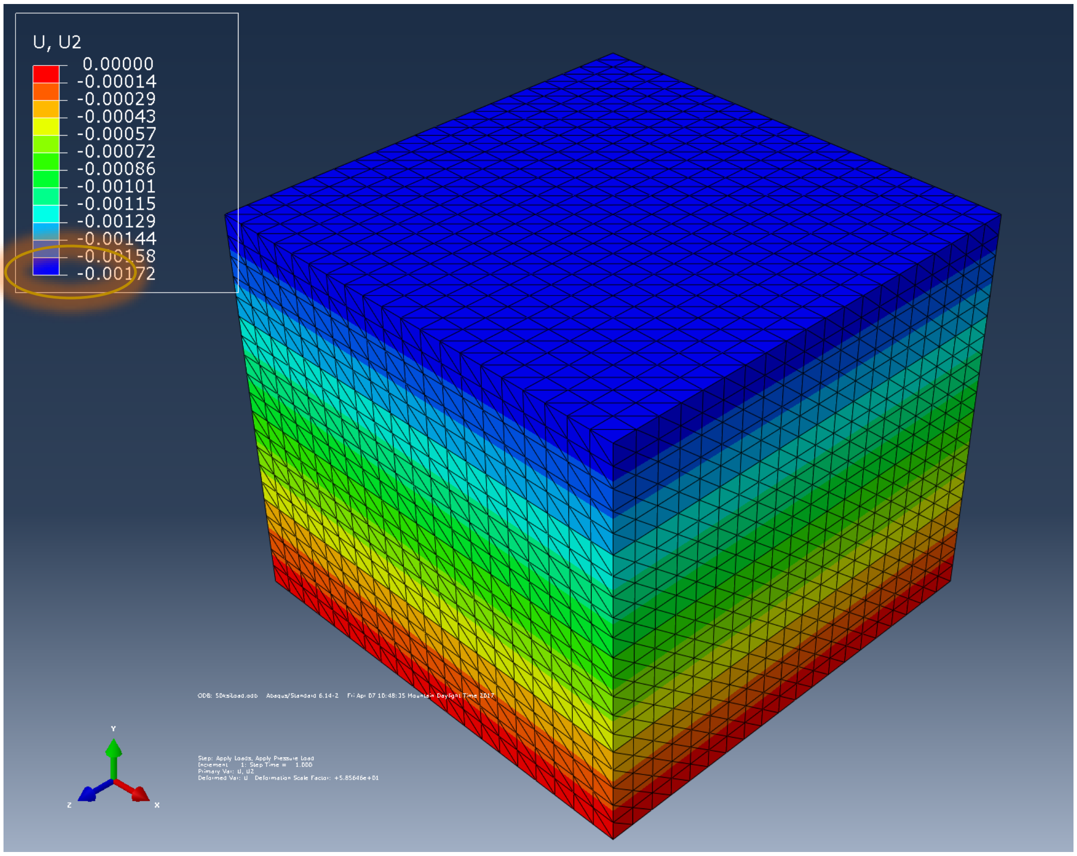

Figure A.5 Displacement Results of Linear Analysis

The analytical solution is calculated as follows:

$$\varepsilon = \frac{l_o - l_f}{l_o} \qquad (A.1)$$

$$where \quad l_o = 1"$$

$$\varepsilon * 1 = l_o - l_f = \Delta$$

$$\therefore \ \varepsilon = \Delta$$

and

$$E = \frac{\sigma}{\varepsilon} \qquad (A.2)$$

$$where\ E = 29e6\ ksi\ and\ \sigma = 50\ ksi$$

$$\therefore\ \underline{\underline{\Delta = 0.00172''}}$$

The analytical solution is exactly as the same as the Abaqus solution for a linear analysis.

Nonlinear Analysis Verification:

A nonlinear analysis includes the linear analysis up until elastic yield. Once the yield stress has been reached, the displacements vary nonlinearly with the applied loads. This is especially true of concrete. Using the equations described in Chapter 3 and the methodology in Chapter 4, concrete material properties are calculated for a 28-day compressive strength of 12,000 psi. These properties are listed in Table A.1 Concrete Material Properties for Nonlinear and the stress-strain is plotted with these table values and is shown in Figure A.6.

Table A.1 Concrete Material Properties for Nonlinear Analysis

Concrete Properties with $f'_c = 12,000\ psi$			
Property	**Value**		**Equation**
Initial Tangent	$E_{IT} = 6.244\ x\ 10^6\ psi$		(3.6)
Tension Yield Stress	$f'_t = 448\ psi$		(3.7)
Compressive Stress as a function of Compressive Strain	Strain (in/in)	Stress (psi)	(3.3) using (3.4) and (3.5)
	0	0	
	0.0005	2861	
	0.0012	5857	
	0.0018	7649	
	0.002	8124	
	0.0024	8929	
	0.0028	9573	
	0.0032	10090	
	0.0036	10505	
	0.004	10838	
	0.005	11412	
	0.006	11737	
	0.007	11909	
	0.008	11985	
	0.009	11999	

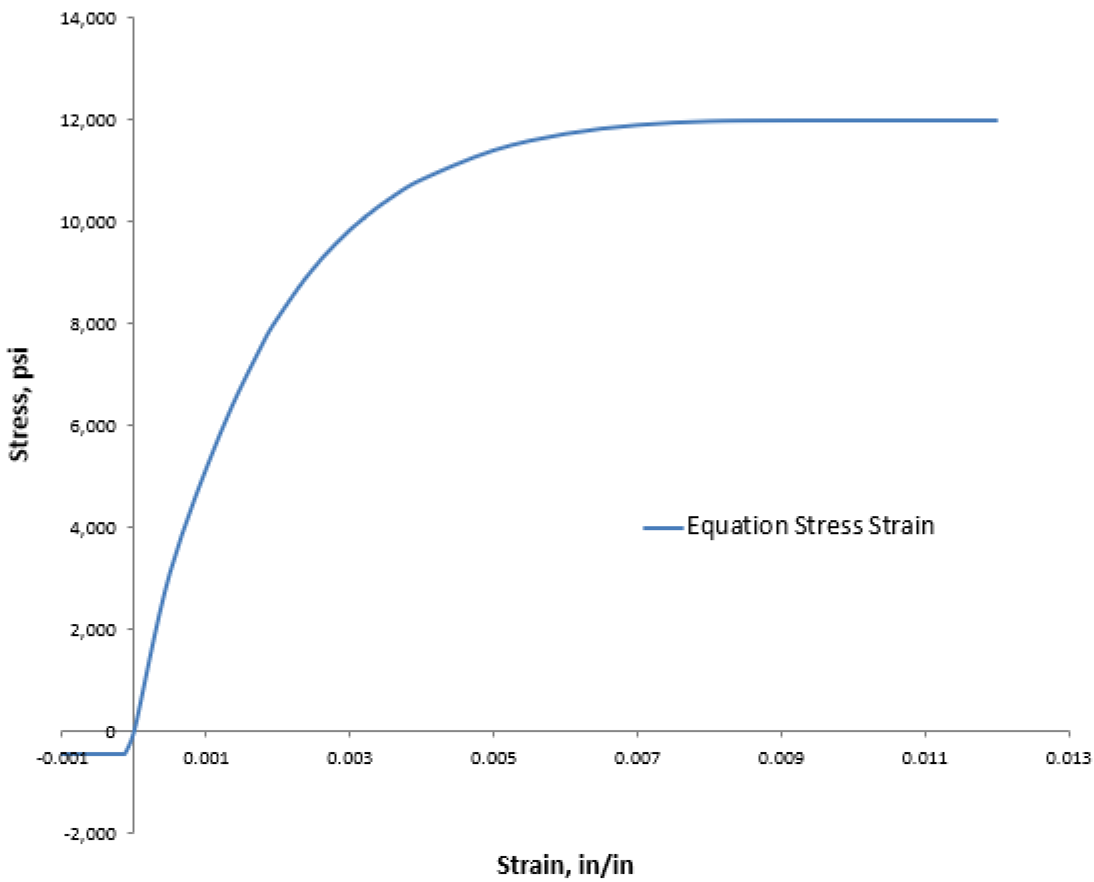

Figure A.6 Stress-Strain Plot of Concrete for Nonlinear Analysis

The plotted values from Table A.1 and Figure A.6 are the inputs entered into the Abaqus material model. It is expected that the Abaqus results will yield similar results.

Just as was done in the Elastic Analysis Verification, a square 1" x 1" x 1" cube was modeled. A vertical displacement, both positive and negative, was placed on the top surface with the bottom surface fixed. The results of displacement and stress on the top node are plotted in Figure A.7. Note that the Abaqus results are an exact match of calculated values showing that the Abaqus nonlinear analysis function is working correctly.

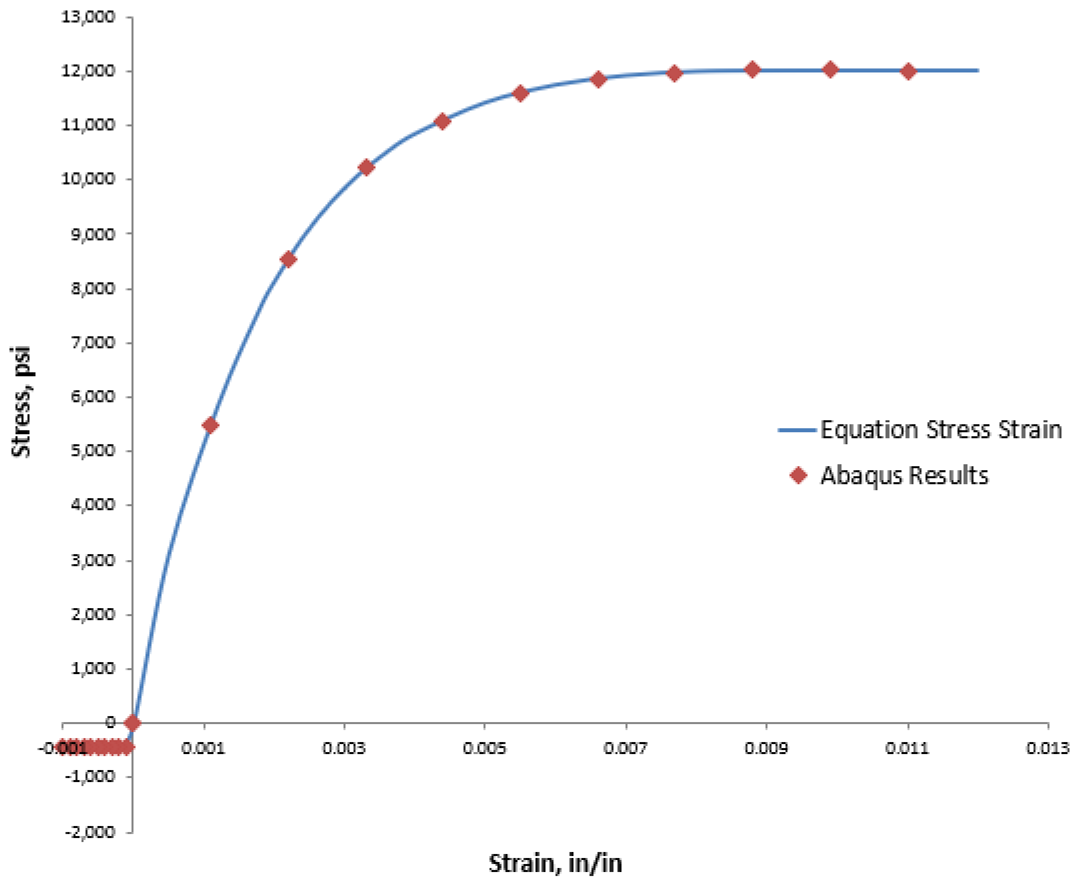

Figure A.7 Abaqus Results of Nonlinear Analysis

APPENDIX B Bond-Slip Finite Element Analysis

The bond between the reinforcing bar and concrete can slip longitudinally in a reinforced concrete member under flexural loading. This interaction is defined as a bond-slip relationship. Initially, the bond resists the load but as the load increases the bond is overcome and slipping occurs. To model properly in FEA, a method must be employed to model this behavior.

Physical Testing of Bond-Slip:

The bond-slip phenomenon is widely characterized with physical testing methods as was performed by Rao (Rao, 2007). Rao created concrete block test specimens of 6" x 6" x 6" and embedded one rebar, #5 (0.62" diameter) in the center. The bar protruded from the block 29 inches for griping to apply an axial tensile force. Materials used are concrete with a 28-day compressive strength of 5,800 psi and steel with a 50 ksi tensile strength. The test setup consisted of pulling on the rebar under controlled displacements. The concrete was mounted in a frame with a steel plate which contained a central opening of 4" for the rebar to pass through. The opening in the plate ensured a free failure of the concrete during testing. Bond stress (τ) was calculated using Equation (B.1).

$$\tau = \frac{P}{\pi d_b l_b} \tag{B.1}$$

Where,

$P = load$, lbf

$l_b = embedment\ length$, inch

$d_b = bar\ diameter$, inch

Error! Reference source not found. shows the bond-slip response comparison. The results s how that the response behaves linearly until the bond strength is exceeded at which point large amounts of slip ensue.

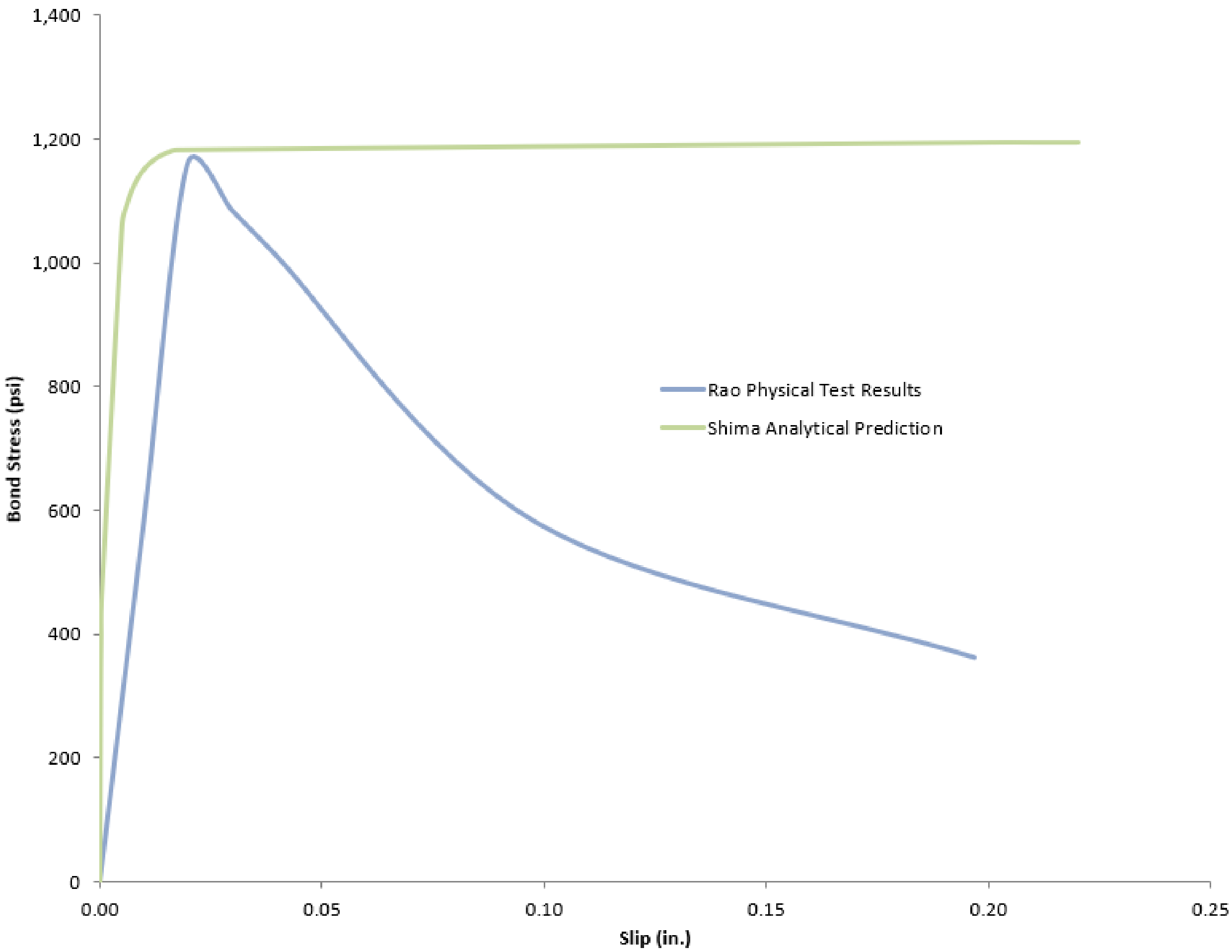

Figure B.1 Bond-Slip Results from Rao Tests and Shima Prediction

Analytical Prediction of Bond-Slip:

An analytical prediction of bond-slip was developed by Shima, 1986. Shima determined that the bond-slip relationship could be represented with mathematical Equation (B.2) (Shima, 1986)

$$\tau = 0.9 f_C'^{2/3}[1 - e^{-40\left(\frac{S}{D}\right)^{0.6}}] \quad \text{(B.2)}$$

Where,

$f_C' = concrete\ 28 - day\ compressive\ strength$, MPa

$\tau = bond\ stress, MPa$

$D = bar\ diameter$, mm

$S = slip\ distance$, mm

The slip distances were entered in Equation (B.2) to calculate associated bond stress. The results are shown on **Error! Reference source not found.** along with the Rao's physical test results.

Verification of Bond-Slip Abaqus Model:

An Abaqus model of the Rao test was created to verify FE results match analytical and physical results. Due to symmetry, a quarter model of the test specimen was prepared. A displacement load was placed on the rebar and a fixed boundary condition was placed on the top surface of the concrete to represent the test fixture. Figure B.2 shows the model. The bond is modeled with a cohesive contact. Figure B.3 shows the contact is set up to damage the bond when the shear stress reaches 1,187 psi. This value is selected as the largest bond stress from Equation (B.2).

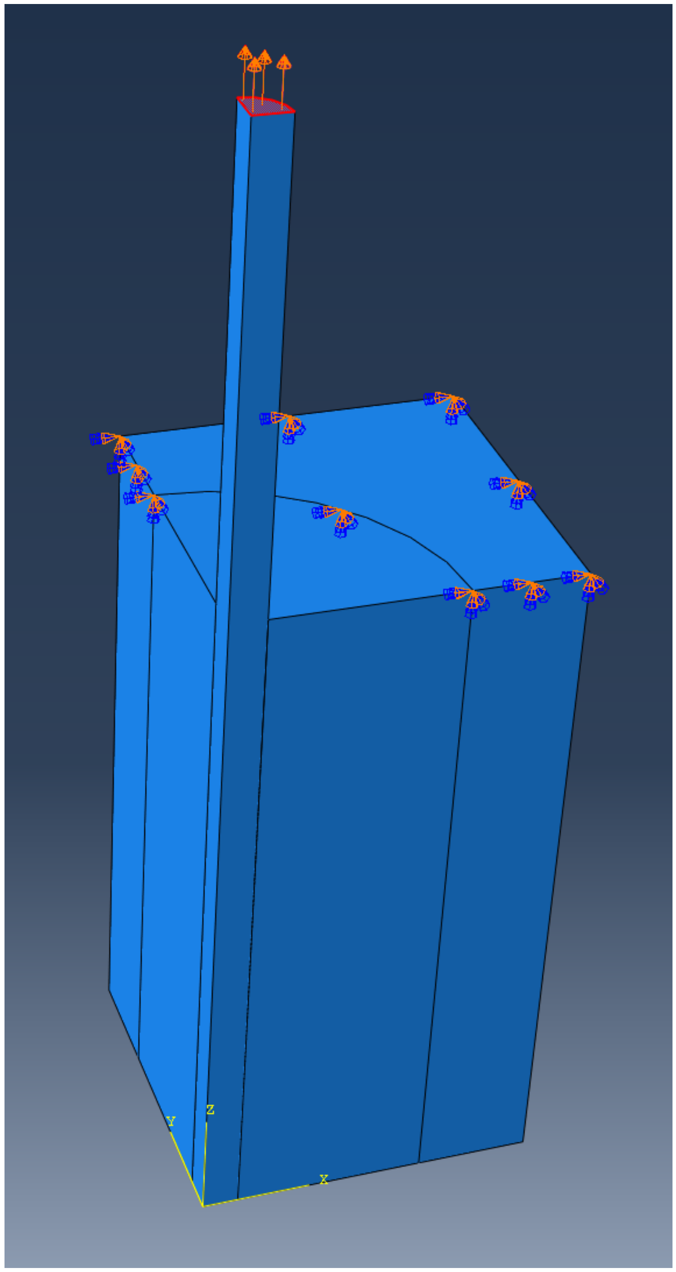

Figure B.2 Abaqus Model of Bond-Slip

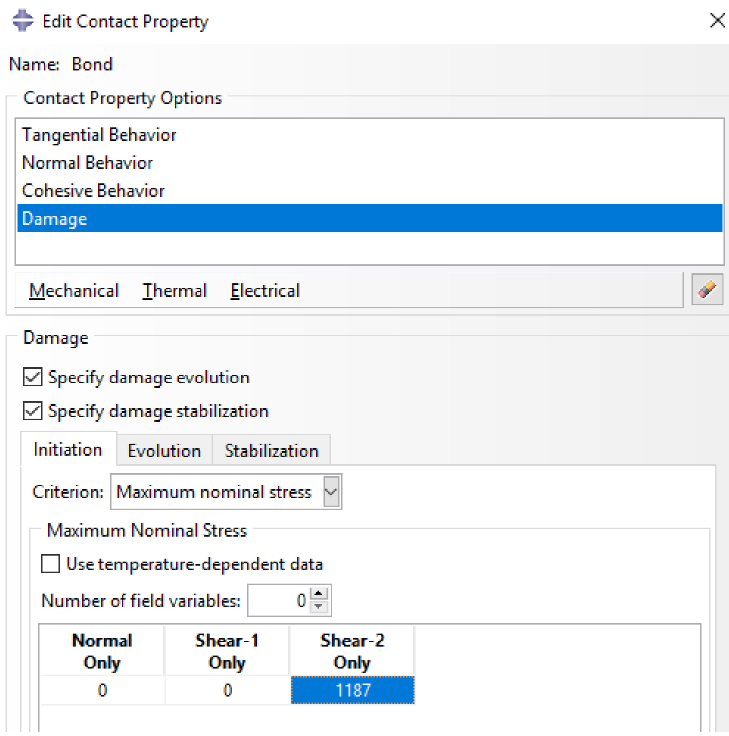

Figure B.3 Abaqus Contact Property for Bond-Slip

A post processing query measured the slip of the node at the top of the concrete where it joined the steel bar at each corresponding bond stress. The results of Abaqus model are shown in Figure B.4 compared with physical and analytical results. The Abaqus model has good agreement with both the physical test and the analytical predictions.

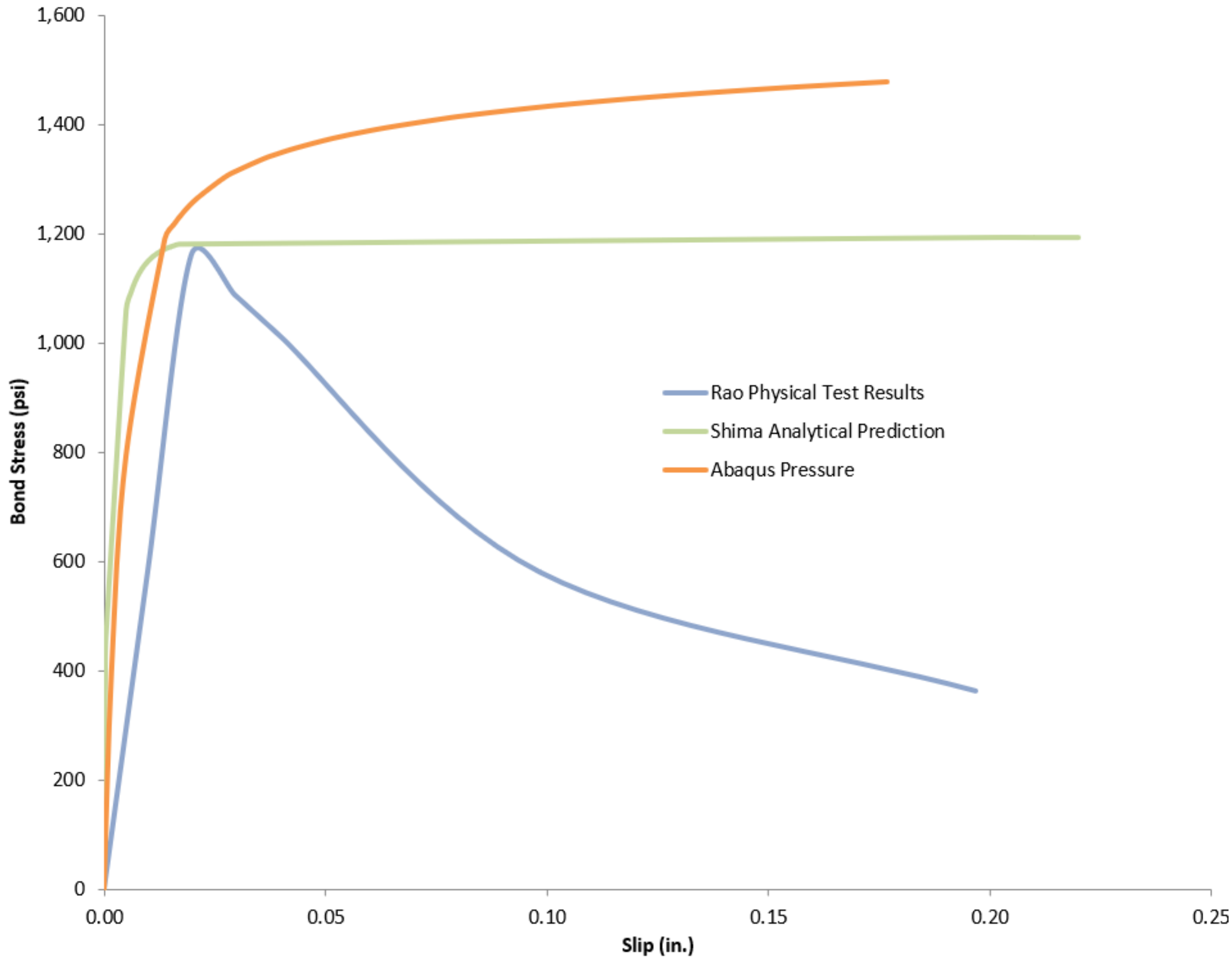

Figure B.4 Bond-Slip Results from Abaqus Model